1-1-2008

PLA-PEO-PLA triblock copolymer hydrogels for soft tissue engineering : properties, assembly, and structure.

Naomi Sanabria DeLong
University of Massachusetts Amherst

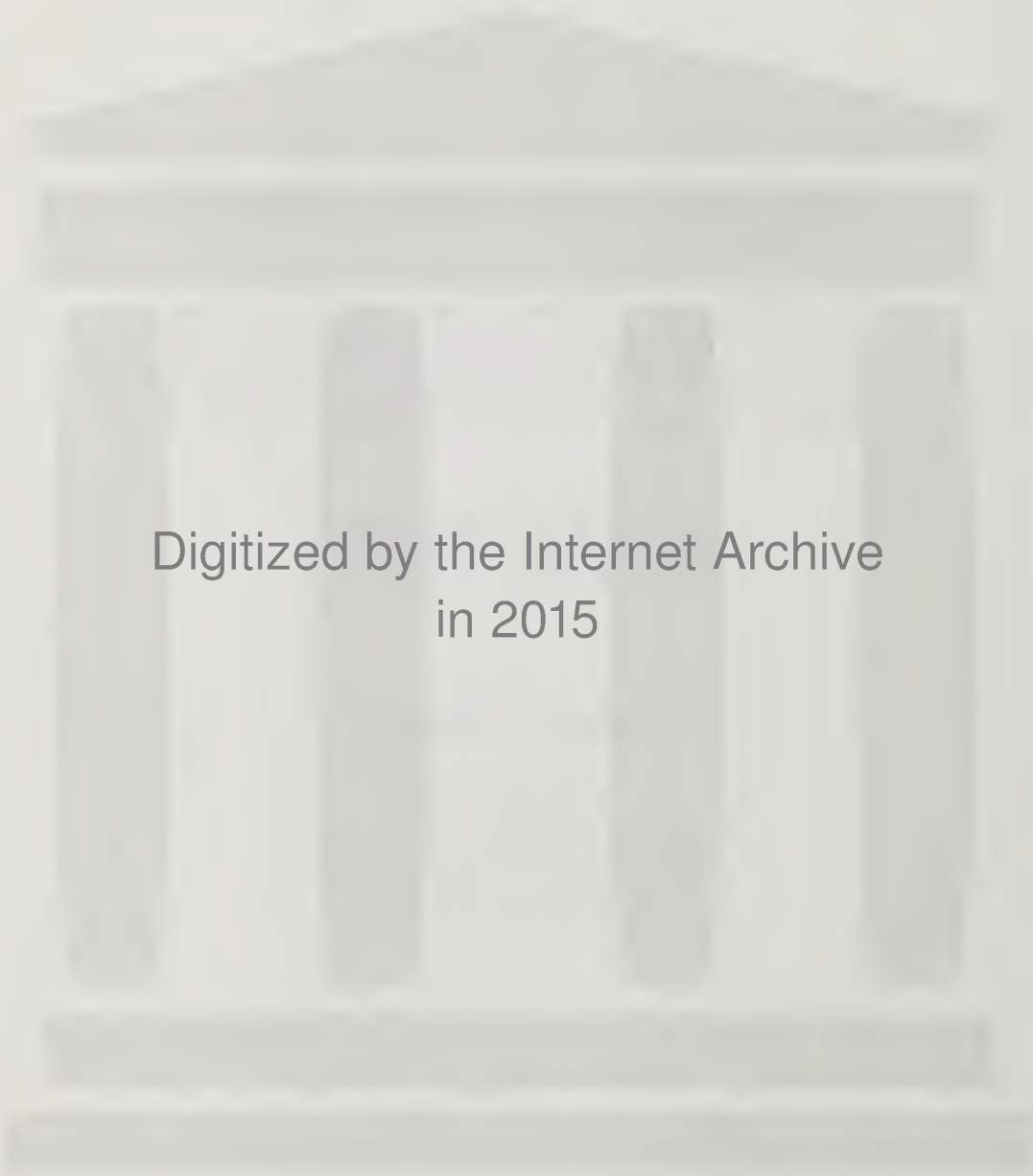

PLA-PEO-PLA TRIBLOCK COPOLYMER HYDROGELS FOR SOFT TISSUE ENGINEERING: PROPERTIES, ASSEMBLY, AND STRUCTURE

A Dissertation Presented

by

NAOMI SANABRIA DELONG

Submitted to the Graduate School of the
University of Massachusetts Amherst in partial fulfillment
of the requirements for the degree of

DOCTOR OF PHILOSOPHY

September 2008

Polymer Science & Engineering

PLA-PEO-PLA TRIBLOCK COPOLYMER HYDROGELS FOR SOFT TISSUE ENGINEERING: PROPERTIES, ASSEMBLY, AND STRUCTURE

A Dissertation Presented

by

NAOMI SANABRIA DELONG

Approved as to style and content by:

_____

Gregory N. Tew, Chair

_____

Alfred J. Crosby, Member

_____

Surita R. Bhatia, Member

_____

Shaw Ling Hsu, Department Head
Polymer Science & Engineering

PLA-PEO-PLA TRIBLOCK COPOLYMER HYDROGELS FOR SOFT TISSUE ENGINEERING: PROPERTIES, ASSEMBLY, AND STRUCTURE

A Dissertation Presented

by

NAOMI SANABRIA DELONG

Approved as to style and content by:

Gregory N. Tew, Chair

Alfred J. Crosby, Member

Surita R. Bhatia, Member

Shaw Ling Hsu, Department Head
Polymer Science & Engineering

DEDICATION

To my loving and supporting husband, Chad DeLong.

ACKNOWLEDGMENTS

I would first like to thank my advisor, Greg Tew. I really believe that you embrace the idea of multi-disciplinary research and that you strive to know as much about a wide variety of subjects as you can. It was this ideality that first attracted me to join your group, and has ultimately turned me into a scientist who can communicate and exchange ideas with researchers with all different types of backgrounds. You've given me the freedom to do research in an area that was unfamiliar to you and encouraged me to learn what I can from the resources around me for which I am grateful. Finally, in the years that I've been here, I've seen your desire to improve the quality of research and scientific writing in the group, as well as your push towards mentoring of students for the department as a whole. I hope that this continues, and I thank you for mentoring me and for knowing both when to push me and when to give me freedom.

I'd also like to thank my committee members, Surita Bhatia and Al Crosby. Surita and her student, Sarvesh Agrawal, were collaborators from the start of my thesis work. They both helped to educate me in the area of rheology, and their expertise in scattering techniques was pivotal towards elucidating the structure of the hydrogel systems. Ideas were raised through conversations with both Surita and Sarvesh that helped progress my work, and I thank them both. Al became an important collaborator later on during my project, and his thoughtful questions helped me to develop my work and ideas. He's also a great teach and mentor, and I thank him for his help in establishing the PSE mentoring program.

There are a number of other collaborators that I must also acknowledge. Khaled Aamer started the work with PLA-PEO-PLA and his passion for science was an

inspiration. Erik Miller and Greg Rolland were my fellow teammates during the IGERT program, and together we dreamed about what it would be like to start our own company. Erik had an incredible drive in this area, enough to overcome my initial reluctance, and together we learned what it takes for commercializing a product (and we even got to go to Hawaii!). Greg was a great asset and made sure we had all the resources we needed. Finally, I'd like to acknowledge those who helped me during my stay at EPFL in Switzerland, Dominique Rothenfluh and André Van der Vlies.

I was fortunate to receive financial support from the Chemistry-Biology Interface (CBI) from the NIH and the IGERT program from the NSF. I thank both of these institutions and those associated with running the IGERT program, especially Mike Wright and Thais Brodeur. The IGERT program allowed me to travel and explore areas outside of my particular project, and I believe it will have a great impact on my professional career. I'd also like to thank the NSF for the support of the Polymer MRSEC and for the CHM for the use of their facilities.

Thanks to all of the Tew group members past and present. Ticora, Khaled, Raja, Sterling, and Lachelle have all helped to establish the research in the group, and I commend them for a job well done! Ticora has particularly been a great mentor for me, and I know that she'll continue to be an inspiration for those she works with. To Raja, my neighbor, I hope that someone will continue to supply gum and candy to your cabinet once you're gone☺ Best of luck in all that you do! To Erin, Ahmad, G, Karen, Jeremy, Zoha, Jeff, Abhi, Morris, Semra, Jing, Casey, Raj, Hitesh, Ozgul, Jun, and Yongping: you're a great group of people and it has been my pleasure to know you all and learn from each of you. I look forward to hearing about your accomplishments in the future.

I'd like to thank all of the friends I've made while here. To the incoming class of 2003, you were a great group, and I hope we keep in touch. I'd especially like to acknowledge Liz, CJ, and Edwin from that class. You've been great scientific resources, but also great friends outside of the classroom. Jess Z., Scott, John, and Jess M. have also been great friends and have listened/critiqued my proposal and prospectus talks, so thank you. To Steve, Liz, and Julie, I'll never forget all the troubles we've had with the GPC's or how we caution taped Steve's door. To Greg Dabkowski thanks for all the work you do for Outreach and ASPIRE, it was my pleasure to take part in these activities with you. And to all of my teammates and friends on the Spare Parts, I'll miss the games, drinking, grilling, and the taunts from "the heckler"!

To my family in Puerto Rico – les quiero mucho y les mando un montón de besos y abrazos, gracias por todo. To all of my Cleveland NASA PR family – you have all been like older siblings to me. Thanks for the support and for being such wonderful and strong examples. To Mami and Papi – you have always encouraged me to set high goals and have given me the confidence to achieve them. I am incredibly fortunate to have such wonderful and caring parents, who I know will always be there for me. Much of my success I owe to you, and I'm very proud to be your daughter, I love you. To my sister, Jessie – I always know that with you and I can revert back to being a fun and carefree kid. Thanks for being my friend, I love you! And finally to my husband Chad – words cannot describe how you've helped me through this whole ordeal of grad school. When I was frustrated and ready to give up, you knew just what to say or do to pick me up. Your confidence in me has never faltered. Even when I didn't believe in myself, you knew that I would pull through. You've also been a collaborator in everything that I do – listening

to my problems in the lab and giving me new ideas and directions to take. I am extremely lucky to have you in my life, thank you, te quiero mucho mi amor!

ABSTRACT

PLA-PEO-PLA TRIBLOCK COPOLYMER HYDROGELS FOR SOFT TISSUE ENGINEERING: PROPERTIES, ASSEMBLY, AND STRUCTURE

SEPTEMBER 2008

NAOMI SANABRIA DELONG, B.S., CASE WESTERN RESERVE UNIVERSITY

M.S., UNIVERSITY OF MASSACHUSETTS AMHERST

Ph.D., UNIVERSITY OF MASSACHUSETTS AMHERST

Directed by: Professor Gregory N. Tew

Biodegradable hydrogels show great promise in the area of biomaterials and specifically for tissue engineering applications. While much work in the past has studied the various biochemical signals associated with cell growth, more recent work has highlighted the importance of the mechanical environment as a stimulus for growth. This dissertation focuses on associative network hydrogels formed for poly(lactide)-b-poly(ethylene oxide)-b-poly(lactide) [PLA-PEO-PLA] triblock copolymers and the factors that influence their mechanical properties, assembly, and structure. By controlling the stereospecificity of the PLA endblocks hydrogels with either amorphous or crystalline hydrophobic domains were formed as characterized using both X-ray and neutron scattering techniques. This change in structure directly impacted the mechanical properties of the hydrogels. Furthermore, complications in synthetic techniques introduced contaminants (asymmetric triblock copolymers or "effective" diblock copolymers) that impacted the assembly of the network to again impact the mechanical properties. Ultimately, the PLA-PEO-PLA triblock copolymer was chemically modified so that the self-assembled physical network served as a template for the covalently

crosslinked network formed by photocrosslinking. The photocrosslinked hydrogels maintained their mechanical integrity in an aqueous environment; however, the measured mechanical properties were dependent on the assumed constitutive relationship.

TABLE OF CONTENTS

LIST OF TABLES

LIST OF FIGURES

Figure Page

CHAPTER 1

SOFT TISSUE ENGINEERING AND HYDROGELS: CURRENT STATUS AND STRATEGIES

1.1. Motivation

There are many people suffering serious health conditions from organ failure or tissue loss due to both disease and injury. The effects of these conditions can range from great physical discomfort to impaired physical function, in some cases ultimately leading to death. To treat these conditions hundreds of billions of dollars are spent per year just in the United States alone, and the treatments are very extensive and time-consuming. Furthermore, a large variety of tissues and organs are affected including the heart, liver, kidney, skin, cartilage, nerves, and bone just to name a small few. Ultimately to repair a tissue or organ, surgeons transplant healthy tissue from a donor to the ailing patient. However, there are a number of complications, risks, and limitations associated with transplants.

The first concern for organ transplantation is rejection. Since the received organ is from another person (allograft), when it is implanted the body's autoimmune system may identify the organ as a foreign material and reject the transplant. To avoid this rejection, patients are treated with immuno-suppressants, and while this helps facilitate the integration, it also lowers the patient's immune system leaving the body much more susceptible to infection. To combat this infection, patients are commonly also treated with antimicrobial drugs.[1] Aside from the risk of rejection and/or infection and the strict immunosuppressive regimen required after transplantation, there is the problem of limited resources. The number of needed organ donations far exceeds the number of

donors available, and as many as 19% of potential candidates have died in the United States while on the waiting list.[2] This shortage coupled with the increasing demand for organ and tissue treatment underscores the rising need for alternatives to current treatments. Xeno-transplantation (transplantation from one species to another) can potentially increase the supply but has the additional risk of transferring animal viruses to the recipient and then to the general population.[3] A more attractive alternative to transplantation lies in the field of tissue engineering.

Tissue engineering is a field that calls on the strengths of both the life sciences and the engineering disciplines to better understand structure-function relationships of tissues, to develop materials to improve tissue function, and ultimately to regenerate healthy tissue.[4-6] The most common approach used in the field of tissue engineering is to cultivate cells within a matrix, followed by implantation into the patient, as demonstrated in Figure 1.1. By using this approach, autologous cells (cells harvested from the patient) can be used to prevent an autoimmune response; although, stem cells are also an attractive cell source as they are undifferentiated and can develop into a wide variety of cell types dependent on certain triggers.[7] The matrix material acts as a scaffold for the cells to produce their own extracellular matrix and finally tissue. Ideally the scaffold acts as just a temporary cellular support and would degrade into bio-resorbable components to leave just healthy intact tissue in place.

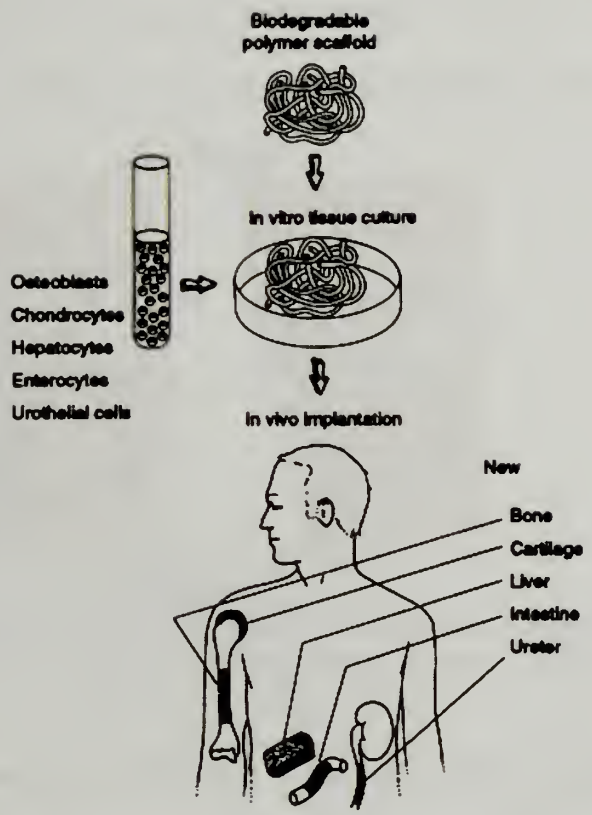

Figure 1.1. Scaffold strategy for tissue engineering using various cell types. (Reproduced from Langer and Vacanti, 1993, Science.)

Tissue engineering not only has potential in the area of organ regeneration, but also has the great potential to address damaged tissues from both disease and injury - of particular interest is the area of orthopedics.[8] A rise in the aging population and sports-related injuries has led to increased occurrences of tissue damage in bone, ligaments, and cartilage. Cartilage deterioration is a particularly pervasive and expensive medical problem leading to 250,000 total knee joint-replacements per year at an average cost of $25,000 in the United States alone (according to the Institute for Cartilage Repair). In addition to this, tens of millions of Americans suffer from osteoarthritis, most commonly in the knee, hands, hip, and spine. In this condition the cartilage between joints that

normally acts as a cushion between bones is degraded causing bones to come in contact, leading to painful inflammation, and limited joint mobility as pictured in Figure 1.2.

Figure 1.2. Healthy knee joint on the left versus an osteoarthritic knee joint on the right. Cartilage is shown in white. (Reproduced from MedLine Plus: Medical Encyclopedia.)

Cartilage is unable to self-repair into healthy articular type cartilage once damaged, and hence presents a very challenging problem. There are current treatments in place to address cartilage deterioration but they all have limitations due to effectiveness and ease of implementation. Most often, patients' joints are treated with pain relieving medications and/or lubricants, but both of these are temporary solutions, which only address the symptoms and not the actual cause of the problem. The most extreme treatment is total joint replacement, which involves an extensive surgery, long recovery, and presents many material challenges in terms of biocompatibility and durability, as metals and ceramics are most commonly used. An alternative to total joint replacement is an orthopedic implant, where the damaged tissue is removed and the implant is placed in the damaged area.[9] The problems here are that the implant must be exactly shaped to the particular patient's damaged area so that it will fit properly, and the implant cannot adapt to the changing stresses within the joint. A more cellular approach implants

chondrocytes (cartilage cells) into the injured area in hopes of regenerating the tissue, however, the success has been rather limited.[10] The final method, autologous chondroctye transplantation (ACT), uses a tissue engineering approach in which healthy chondrocytes are removed from the patient, cultured *in vitro* for several weeks in a collagen scaffold, and reimplanted into the body.[11] Although this method can be effective in some patients, two surgeries are necessary, specialized technicians are required, and the process is costly.

Due to the aforementioned complications with the more common orthopedic treatments (joint replacement and orthopedic implants), tissue engineering is a much more attractive alternative. By utilizing tissue engineering, growth would be spurred to generate natural tissue. In doing this we address the root of the problem, as opposed to temporarily patching the area with foreign materials. Furthermore, although ACT uses a tissue engineering approach, there are many opportunities to improve on the method. More specifically, the scaffold material used in ACT is made of collagen from bovine sources, which can induce an immunological response. A synthetic scaffold is much more attractive because the material properties including degradation, mechanical strength, chemical functionality, and cellular adhesion can be controlled and tuned as desired to achieve the best properties for cellular growth.

1.2. Stimuli for Cellular Growth and Adhesion

1.2.1. Biochemical and Physical Signaling

There are a number of critical factors in tissue development to consider for the successful design of a cellular scaffold. The most obvious and well-studied factor is the

variety of biochemical signals that are sent to cells via growth factors to help stimulate growth and proliferation. Growth factors are natural proteins that help regulate a variety of cellular processes including angiogenesis (new blood vessel formation), bone regeneration, and wound healing. Since these growth factors are known to help stimulate the aforementioned processes, many researchers have worked towards developing strategies to incorporate these molecules into cell scaffolds for tissue engineering.[12-14] In using this strategy, it is hoped that cells can be directed to differentiate and proliferate at the proper location and at the proper time.

Insoluble extracellular matrix molecules are the second critical factor in tissue development and are responsible for physical signaling towards cellular adhesion. Cell adhesion through focal adhesion contacts is vital for cell growth and proliferation on surfaces or three-dimensional scaffolds. Once a part of the cell is adhered, the cell can spread and move by releasing and depositing more of these adhesions.[15-17] The most commonly studied cellular adhesive interaction is through the protein, fibronectin. This protein, along with others, has a short peptide sequence of arginine-glycine-aspartic acid (RGD) that interacts with integrins on the cellular membrane allowing cells to adhere.[18, 19] These two factors, biochemical signaling and adhesion mediated through peptides, along with cell-cell interactions are demonstrated in Figure 1.3 and are often seen as the most essential when considering polymer cellular scaffolds.[15]

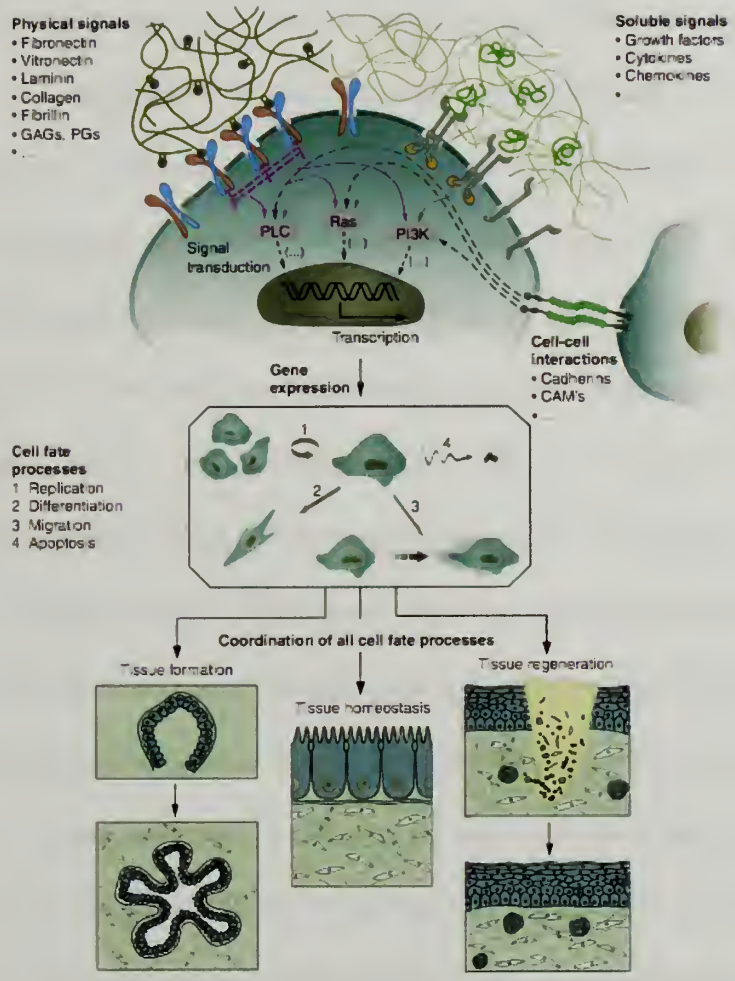

Figure 1.3. The dynamic state of cells mediated by soluble signals, physical signals, and cell-cell interactions. (Reproduced from Lutolf and Hubbell, 2005, Nature Biotechnology.)

1.2.2. Mechanical Signaling

Although chemical and physical signaling play an important role in cell adhesion, differentiation, and growth that ultimately guides tissue regeneration, more recent work explores the influence of mechanical signaling on cells. Extensive work has tried to elucidate the role of mechanics in cell growth and proliferation and has found that cells indeed receive mechanical, as well as, biochemical signals.[16, 20, 21] Cells typically bind to the extracellular matrix through surface receptors (which commonly have an RGD binding domain as described earlier), but to migrate traction forces must be generated.

The underlying substrate must be able to withstand these traction forces so that the cell can grow and spread properly. One report has shown that cells can sense the restraining force of the underlying substrate and can respond by locally strengthening cytoskeleton linkages.[22] This supports the work of many others who suggest that cells can probe the stiffness of the surrounding environment to provide a feedback loop that can help determine the cell morphology, growth, and proliferation. [23-28] Ultimately, cells prefer to grow on substrates with similar modulus to their corresponding tissue.

Further work has also demonstrated that undifferentiated mesenchymal stem cells differentiate into specific cell types based on the substrate elasticity.[29] Softer substrates with elasticity similar to brain tissue yielded neurons, intermediate substrate stiffness similar to muscle yielded myoblasts (muscle forming cells), and stiffer substrates similar to bone yielded osteoids (bone forming cells). Refer to Figure 1.4 to see how substrate stiffness affects the markers for each cell type. These results suggest that stem cell differentiation can be guided based on mechanical stimuli alone and presents an opportunity in the area of tissue engineering. In conclusion, since the healthy survival of cells so greatly depends on the mechanical properties, it is important to design cell scaffolds with similar mechanical properties to the target native tissue so that cells can grow and proliferate properly.

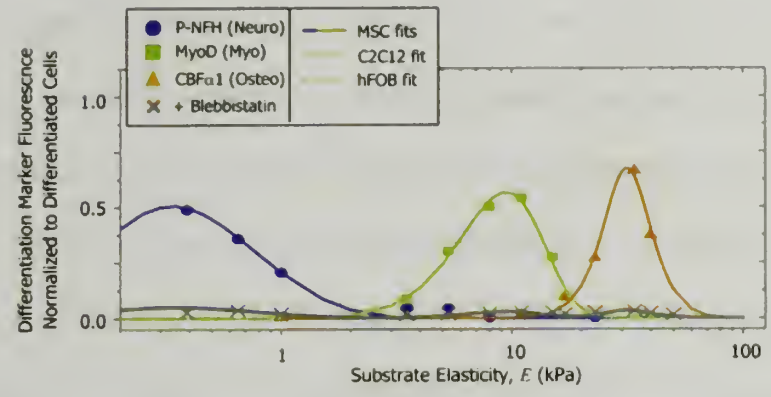

Figure 1.4. Protein profiles associated with certain cell types (neurons, myoblasts, and osteoblasts) generated from stem cells are elastically dependent under identical media conditions. (Reproduced from Engler et al., 2006, Cell.)

1.2.3. Properties of Cartilage

To best design a scaffold for cartilage, it is important to consider its structure and properties. Cartilage is made up of a 3-dimensional array of collagen fibrils, proteoglycan complexes, chondrocytes, glycoproteins, and lipids, and when fully hydrated, contains 60-80% water. The collagen (most commonly type II) forms a fibrillar network that immobilizes the highly negatively charged proteoglycans and leads to repulsion of proteoglycans, high osmotic pressure, and ultimately a framework that has a preloaded stress. Chondrocytes only make up about 1% (by volume) of cartilage but are responsible for replacing degraded matrix and maintaining the tissue. The tissue fluid provides nutrients and oxygen to the avascular (having no blood vessels) cartilage.[10]

The structure described above leads to remarkable characteristics including: high permeability, stiffness in compression, dissipation of stresses through fluid flow,[30] and mechanical properties that are dependent on the rate of loading.[31, 32] At low compressive strain rates, water can be exuded from the charged proteoglycans lubricating the joints while charge repulsion between proteoglycans bears the load. However, at high compressive strains, cartilage acts like an elastic material (refer to Figure 1.5). Reports

have varying numbers, due to different forms of mechanical testing and different types of cartilage, but show that cartilage can have a compressive modulus between 0.7 – 60 MPa.[30-33] Other potential soft tissue targets include: bovine hippocampal brain (G' ~ 0.3 kPa) and retinae (G' ~ .05 kPa) [34], cardiovascular tissue (E ≈ 5 kPa – 1.7 MPa) [33, 35-37], skin (E ≈ 0.1 MPa – 50 MPa) [33, 38], tendon (E ≈ 100's of MPa) [33, 39], canine lung parenchyma (E ~ 5 kPa) [40], and pig kidney (G' ≈ 1-10 kPa) [41]. Thus, based on the correlation between mechanical properties and cell growth and differentiation described above, scaffold modulus should be designed to fall in the range of tenths of a kilopascal to the hundreds of kiloPascals.

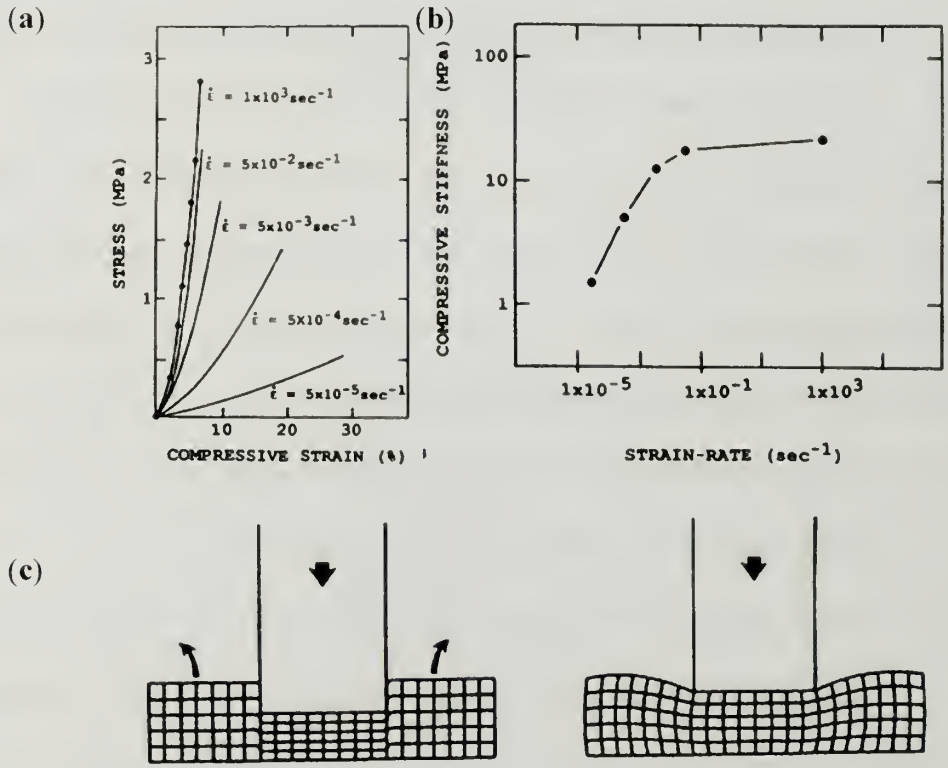

Figure 1.5. Mechanical response of cartilage while under compression. **(a)** Stress versus strain at various strain rates. **(b)** Stiffness as a function of strain rate. **(c)** At low strain rates water is exuded (left), while at high strain rates it behaves elastically. (Reproduced from Oloyede et al., 1992, Connective Tissue Research.)

1.3. Hydrogels as Biomaterials

Hydrogels are polymer network structures containing hydrophilic components allowing absorption of water, sometimes up to thousands of times their original dry weight. The hydrogel's network structure is held together through crosslinks, or junction points, within the system (Figure 1.6). This structure leads to a great number of properties that make hydrogels particularly attractive for use as biomaterials.[42-45] First and foremost, hydrogels are high in water content (typically greater than 70% water by weight). The high water content is ideal for biomedical applications since the body is a primarily aqueous environment. Hydrogels also have a porous structure, allowing for influx or efflux of small molecules, more specifically cell nutrients and waste or therapeutic drugs. Biocompatibility and/or biodegradability can be designed into the hydrogel using certain chemistries in the backbone and at the crosslink sites. Finally, hydrogels can often begin as injectable polymer solutions that form a gel once in the body (gelation is stimulated through temperature or pH).[46] For these reasons, hydrogels are already being used in a variety of biomedical applications including soft contact lenses, formulations for drugs (both as coatings and capsules), wound dressings, delivery membranes, and bioadhesives.

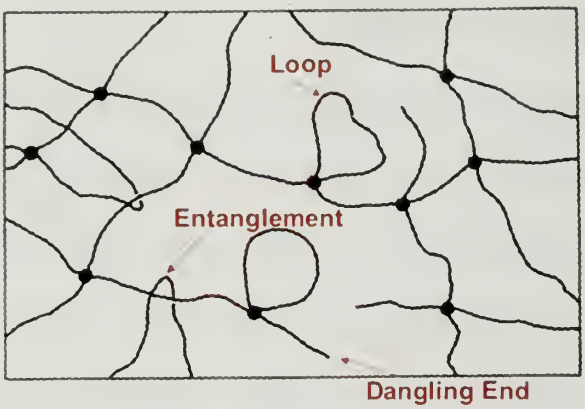

Figure 1.6. Network structure with crosslinks shown as black dots and common defects including entanglements, ineffective loops, and dangling chain ends.

Hydrogels also have great potential in the area of tissue engineering for the same reasons as listed above. Ideally, the hydrogel would act as a temporary tissue substitute, so the material must have the appropriate properties to withstand the forces associated with the site of injury. Moreover, as already discussed in the previous section, mechanical matching between the cell scaffold and the target tissue is an important stimulus towards proper cell growth and differentiation. However, ultimately, the hydrogel should degrade over the proper time scale allowing the cells to grow and leaving behind only healthy tissue as a product. Drugs, including peptides and proteins, may also be incorporated into the hydrogel to couple the effects of mechanical and biochemical stimuli and help facilitate cell growth, attachment, and proliferation.[12] By keeping all of these factors in mind, one should be able to tune the hydrogel properties to the ideal conditions for specific tissue types by changing the chemistry and structure of the polymer used. In the next sections, we will discuss some of the biocompatible polymers (both natural and synthetic) that are commonly employed in biomaterials as well as in hydrogel scaffolds for tissue engineering.

1.3.1. Natural Polymers

Cell scaffolds derived from naturally occurring polymers are particularly attractive because they have many similarities to the cell's natural extracellular matrix (ECM), and they're known to be biocompatible.[47] The most commonly used natural polymer for tissue engineering is collagen,[48, 49] a matrix of fibrous structural protein. Collagen is a protein found in the ECM of many soft tissues including skin, bone, cartilage, tendon, and ligament and is recognized by cells. It is already used for implants replacing the meniscus of the knee[9] and is the base scaffold material used in the ACT process for cartilage regeneration described in section 1.1.[11] However, collagen scaffolds are lacking in strength, there is a risk of an immunogenic response, and they can be expensive.

Fibrin gel is a network of polymerized fibrinogen catalyzed by the enzyme thrombin. In contrast to collagen, fibrinogen can be isolated from the patient's own blood, essentially eliminating the risk of infection or immunogenic responses. Most often fibrin is used as a glue to seal and aid in wound healing. However, a commercial version of fibrin is not available, and it is typically polymerized in house in a clinical setting.[50] The polymerization is dependent on the concentration of thrombin used leading to a large variation in the mechanical properties.[51] Furthermore, the mechanical properties of fibrin alone do not match those of cartilage.[52] Only when combined with other polymers for reinforcement (like collagen) do the mechanical properties begin to approach the proper range for cartilage (~100 kiloPascals).[53]

Polysaccharides are a class of complex carbohydrates, as well as natural polymers, and are commonly utilized for tissue engineering. One example, hyaluronan,

is a glycosaminoglycan common in the ECM of connective tissue (also present in cartilage) and plays a role in wound healing. Most commonly hyaluronan is chemically modified through pendant hydroxyl and carboxyl groups so that is it crosslinkable through radical polymerization. Work has shown that both smooth muscle cells[54] and chondrocytes[55] can be successfully encapsulated within the photocrosslinked gels. The compressive modulus could also be tuned from 1 to 100 kPa by varying the hyaluronan molecular weight and concentration.[56] Chitosan is a cationic polysaccharide derived from the deacylation of chitin (found in the exo-skeleton of marine invertebrates) that forms a porous gel. It is known for its biodegradability and anti-bacterial qualities and is similar in structure to glycosaminoglycans. Chitosan is able to support chondrocyte growth and has potential for a variety of applications in tissue engineering.[57, 58]

Other hydrogels from polysaccharides include alginate and agarose (both derived from algae). Alginate gels are formed through the ionic interactions of negatively charged moieties on the linear polysaccharide with divalent cations (usually Ca^{2+} and Mg^{2+}). The compressive modulus can be tuned from 1 kPa to as high as 500 kPa by controlling the source and concentration of cation and alginate;[59] however, although the scaffolds were able to support chondrocytes, they did not develop into normal hyaline cartilage.[60] Agarose gel is formed by the aggregation of associated double helices and is reversible. The range of attainable modulus can also reach up to 100's of kPa, but the modulus greatly depends on the processing conditions including the type of agarose used, concentration, and whether it was subject to mechanical loading (when seeded with chondrocytes).[61, 62]

1.3.2. Synthetic Polymers

While natural polymer hydrogels are attractive for a number of reasons including their biocompatibility, similarities in chemical structure and functionality to natural ECM, and tunable modulus, there are a number of challenges associated with them. The supply of natural polymers usually comes from either an animal or plant source and thus must be extensively purified. Furthermore, there is not always consistency from batch to batch since the purification process can lead to a wide variety of molecular weights and degrees of functionality within the polymer backbone. This inconsistency will have a direct effect on its performance as a scaffold. Finally, there is the risk of an immune response as well as disease transmission between species when the polymer is supplied from an animal source. Conversely, by utilizing controlled conditions, synthetic polymers have none of these problems but can still potentially achieve similar advantageous characteristics of naturally derived polymers for tissue engineering.

Poly(ethylene oxide) [PEO] is already approved by the Food and Drug Administration (FDA) for a number of biomedical applications. It is well known for its hydrophilicity, biocompatibility, and its ability to decrease protein adsorption making materials less susceptible to immune responses. For these reasons PEO has been incorporated into the following systems: polymer-drug and polymer-protein conjugates to prolong circulation time, polymeric micelles to encapsulate therapeutics, polyplexes with DNA for gene delivery to improve biocompatibility, and as a hydrophilic component in hydrogels.[63] PEO is commercially available but can be synthesized using anionic or cationic polymerization of ethylene oxides, or through polycondensation of ethylene glycol and can have a variety of different polymer architectures.

Synthetic degradable polyesters were first used as sutures several decades ago, and still remain one of the most widely utilized class of polymers for biomaterials. They are typically synthesized via ring-opening polymerization of cyclic monomers, polycondensation of bifunctional monomers, or via biosynthesis using bacteria.[64, 65] Some examples of commonly used polyesters include poly(lactide) [PLA], poly(glycolide) [PGA], poly(caprolactone), [PCL], and poly(hydroxyalkanoate) [PHA]. Degradation of polyesters occurs through hydrolysis of the ester linkages and can be tuned based on molecular weight, crystallinity, and the specific monomer used; unfortunately, the acidic byproducts can often cause an anti-inflammatory response in the body. In general these polymers are hydrophobic and thus are typically co-polymerized with another more hydrophilic component.

Although the above two classes of polymers (PEO and polyesters) are the most prevalent in biomaterials, other potential biodegradable polymers include polyamides, polypeptides, and polyurethanes.[66] Polyamides and polypeptides are similar in structure to proteins since the monomers are connected through amide linkages. Furthermore, polypeptides are made up of amino acids, contributing to their biocompatibility. Normally they exhibit relatively low biodegradation due to strong intermolecular hydrogen bonding, but the degradation can be modified by co-polymerizing with esters or by other chemical and/or processing modifications. Polyurethanes can undergo oxidative degradation as well as enzymatic hydrolysis in polyester-based poly(urethane-urea) systems. Varying the size of the hard versus soft micro-domains can also influence the degradation rate. While the aforementioned polymers are not an all inclusive list in the

area of biomaterials, they are the most common, and some of their structures are shown in Table 1.1.

Table 1.1. Structure of synthetic polymers used in biomaterials.

Synthetic Polymer	*Structure*
Poly(ethylene oxide) [PEO]	
Poly(lactide) [PLA]	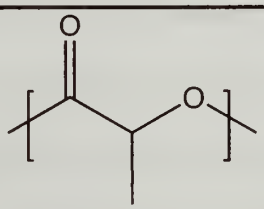
Poly(glycolide) [PGA]	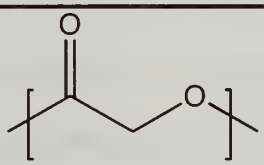
Poly(caprolactone) [PCL]	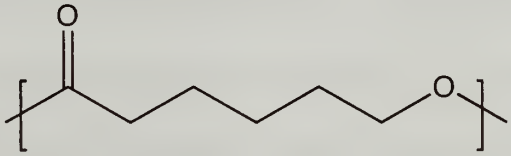
Polyhydroxyalkanoate [PHA]	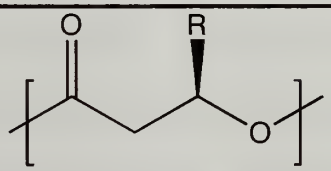
Polypeptide	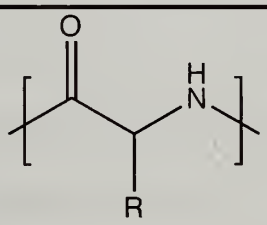
Polyurethane [PU]	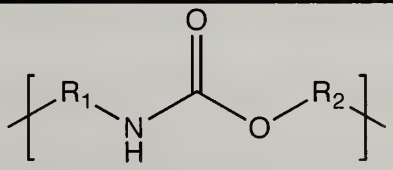

1.4. Strategies for Hydrogels

1.4.1. Chemically Crosslinked Hydrogels

Chemically crosslinked hydrogels have hydrophilic components and junction points that are held together through covalent bonds. The covalent bonds lead to stable hydrogels that absorb an equilibrium amount of water. The stability allows for easy handling and characterization. Furthermore, by varying the molecular weight between crosslinks and the crosslink density, the degree of swelling and the mechanical properties of the hydrogel can be tuned as desired. However, the ultimate goal in tissue engineering is to use the hydrogel as a temporary implant that gradually degrades, and the degradation of these gels can be more complicated because the crosslinks are covalent.

Chemically crosslinked hydrogels are most commonly formed through free radical reactions. One approach is to co-polymerize a vinyl monomer with a divinyl monomer. As already mentioned the hydrogel properties depend on the molecular weight and crosslinker, but the hydrogel can also become stimuli sensitive by copolymerizing with certain monomers. N-isopropyl acrylamide has a lower critical solution temperature in water and thus hydrogels with this monomer are temperature sensitive,[67] while hydrogels with methacrylic acid are pH sensitive.[68, 69] Another approach is to end-functionalize water-soluble polymers, such as PEO and poly(vinyl alcohol), with acrylates followed by free-radical crosslinking using a photoinitiator and ultra-violet (UV) light.[70, 71] This second method can be particularly useful because one starts with an aqueous pre-polymer solution that can also include cells and will not crosslink until triggered by UV light. The water-soluble polymers can also be modified with polyesters to yield a hydrogel that is biodegradable (refer to Figure 1.7),[72, 73] and adhesive peptides

can be added to aid in cellular adhesion. Condensation reactions are more generally used for polyurethane hydrogels (using isocyanates and amines or alcohols) but can also utilize Michael additions, formation of amides, and formation of esters.[44, 68, 74]

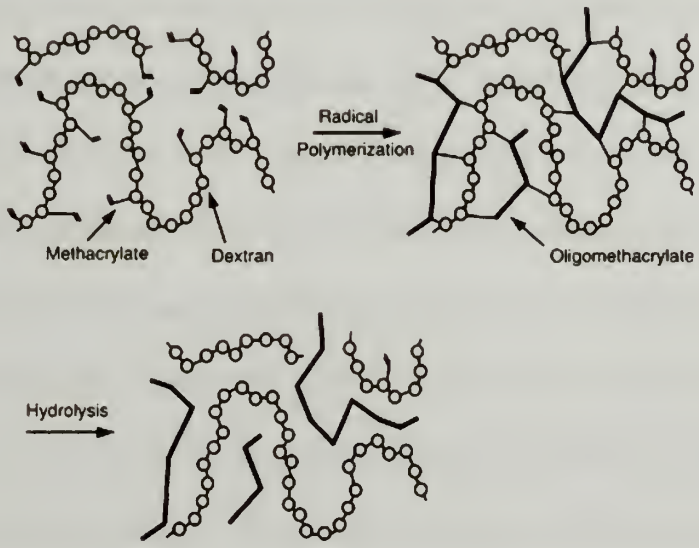

Figure 1.7. Network formation and degradation of a radically polymerized water-soluble polymer. (Reproduced from Hennink, 2002, Adv Drug Del Rev.)

1.4.2. Physically Crosslinked Hydrogels

The crosslink sites in physical hydrogels are held together through a variety of non-covalent interactions including: ionic interactions, hydrogen bonding, crystallization, molecular entanglements, and hydrophobic interactions. The advantage with these hydrogels is no crosslinker needs to be added, which minimizes the chance of cytotoxicity in cells. Also the crosslinks are often reversible or not permanent, potentially easing the degradation, but the weaker interactions at the junction point could cause the system to dissolve or precipitate in excess water. Most importantly, physical hydrogels self-assemble into network structures. In the following sections, examples of hydrogels using non-covalent interactions will be further explored. Note that an example

of a hydrogel formed through ionic interactions (between charged carboxylates and divalent cations) was already discussed previously (Section 1.3.1) using alginate.[75, 76]

Polypeptides and proteins self-assemble into secondary and tertiary structures to form network structures through a variety of interactions including hydrogen bonding and charge attraction/repulsion.[77, 78] In one example the peptide begins in the random coil configuration at ambient conditions, but once salt is added the configuration converts to a β-hairpin due to intramolecular electrostatic and hydrophobic interactions. The β-hairpins can then further associate via intermolecular hydrogen bonding and hydrophobic interactions into a fibrillar network with a shear modulus as high as 2 kPa.[79] UV light can also act as a trigger for peptide folding and self-assembly. By photocaging the peptide it was unable to assume the β-hairpin conformation, and hydrogels were only formed once the peptide was released from the cage by activating with UV light.[80] Fibrillar networks are also formed using oligomers or block co-polymers containing peptide segments with α-helical secondary structures.[81] Unfortunately, the design and synthesis of folding peptides for use in hydrogels can be both time consuming and expensive, respectively, and the hydrogels are softer than certain target tissues, including cartilage.

Crystalline domains within a swollen hydrogel can also act as crosslink points. Two examples of these types of hydrogels include poly(vinyl alcohol) [PVA] and liquid crystalline gels. In the case of PVA, gelation starts first with hydrogen bonding following by crystallization. By repeated freeze-thaw cycles the degree of crystallinity is increased and directly correlates to an increase in the shear modulus.[82-85] For example, a gel of 14.6 wt% PVA initially had a storage modulus of 7 and increased to 20 kPa after 7

freeze/thaw cycles. Similarly, networks with liquid crystalline domains have significant crosslinking from the association of crystalline microdomains;[86-90] however, these gels have relatively low water content (15.3 wt% and less water). Finally, there are associative network hydrogels formed through hydrophobic interactions, but these will be further discussed in the next section.

1.5. Associative Network Physical Hydrogels from Amphiphilic Block Copolymers

Physical hydrogels can also be formed using amphiphilic AB diblock copolymers or ABA and BAB triblock copolymers, in which the A block is hydrophobic, while the B block is hydrophilic. The hydrophobic blocks associate into ordered aggregates, typically micelles, due to the hydrophobic effect. The micelles have a hydrophobic core that is surrounded by a hydrophilic corona, and when the concentration is increased, the micelles begin to pack. The association of these micelles, either due to packing or due to bridging between micelles, act as reversible physical crosslinks (Figure 1.8). The great advantage with these systems is that they assemble on their own.

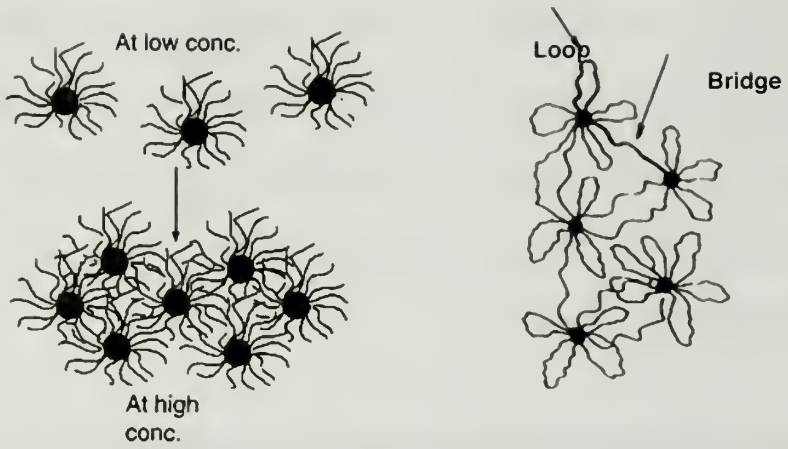

Figure 1.8. Schematic of associative network formed from diblock copolymer on the left and triblock copolymer on the right. (Reproduced from Tae et al, 2001, Macromol and Semenov et al, 1995, Macromol, respectively.)

There are many amphiphilic block copolymers currently being studied, but thus far, few physical hydrogels have approached the necessary mechanical properties of some of the previously described soft tissues. Fluoroalkyl end-capped PEOs form gel-like materials, but rheological studies show mechanical behavior more closely resembling a Maxwell fluid.[91-93] Similar behavior is seen for alkyl end-capped PEOs, in which the shear storage modulus (G', elastic component) surpasses the shear loss modulus (G'', viscous component) only at mid to high frequency ranges.[94] Systems using poly(butylene oxide)-poly(ethylene oxide)-poly(butylene oxide) [PBO-PEO-PBO] also show Maxwell fluid-like behavior at low temperatures (10 °C), but then display typical gel-like behavior (G' > G'') at 20°C and higher over the entire frequency range with a plateau modulus of approximately 20 kPa.[95] PBO-PEO diblock copolymers with liquid crystalline phases can have a shear modulus as high as 200 kPa.[96, 97] However, PBO may have problems with biocompatibility. Poly(ethylene oxide)-poly(propylene oxide)-poly(ethylene oxide) [PEO-PPO-PEO] triblock copolymers (also known by the commercial names of Pluronics

or Poloxamers) also go through a sol to gel transition with increasing temperature. The gelation temperature is inversely proportional to the concentration, the measured G' is as high as 15 kPa, and both can be tuned by varying the ratio of PEO:PPO and the molecular weight.[98-100]

For this thesis project we chose to study associative network physical hydrogels formed from poly(lactide) – b – poly(ethylene oxide) – b – poly(lactide) [PLA-PEO-PLA] triblock copolymers. This polymer is particularly attractive because its components are already FDA approved due to the biocompatibility of the PEO block and the biodegradable ester linkages of the PLA blocks. Furthermore, the polymer can self-assemble in water to form a hydrogel structure with high water content, the chemistry can be well controlled, and it can act as a carrier for therapeutics.[45, 101, 102] Past work done with these types of polymers (both linear AB diblock and ABA triblock copolymers, where the A block is a polyester) showed that hydrogels were formed and the sol-gel transition point was tuned using temperature, concentration, differences in molecular weight, ratio of block A to block B, and by the type of polyester used in the A block.[103-111] An example of a phase diagram when changing the ratio of hydrophobic to hydrophilic block (poly(lactic acid – co – glycolic acid) [PLGA] random copolymer and PEO, respectively) is shown in Figure 1.9. In this case, at low temperatures the triblock copolymer had minimal aggregation and was able to diffuse between micelles. As the temperature increased, the aggregation increased leading to bridging between micelles and a sol to gel transition. When the temperature was further increased, the hydrophobic micelle cores shrank and the PEO block was dehydrated, leading to precipitation and a gel to sol transition.[103]

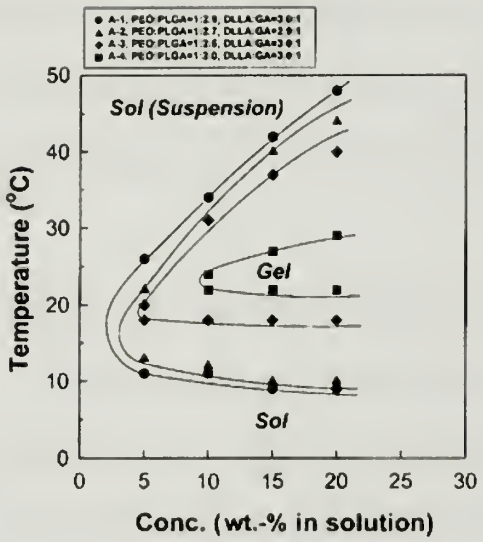

Figure 1.9. Phase diagram of PLGA-PEO-PLGA with varying ratio of PEO:PLGA. (Reproduced from Lee et al, 2001, Macromol. Rapid Commun.)

Many groups have also used stereocomplexation and different architectures to form gels using PLA and PEO based block copolymers. The monomeric unit of PLA has a chiral carbon center, so semi-crystalline poly(L-lactide) [PLLA], poly(D-lactide) [PDLA], or amorphous PLA can be synthesized by using the proper monomer (in the case of amorphous PLA, a racemic mixture of L- and D-lactide is used). Since, PLLA and PDLA are enantiomeric, they form a stereocomplex with a higher crystalline melting temperature and a different crystalline structure than the single enantiomer polymer alone.[112, 113] When block copolymers containing PLLA and PDLA are mixed in the presence of water a hydrogel with stereocomplexed micellar cores is formed.[114, 115] The triblock copolymer architecture can also be changed to a BAB system where the outer blocks are hydrophilic PEO or to a star polymer. In this case no bridging between micelles occurs to form crosslinks; instead, the gelation is similar to that of AB diblock copolymers where micelles associate due to crowding and entanglements. The sol to gel transition is also tunable, and the hydrogel can be injectable.[116, 117]

Unfortunately, the mechanical properties of the biocompatible amphiphilic block copolymer hydrogels were often not well characterized,[103, 105, 115, 117, 118] and as described in Section 1.2.2, this is an important parameter for success as a tissue engineering scaffold. Furthermore, those that have been characterized using rheology had a storage modulus typically less than 1 kPa, [104, 114] which is several orders of magnitude lower than the modulus of cartilage. While novel chemistries may be able to broaden the range of attainable modulus to be more similar to biological soft tissues, cytocompatibility tests and the long process for FDA approval will slow their progress. Instead, we proposed to study how the mechanical properties of PLA-PEO-PLA triblock copolymer hydrogels could be tuned, as there are several biomaterials with these components already in clinical use. We began first by comparing PLA-PEO-PLA triblock copolymer hydrogels with very small changes in the chemical structure, more specifically, stereochemistry and hydrophobic block length. From there, we explored differences in stiffness when the synthetic technique was changed and when the triblock copolymer was mixed with various homopolymers. Finally, we combined two gelation techniques (self-assembly through hydrophobic interactions and photocrosslinking) to synthesize a novel hydrogel with enhanced mechanical properties.

CHAPTER 2

SYNTHETIC CHALLENGES FOR PLA-PEO-PLA TRIBLOCK COPOLYMERS

2.1. Introduction

Polylactides are polymerized with a variety of polymerization techniques including condensation, coordination-insertion, and anionic polymerizations.[45, 64, 119] Most often, controlled polymerizations are achieved by using an organo-metallic catalyst that coordinates with the active chain-end to drive the opening of a cyclic monomer.[119-121] For our synthesis, we have used the organo-tin catalyst, tin (II) 2-ethyl hexanoate, and we began by using an established procedure involving bulk-polymerization in the melt.[122] While this polymerization initially was well-controlled and had low molecular weight distributions, with time the distributions began to broaden. Due to this complication, we explored how we could narrow the distribution by using fractioning techniques and by changing the synthetic conditions. Better control was achieved by modifying the synthesis to a solution polymerization; however, with time the solution synthesis also began to show broadened polydispersity. In this chapter, we conclude that contamination with water, which can initiate poly(lactide) homopolymer, leads to the broadened molecular weight distribution. The best results were achieved by adding molecular sieves to the reaction and by washing the product with ethyl acetate. Molecular sieves removed the majority of the water contaminant, and washing with ethyl acetate solublized and removed any poly(lactide) homopolymer to yield polymers with lower polydispersity. Furthermore, we established a method for determining sample purity using a thermal technique coupled with ^{1}H Nuclear Magnetic Resonance (NMR) spectroscopy. The modified synthetic conditions using molecular sieves in a solution-

polymerization coupled with this new method led to triblock copolymers with controlled degrees of polymerization and low polydispersity.

2.2. Synthetic Challenges for PLA-PEO-PLA in the Bulk

2.2.1. Synthetic Methodology for Bulk Polymerization

(3*S*)-*cis*-3,6-Dimethyl-1,4-dioxane-2,5-dione (L-lactide) and 3,6-Dimethyl-1,4-dioxane-2,5-dione (DL-lactide, a mixture of D-lactide and L-lactide) (Sigma Aldrich) were recrystallized from ethyl acetate and sublimated prior to use. Tin (II) 2-ethylhexanoate catalyst (Alfa Aesar) and PEO (M_p = 8 kDa, Sigma Aldrich, previous MALDI-ToF analysis showed the actual molecular weight to be 8.9 kDa) were used without further purification.

To prepare PLA-PEO-PLA triblock copolymers, telechelic PEO macroinitiator (1 equiv, 12.0g, 1.36 mmol) was weighed into a dried round-bottom flask. The flask was heated in a 150°C oil bath while stirring and purging with nitrogen until no bubbles were visible. This step was meant to remove any water in the PEO. Tin (II) 2-ethylhexanoate (0.5 equiv, 221 μL, 0.68 mmol) was added to the mixture, followed by the immediate addition of lactide (45 equiv, 8.84g, 61.4 mmol). The amount of lactide monomer added to the solution was half of the desired degree of polymerization (since lactide is a cyclic dimer and for every one equivalent of lactide two equivalents of lactic acid are added) plus 10 equivalents to account for incomplete polymerization. For example if the total desired degree of polymerization (DP) was 70, then 45 equivalents of lactide monomer was added. The reaction was capped with a rubber septum and reacted at 150°C for 24 hours. The high temperature caused the lactide to sublime and crystallize on the top of

the flask where it was cooler. Every so often, the lactide monomer was re-melted by heating with a torch. After reaction, the mixture was quenched with methanol, and the product was a creamy-brown solid. The product was dissolved in tetrahydrofuran (THF) and precipitated using hexanes. Dissolution and precipitation was repeated 3 more times. The recovered powder was mostly white with a slight brown tinge and was dried under vacuum at room temperature. The reaction scheme is shown in Figure 2.1a. The synthesized triblock copolymer degree of polymerization (DP) was characterized using ^{1}H Nuclear Magnetic Resonance (NMR) spectroscopy. Figure 2.1b shows a typical ^{1}H NMR spectrum of PLLA-PEO-PLLA triblock copolymer synthesized with L-lactide: methyne proton of PLLA δ 5.12 - 5.19 (q), methylene protons of PEO δ 3.64 (s), methyl protons of PLLA δ 1.48 - 1.59 (d). The total DP of PLLA was calculated by using PEO as a standard, since the molecular weight was already known by using Matrix Assisted Laser Desorption/Ionization - Time of flight (MALDI-Tof). The integration of the methyne proton of PLLA was compared to the integration of the methylene protons of the PEO midblock to give the total degree of polymerization for PLLA.

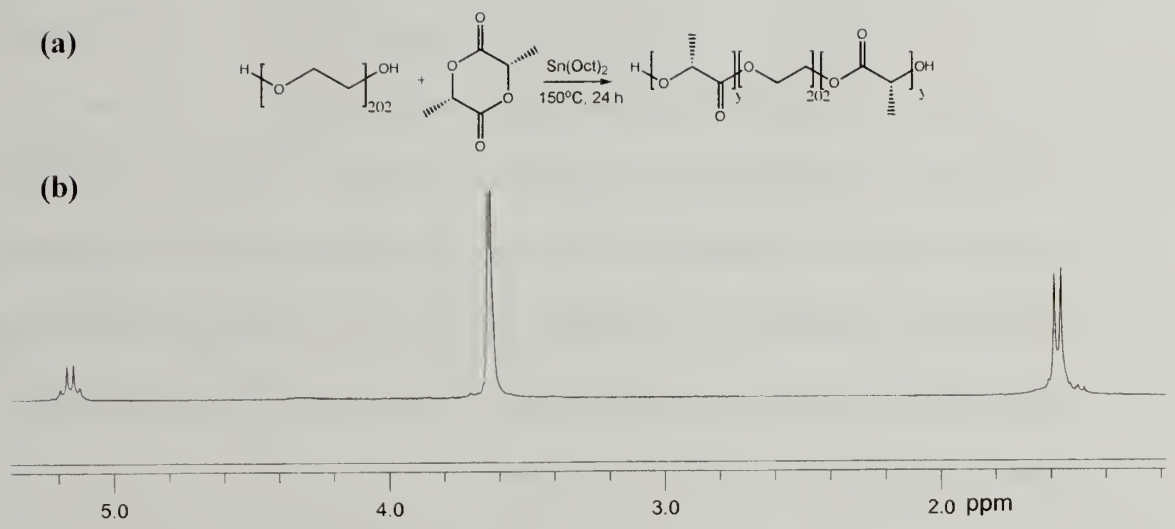

Figure 2.1. PLLA-PEO-PLLA synthesis. (**a**) PLLA-PEO-PLLA reaction scheme. (**b**) ^{1}H NMR spectrum of PLLA-PEO-PLLA triblock copolymer.

2.2.2. Characterizing Control of Bulk-Synthesized PLA-PEO-PLA

The DP and molecular weight of PLA-PEO-PLA triblock copolymers were characterized as already described in the previous section. The molecular weight distribution was determined by Gel Permeation Chromatography (GPC). The GPC system had two PLGel Mixed D columns, a 5 μm guard column, and a refractive index detector. The eluent was N,N-dimethyl formamide with 0.01 M LiCl at 1 mL/min flow, and the GPC was calibrated with narrow poly(styrene) standards. By synthesizing PLA-PEO-PLA in the bulk, we could target the desired DP of PLA with good accuracy indicating the reaction was controlled (Figure 2.2a). Furthermore, the polydispersity indices, as characterized by GPC, were typically less than or equal to 1.2. However, the PDI occasionally was higher and almost always showed a small amount of tailing on the lower molecular weight side of the peak (Figure 2.2b). After using this polymerization method for about a year and a half, the molecular weight distribution began to increase substantially. The low molecular weight tailing became much more prominent, and there

often appeared to be multi-modal distributions (Sample GPC's are shown in Figure 2.3). The increase in polydispersity indicated a side reaction; most likely there was a contaminant or impurity in the reaction to yield a mixture of polymers with varying molecular weights. Unfortunately, the source of contaminant was unclear initially, since all purification, preparation, and synthesis was consistent. Since polymers with bimodal distributions or tailing were not ideal, we decided not to use them, and we explored routes for purifying the synthesized polymer.

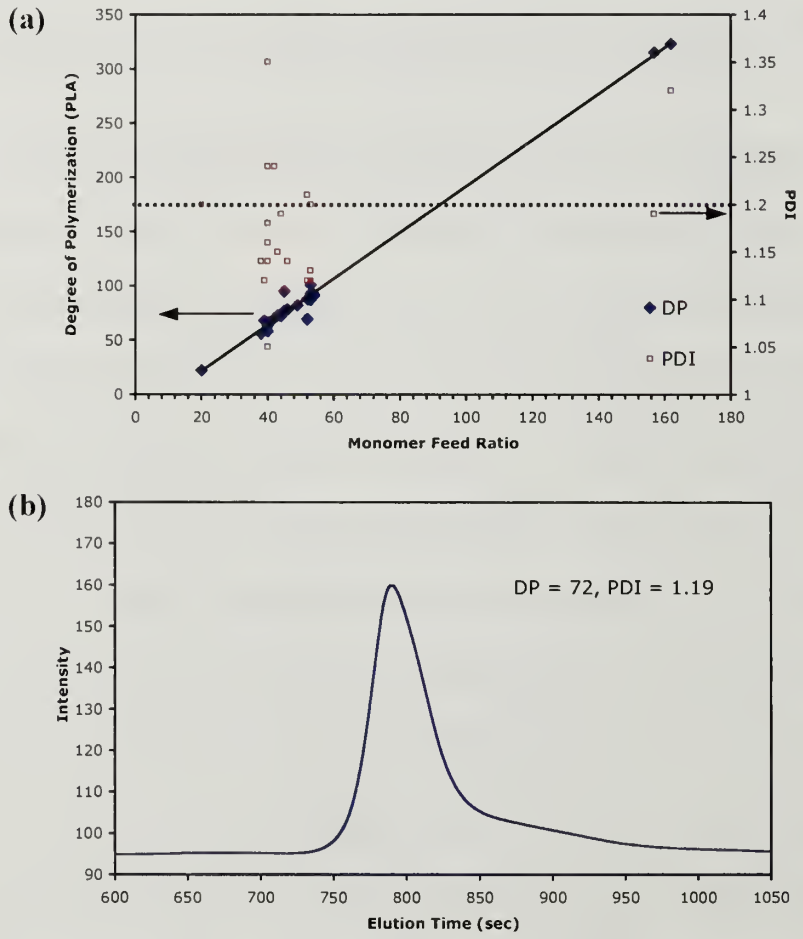

Figure 2.2. Characterization of bulk-synthesized PLA-PEO-PLA. (**a**) DP and PDI versus monomer feed ratio. (**b**) GPC of bulk-synthesized PLA-PEO-PLA, $DP_{PLA} = 72$ by ^{1}H NMR and PDI = 1.19.

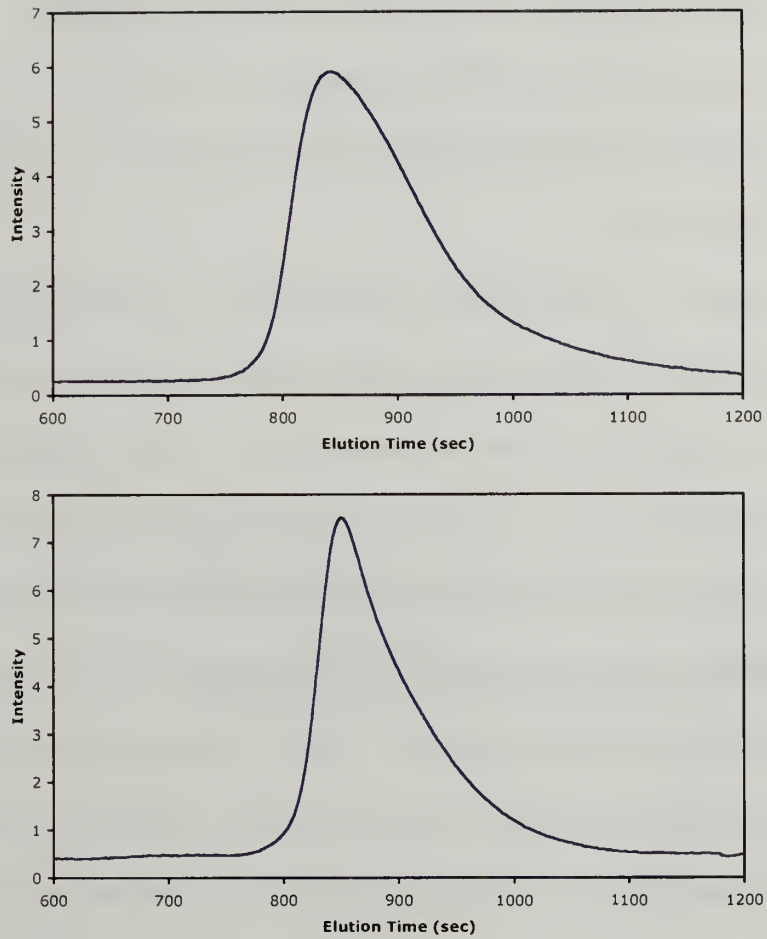

Figure 2.3. GPC chromatograms of bulk-synthesized PLA-PEO-PLA with broadened PDI.

2.2.3. Fractioning Bulk-Synthesized PLA-PEO-PLA

Since the polymers with higher polydispersity seemed to broaden more in the lower molecular weight range, we tried fractioning to separate the higher molecular weight polymer from the lower molecular weight polymer. During the process of fractioning the polymer is dissolved in a fair solvent, then by slowly adding a bad solvent, the higher molecular weight polymer precipitates first. Polymer fractions with different molecular weights can be collected by repeating this process. More specifically, PLA-PEO-PLA (1.00 g) was dissolved in approximately 100 mL of THF while stirring overnight. After allowing sufficient time for full equilibration, a mixture of hexanes (a

non-solvent) was added drop-wise until the solution became turbid. The precipitate was filtered off, redissolved in THF, and precipitated in hexanes to give the first fraction. Subsequent fractions were collected in the same manner using the leftover filtrate from the previous fraction.

Figure 2.4 shows the GPC chromatograms of the starting triblock copolymer with a large molecular weight distribution (PDI = 1.66) and the subsequent fractions. Looking at the chromatograms, we saw we were successful in separating fractions of polymers with different molecular weights. Even more promising, the first fraction appeared to have the same elution time as the starting polymer but without any lower molecular weight tailing, and each subsequent fraction was lower in molecular weight. It therefore appeared that fractionation was a good method to purify triblock copolymers with broad molecular weight distributions. We further analyzed the fractions with ^{1}H NMR to determine the total degree of polymerization of PLA and the corresponding molecular weight.

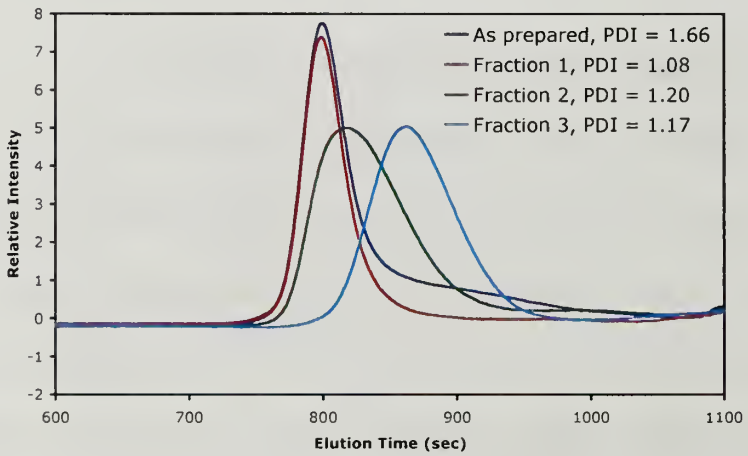

Figure 2.4. GPC of PLA-PEO-PLA before and after fractionation.

The DP and molecular weight were calculated by comparing the PLA protons to the PEO protons (assuming that the PEO molecular weight was 8.9 kDa) as described in Section 2.2.1, and the results are listed in Table 2.1. Based on these calculations, Fractions 2 and 3 had higher molecular weights than both Fraction 1 and the original starting polymer, but the GPC clearly showed they had lower molecular weights (higher elution times). Furthermore, the calculated molecular weights for Fractions 2 and 3 are the same, but again, the GPC clearly showed Fraction 2 had higher molecular weight than Fraction 3 based on elution times. The discrepancy suggested the calculation for molecular weight based on ^{1}H NMR was inaccurate. We believe the inaccuracy was brought about by the assumption of the PEO molecular weight. We knew the molecular weight of the PEO macroinitiator when polymerizing triblock copolymer; however, the data suggested that the purification process actually fractionated PEO as well. Since THF is a poor solvent for PEO and hexane is a bad solvent, polymer with higher PEO may also precipitate first, followed by polymers with lower molecular weight PEO. Therefore, for later fractions the assumption that the PEO molecular weight was 8.9 kDa was no longer accurate. Instead, for Fractions 2 and 3, the PEO block must be very short. The incorrect assumption led to an overestimation of the PLA block length and, correspondingly, to an overestimation in the total molecular weight. This problem arises because there are two blocks with different chemistries and solubilities that affect the fractionation process. Therefore, while fractioning is a useful tool for purifying polymers with broad polydispersities, calculation of molecular weight and composition in triblock copolymers becomes non-trivial and should be used with caution. It is also possible to calculate the degree of polymerization for PLA using the integration of the methylene protons closest

to the ester unit if the NMR solvent were changed to dimethyl sulfoxide. We discovered this after moving away from this technique, so we did not pursue it; however, it should be straight-forward in principle.

Table 2.1. Molecular weights of PLA-PEO-PLA before and after fractionation.

Sample	PDI	DP_{PLA}	M_n
As prepared PLA-PEO-PLA	1.66	65	13.6 kDa
Fraction 1	1.08	52	12.6 kDa
Fraction 2	1.20	166	20.9 kDa
Fraction 3	1.17	167	20.9 kDa

2.3. Synthetic Challenges for PLA-PEO-PLA in Solution

2.3.1. Synthetic Methodology for Solution Polymerization

Monomer was purified as before (Section 2.2.1). Activated molecular sieves were added to tin (II) 2-ethylhexanoate catalyst (Alfa Aesar). PEO (M_p = 8 kDa, Sigma Aldrich, MALDI-ToF analysis showed the actual molecular weight to be 8.8 kDa) was used without further purification.

Telechelic PEO macroinitiator (2.50 g, 0.284 mmol, 1 equiv) was weighed into a dry 3-neck round bottom flask with a stir bar and attached to a condenser. The PEO was stirred and heated at 130°C under nitrogen flow to expel any water. Tin (II) 2-ethylhexanoate (46 μL, 0.142 mmol, 0.5 equiv) was added to the PEO, followed by immediate addition of lactide (1.43 g, 9.94 mmol, 35 equiv). The amount of lactide monomer added to the solution was half of the desired degree of polymerization (since lactide is a cyclic dimer and for every one equivalent of lactide two equivalents of lactic acid are added), and the reaction went to completion. For example if the total desired degree of polymerization (DP) was 70, then 35 equivalents of lactide monomer was added. The condenser was turned on and toluene was added to the reaction mixture

(approximate [PEO] = 28 mM). The mixture was refluxed for 24 hours under nitrogen flow, quenched with methanol, diluted with THF, and precipitated using hexanes. The recovered white powder was separated with a filter funnel, collected, and dried under vacuum at room temperature.

2.3.2. Characterizing Control of Solution-Synthesized PLA-PEO-PLA

When synthesizing PLA-PEO-PLA with a solution polymerization we could target the desired DP of PLA with good accuracy indicating the reaction was controlled. Also, in contrast to the bulk-synthesis, the monomer feed ratio directly correlated to the degree of polymerization. More specifically, for every one dimer monomer of lactide added, two lactic acid units were added to the chain indicating the reaction went to completion and there was no depolymerization (Figure 2.5a). Additionally, the measured polydispersities for the solution-synthesized polymers were less than the bulk-synthesized polymers (typically PDI $\leq$ 1.1), and the GPC's showed no evidence of tailing (Figure 2.5b).

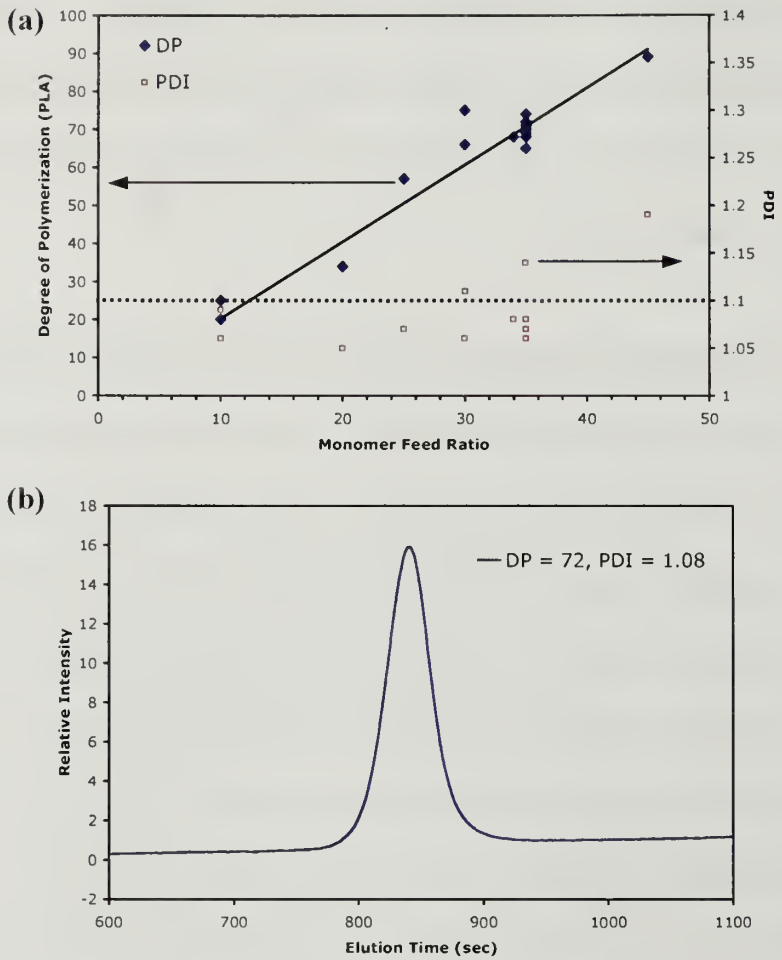

Figure 2.5. Characterization of solution-synthesized PLA-PEO-PLA. (**a**) DP and PDI versus monomer feed ratio. (**b**) GPC of solution-synthesized PLA-PEO-PLA, DP_{PLA} = 72 by ^{1}H NMR and PDI = 1.08.

The solution polymerization had narrow polydispersity and good control and yielded many batches of triblock copolymer (several hundreds of grams of PLA-PEO-PLA were synthesized); however, as with the bulk polymerization, with time the polymerizations started to show broadened molecular weight distributions. Most commonly the distributions showed lower molecular weight tailing, but sometimes the distributions were bimodal. These looked similar to the previous GPC's from the bulk method. As before, we believed there was a contaminant leading to a side reaction. More specifically, we believed water was present and initiated PLA homopolymerization.

A number of modifications to the synthesis were tried to eliminate water including: using new catalyst, using anhydrous toluene as the solvent, re-purifying the lactide monomer, drying the monomer and PEO initiator under vacuum prior to use, and azeotropic distillation of both lactide and PEO prior to polymerization. Unfortunately none of these methods worked to give unimodal and symmetrical molecular weight distributions, and we looked to alternative approaches for purifying PLA-PEO-PLA triblock copolymer.

2.3.3. Purifying Solution-Synthesized PLA-PEO-PLA and Characterization

Water was the likely contaminant leading to broadened PDI, since water can initiate lactide to yield small molecular weight PLA homopolymer and oligomer. Since we wished to separate the suspected PLA oligomer contaminant from PLA-PEO-PLA triblock copolymer, we probed the solubility of each polymer in a variety of solvents including: acetone, THF, hexanes, ether, ethyl acetate, and toluene. Both polymers were soluble in acetone and THF and insoluble in hexanes and ether. However, PLA homopolymer was soluble in ethyl acetate, while triblock copolymer was not, and had limited solubility in toluene, while triblock copolymer was optically transparent. We took advantage of the differences in solubility to separate homopolymer from triblock copolymer.

Solution synthesized PLA-PEO-PLA triblock copolymer was dissolved in THF then precipitated in hexanes. The precipitate was filtered, and while filtering, was washed several times with ethyl acetate. The triblock copolymer should stay insoluble and not be passed through the filter, while PLA homopolymer should dissolve and pass through the filter. The solvent in the filtrate was evaporated, and the remaining product was dissolved in THF and precipitated in hexanes. Each of these samples was compared

to the as-prepared triblock copolymer to evaluate how effectively it was purified. Figure 2.6 shows the GPC chromatogram (THF GPC vs. PS standards) for the starting triblock copolymer (Figure 2.6a) with a broad (bimodal) distribution, as well as the samples obtained from the ethyl acetate wash. As shown in Figure 2.6b, the PDI was significantly reduced by washing with ethyl acetate; however, it appeared as though some amount of triblock was soluble in ethyl acetate as evidenced by the bimodal peak. Nevertheless, this strongly suggested that PLA homopolymer was present in the samples with broad distributions and could be effectively eliminated by this protocol.

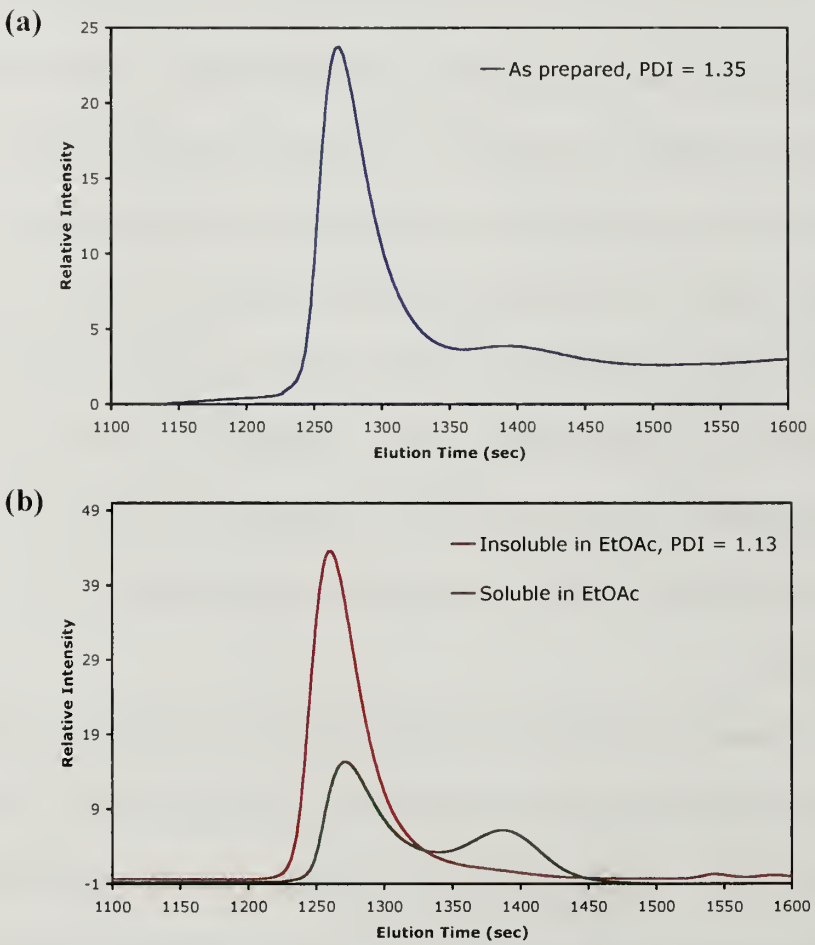

Figure 2.6. GPC's of PLA-PEO-PLA. **(a)** As-prepared solution-synthesized PLA-PEO-PLA. **(b)** After ethyl acetate wash.

In the previous section we learned that determining the DP and molecular weight through ^{1}H NMR could be unreliable after purification of triblock copolymer since each of the blocks have different solubilities that will affect the resulting composition. However, we previously determined that Thermogravimetric Analysis (TGA) accurately tracked the degree of polymerization of each block (by weight) from pure, narrow PDI samples.[123] Therefore, we speculated that TGA could be used as another technique to confirm the calculated molecular weight compositions. The samples were heated from room temperature to 600°C at a rate of 10°C/min under nitrogen flow using a TGA TA Instruments Thermogravimetric Analyzer 2950. When heated, there was a transition starting at approximately 175°C, and the polymer continued to lose weight until about 260°C where the weight loss leveled off. This first transition was due to degradation of the PLA endblocks. As the temperature was increased, there was a second transition (300°C - 400°C) due to degradation of the PEO midblock (Figure 2.7).

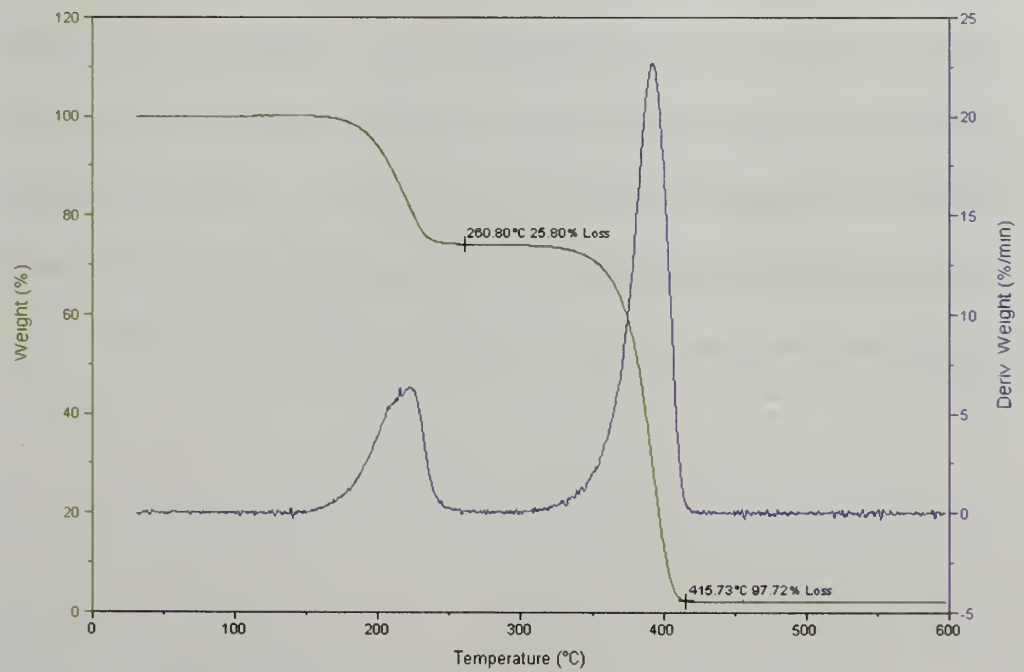

Figure 2.7. TGA of PLA-PEO-PLA triblock copolymer.

We determined the weight percentage of each component (PLA and PEO) by tracking the weight loss at the two transition temperatures. Table 2.2 lists the weight percent of each component (PLA and PEO) as determined by ^{1}H NMR and TGA analysis for triblock copolymers both before and after purification with an ethyl acetate wash. Interestingly, the weight percent compositions determined from NMR and TGA disagree for polymers with high PDI. The discrepancy arose because when using the NMR calculation, we assumed that 8.8k PEO was attached to the PLA. However, since we know that there was a large amount of PLA homopolymer that was not covalently bound to the PEO, the NMR integration underestimated the weight percentage of PLA. After purification, the two methods were in agreement, since all of the PLA homopolymer was washed away and the only product left was PLA-PEO-PLA triblock copolymer. Therefore, TGA coupled with NMR can serve as a test for purity since TGA allows direct comparison of weight percentages within the triblock copolymers. Finally, although washing with ethyl acetate was an effective way to clean polymers with broad polydispersity, it made targeting specific molecular weights difficult since some lactide monomer was consumed to make PLA homopolymer. However, as displayed in Figure 2.8, preliminary data showed that one could account for the extra monomer needed since the feed ratio and degree of polymerization were still linearly related.

Table 2.2. Weight % composition from NMR and TGA.

Sample	Wt% PLA, NMR	Wt% PLA, TGA	PDI
As-prepared, DP = 77	38.7	42.6	1.35
Washed, DP = 44	26.6	26.4	1.13
Washed, DP = 52	30.7	30.5	1.15
As-prepared, DP = 101	45.3	48.7	1.38
Washed, DP = 79	40.2	39.9	1.11
Washed, DP = 82	39.2	39.0	1.10

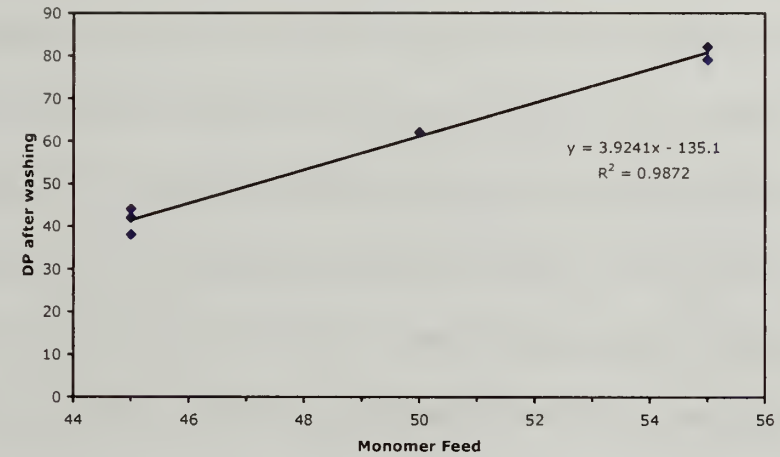

Figure 2.8. Monomer feed vs. DP_{PLA} after purifying with ethyl acetate wash.

2.4. PLA-PEO-PLA Solution Synthesis with Molecular Sieves

We believed water was the cause for broadened polydispersity of PLA-PEO-PLA, and while washing with ethyl acetate narrowed the distribution, the extra purification/cleaning step was non-ideal. We wished to tune the conditions so that one could perform a one-pot synthesis without extra purification steps and without having to add extra monomer to account for side reactions. With this in mind, molecular sieves (Acros Organics, 4A, 8-12 mesh) were added to the reaction in the hopes of having dryer conditions. Sieves were activated by heating in an oven (~ 200°C) and then cooling to room temperature under vacuum. Since we had previously tried drying the PEO initiator and lactide monomer through azeotropic distillation but the PDI still remained broad, the

catalyst was the likely source of water. Therefore, the sieves were added to the catalyst to remove any residual water. PEO (1.00 g, 0.114 mmol, 1 equiv) was weighed into a dried 3-neck round bottom flask attached to a condenser. The flask was heated to 130°C under nitrogen flow for half an hour to remove water. The flask was removed from heat and ~ 6 mL of anhydrous toluene (99.8%, Aldrich) was added to the PEO. Once dissolved and cooled to room temperature, activated molecular sieves were added to the solution as well to ensure water was removed from all sources (catalyst, macroinitiator, and monomer). The condenser was turned on, the flask was placed back in the oil bath (130°C) under nitrogen flow, and the solution was refluxed. Tin (II) 2-ethyl hexanoate (18 μL, 0.057 mmol, 0.5 equiv) was added to the mixture, followed by the immediate addition of recrystallized and sublimated lactide (0.592 g, 4.10 mmol, 36 equiv). The reaction mixture was refluxed under nitrogen flow for ~ 6 hours. The reaction was then quenched with methanol, diluted with THF, precipitated with hexanes, and dried under vacuum.

Figure 2.9 shows that the reaction was controlled because the degree of polymerization could be targeted and the polydispersity was greatly reduced with no significant tailing for most of the reactions. Since molecular sieves reduced the molecular weight distribution, it was confirmed that water acting as an initiator was the contaminant in the reaction. However, at the highest feed ratio tried, the PDI increased and low molecular weight tailing was evident. The PDI also increased when a large scale reaction was tried (~70 g). This suggested there was also some water present in the lactide monomer, and as more monomer was added, the amount of water was significant enough to initiate PLA homopolymer as evidenced by GPC. Therefore, for higher

molecular weight polymers an ethyl acetate wash should be coupled with the use of molecular sieves to reduce the tailing, or the lactide monomer should be more thoroughly dried with sieves or azeotropic distillation before use in the polymerization.

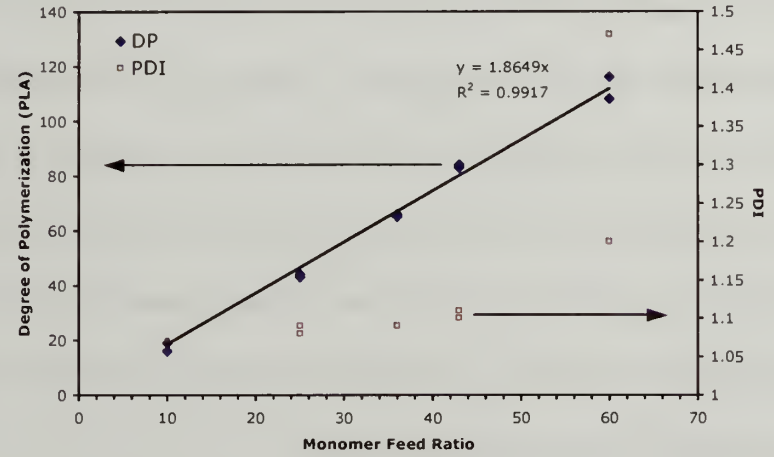

Figure 2.9. DP_{PLA} vs. feed ratio for solution-synthesized PLA-PEO-PLA with molecular sieves.

2.5. Conclusions

Despite the elusive nature of the water impurity, over half of a kilogram of PLA-PEO-PLA triblock copolymer with various molecular weights and low polydispersities (PDI $\leq$ 1.2) were synthesized, and batches were synthesized on scales as high as 100g. The elusive water caused us to pursue several alternative routines including fractionation, converting to solution synthesis, and addition of molecular sieves. Fractioning proved to be an effective method for narrowing the PDI; however, due to differences in solubility of each block, it became difficult to accurately determine the percent composition of each block. The synthesis was changed from the bulk to solution and the molecular weight distribution was significantly reduced (PDI $\leq$ 1.1), but as with the bulk synthesis, the distribution began to broaden and showed significant tailing on the lower molecular weight end of the chromatograms. Since water was initiating PLA homopolymer, we

added a washing step using ethyl acetate that successfully eliminated the low molecular weight tailing. TGA was also used as a technique to confirm the weight percent composition of each block. Finally, the water contaminant causing the broadened PDI was reduced by adding molecular sieves to the reaction mixture and led to controlled molecular weight and low polydispersity. Keeping all of these modifications in mind, the best approach to synthesizing PLA-PEO-PLA triblock copolymers is to use a solution polymerization with molecular sieves and couple this with an ethyl acetate wash after precipitating. By doing this, the water contaminant should be reduced, and any PLA homopolymer synthesized from residual unremoved water should be removed to yield controlled polymerizations and narrow PDI's.

CHAPTER 3

PROPERTIES AND STRUCTURE OF PLA-PEO-PLA PHYSICAL HYDROGELS

3.1. Introduction

Amphiphilic block copolymers have been extensively studied in the area of hydrogels because of their ability to self assemble in water. More specifically in the area of biomaterials, poly(ethylene oxide) [PEO] is often incorporated due to its biocompatibility and polyesters such as poly(lactide) [PLA], poly(caprolactone) [PCL], poly(glycolide) [PGA], and various copolymers thereof, are used for their biodegradability.[45] By using these polymers to make block copolymers, an associative network can be formed. Past work done with these types of polymers (both AB diblocks and ABA triblock copolymers, where the A block is a hydrophobic polyester and the B block is PEO) showed that hydrogels were formed and the sol-gel transition point was tuned using temperature and concentration gradients, but the mechanical properties of the gels were often not well characterized.[103, 105, 115, 117, 118] Those that have been characterized using rheology had a storage modulus typically less than 1 kPa which is lower than many target soft tissues.[104, 114]

We proposed to synthesize and characterize the mechanical properties of PLA-PEO-PLA triblock copolymer hydrogels while making small chemical changes in the structure. The components of the triblock were chosen because they were already approved by the FDA for a number of biomaterials and because the amphiphilic character allows for facile hydrogel assembly. First, we explored the influence of crystallinity on the rheological properties. While past reports have used crystalline domains within the hydrogel structure to improve mechanical properties,[96, 97] there had not been a system

where one could directly compare the crystalline system with an amorphous analogue. For example, poly(vinyl alcohol) [PVA] hydrogels stiffened after multiple freeze-thaw cycles due to an increase in crystallinity.[82-85] Similarly hydrogels with liquid crystalline domains also have significant degrees of crystallinity,[86-90] but for both of these cases there is no amorphous equivalent for comparison. In fact, if the crystalline domains were removed from these networks, the overall structure would be considerably altered. Here we compared two chemically equivalent polymer systems in which only the stereochemistry was changed by either using L-lactide to give stereoregular PLLA endblocks or DL-lactide to give stereorandom PRLA endblocks using rheology, thermal, and scattering techniques. Also, since the hydrogel network junctions are formed through hydrophobic interactions, we investigated the influence of the PLA hydrophobe length on the rheological properties.

3.2. Methodologies: Synthesis and Characterization

3.2.1 Synthesis by Bulk Polymerization

PLA-PEO-PLA triblock copolymer was synthesized in the bulk and characterized using ^{1}H Nuclear Magnetic Resonance (NMR) spectroscopy and Gel Permeation Chromatography (GPC) as described in Sections 2.2.1 and 2.2.2. The reaction scheme is shown in Figure 3.1a using either the stereorandom monomer, DL-lactide, or the stereo-regular monomer, L-lactide. Figure 3.1b shows a typical ^{1}H NMR spectrum of PLLA-PEO-PLLA triblock copolymer synthesized with L-lactide, and the inset shows the difference seen in the PLA methyne proton for PLA-PEO-PLA triblock copolymer synthesized with DL-lactide (multiplet versus a quartet for PRLA versus PLLA,

respectively). The nomenclature for the triblock copolymers is the total degree of polymerization of PLA followed by L if the L-lactide monomer was used or R if the racemic DL-lactide monomer was used. For example a triblock copolymer with DP_{PLA} = 70 synthesized from DL-lactide was called 70R. Characterization with GPC showed that polymers had a PDI less than or equal to 1.2.

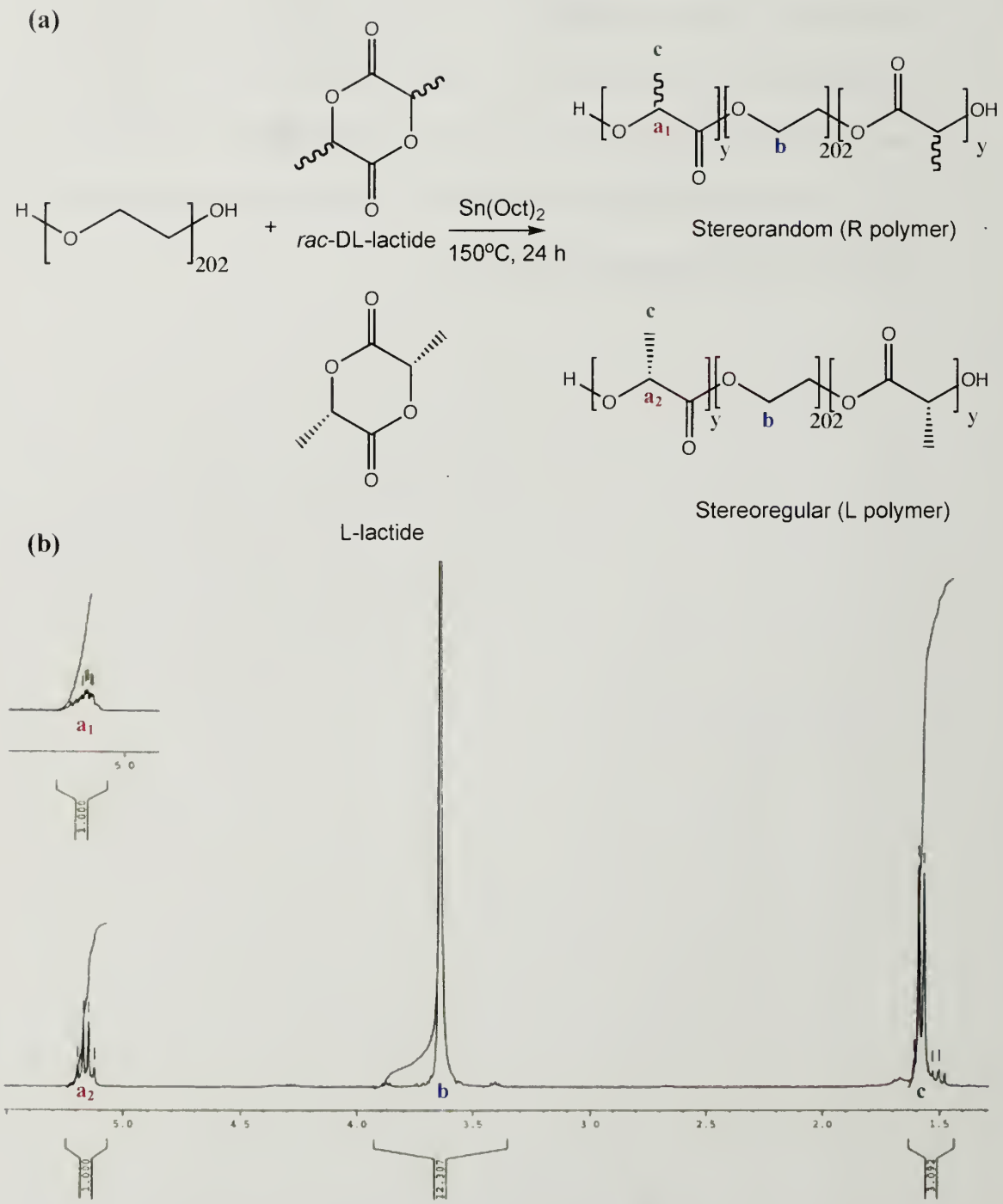

Figure 3.1. Polymerization of PLA-PEO-PLA using both DL- and L-lactide. (**a**) Reaction scheme. (**b**) ^{1}H NMR of PLA-PEO-PLA.

3.2.2. Rheology, X-Ray Diffraction, and Differential Scanning Calorimetry Characterization

In a typical method of preparation, water was added to a measured amount of polymer to form the dispersion at various concentrations (in weight percent). These samples were kept at equilibrium for 1 day at room temperature and then heated at either 40°C or 80°C for 20 hours (most typically at 80°C). The gels were again allowed to sit for 2 days before being transferred to a TA instruments AR2000 stress controlled rheometer for oscillatory measurements. Rheological measurements were performed using a cone and plate geometry (40 mm diameter cone with a 2° cone angle). A solvent trap was used and water evaporation was not significant for the temperature and timescales investigated. A stress sweep at a constant frequency of 1 Hz was first performed to obtain the linear viscoelastic region for collecting subsequent data. Frequency sweep tests over a frequency range of 0.01 Hz to 100 Hz were done at constant stress amplitudes to measure G' and G'' (storage and loss moduli, respectively) corresponding to the linear response.

Powder X-ray diffraction (XRD) measurements of the gels were performed on a Panalytical X'Pert Powder Diffractometer. The voltage was set at 45 kV, and the current was set at 40 mA. A Ni filter and a 1/2° slit width were used. The samples were scanned from 2θ = 5-55°.

Differential Scanning Calorimetry (DSC) of the polymer and the hydrogels was performed using a DSC 2910 DuPont Instrument. The polymer samples were heated at 10°C/min from room temperature to a maximum temperature of 180°C in a hermetically sealed aluminum pan for the first run. The samples were quenched with liquid nitrogen

to remove previous thermal history and then heated again at 10°C/min for the second run. The hydrogel samples were quenched to -50°C using liquid nitrogen, then heated at 10°C/min to a maximum temperature of 70°C.

3.3. Influence of Stereospecificity/Crystallinity in the Hydrophobic (PLA) Block

PLA-PEO-PLA triblock copolymers were synthesized with various block lengths (DP_{PLA} = 40-88) while keeping the PEO mid-block constant (M_n = 8900 Da). When in an aqueous environment the hydrophobic PLA end-blocks segregate from the water into flower-like micelles due to the hydrophobic effect. As the concentration of polymer is increased, micelles become more packed. At a certain critical concentration the micelles are close enough that the PEO mid-block may bridge to another micelle core instead of looping back to the same core. This assembly leads to an associative network with reversible physical crosslinks[124-126] at the PLA micelle cores (refer to the illustration in Figure 3.2). To take advantage of this assembly, the synthesized polymers were dispersed in water at concentrations ranging from 10 wt% to 25 wt%. These dispersions were separated into the categories of gel or sol based on the vial-inversion test (inverting the vial and seeing if there is flow after approximately 30 seconds). Using this test all of the R-series polymer dispersions were transparent sols, while the L-series were opaque gels when at concentrations greater than 16wt% as shown in Figure 3.3. However, this test is only qualitative at best, since only a modulus of 65 Pa is needed to pass vial inversion.[110] Nevertheless, this qualitative test demonstrated that although two polymers were chemically equivalent (the sole difference was stereospecificity), the properties were very different.

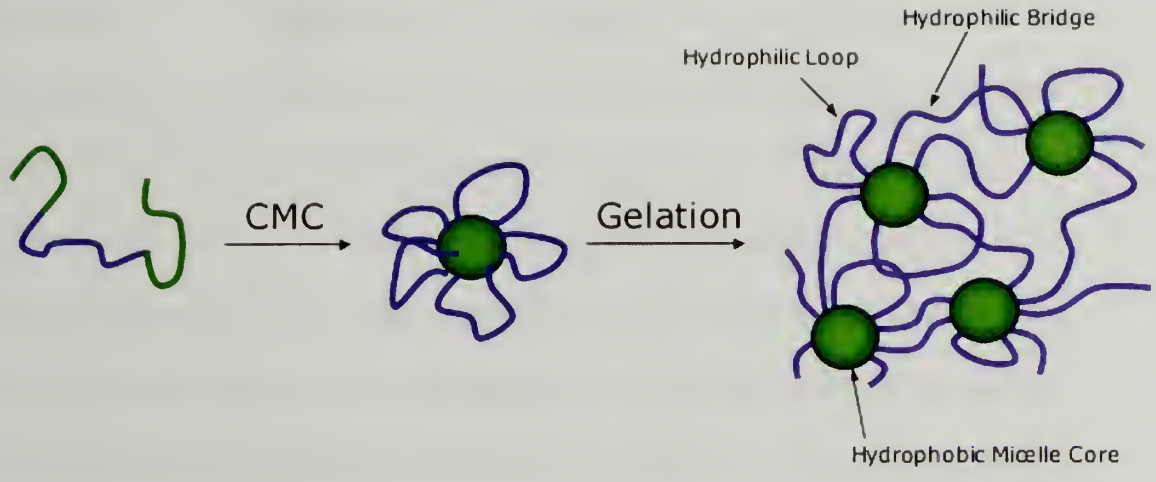

Figure 3.2. Formation of physical hydrogel structure. PLA end-blocks are represented in green and PEO mid-blocks in blue.

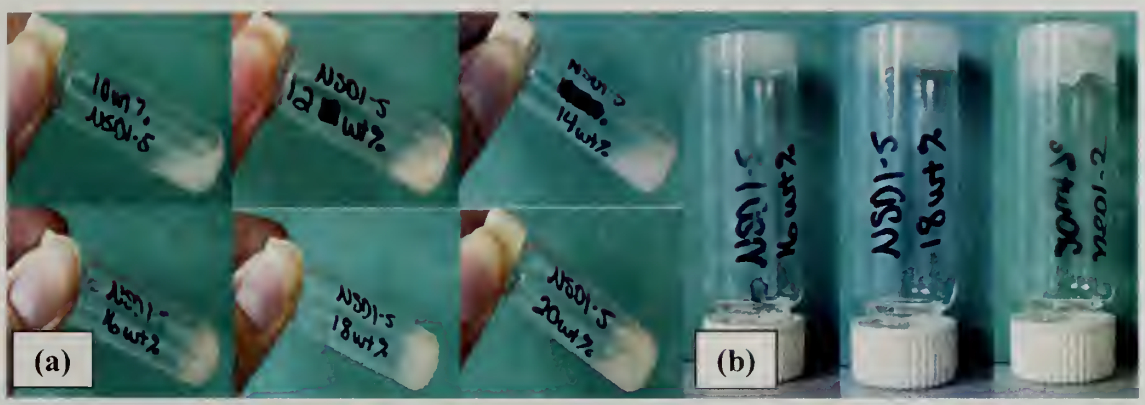

Figure 3.3. PLLA-PEO-PLLA hydrogels at various weight%. **(a)** Below 16wt% the dispersions appear to be sols. **(b)** Above 16wt% the samples are gelled and pass vial-inversion.

The mechanical differences between L- and R-polymers were more quantitatively compared with rheological measurements to find that the modulus of the materials was strongly dependent on the stereochemistry of the PLA blocks. Keeping molecular weight and concentration constant, the L-polymer series led to significantly stiffer materials than the racemic R-polymer series. Two examples with different molecular weights comparing the storage and loss modulus (G' and G'', respectively) versus frequency for

the L- and R-series are shown in Figure 3.4. For the L-series G` > G`` over the entire frequency range, and the moduli were fairly frequency independent, indicating a stiff hydrogel. Conversely, G` only began to approach G`` at high frequencies for the R-series, and the moduli were very frequency dependent demonstrating behavior that is more typical of a viscoelastic fluid. Furthermore, the L-series was overall much stiffer (higher modulus) than the R-series. For example, the 72L sample shown in Figure 3.4a had a storage modulus of 14 kPa at 1 Hz, while the 72R sample's storage modulus was only 0.1 kPa. This behavior was consistent even if the overall molecular weight was changed (Figure 3.4b).

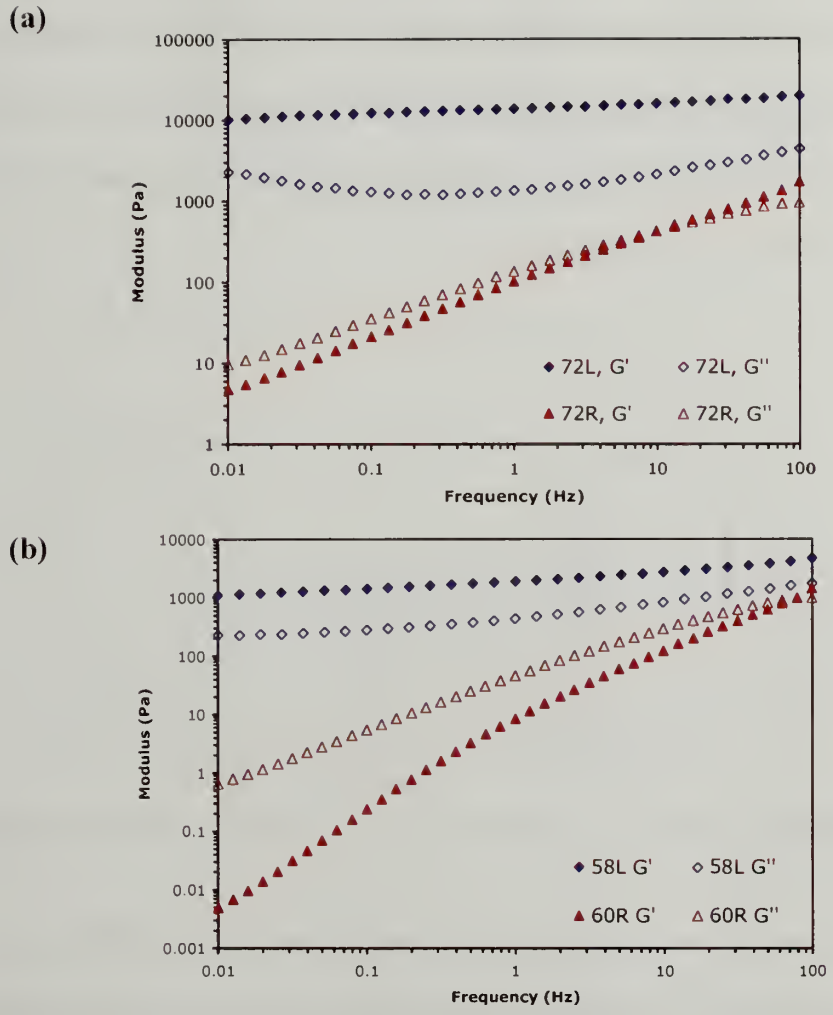

Figure 3.4. Rheology of stereoregular and stereorandom PLA-PEO-PLA in water. (**a**) 25 wt% PLA-PEO-PLA using L-lactide monomer (L) and racemic DL-lactide monomer (R) in water with $DP_{PLA} = 72$. (**b**) 25 wt% PLA-PEO-PLA using L-lactide monomer (L) and racemic DL-lactide monomer (R) in water with $DP_{PLA} = 58$ and 60, respectively.

We speculated that the increased stiffness for L-series hydrogels was due to the formation of longer-lived, crystalline, hydrophobic domains in the network junctions. In contrast, the racemic R-series materials were thought to have shorter-lived amorphous hydrophobic domains due to its stereorandom structure. To test this hypothesis, the samples were probed for crystallinity using differential scanning calorimetry (DSC) and powder X-Ray diffraction (XRD). Using DSC on the bulk triblock copolymers, a melting endotherm for crystalline PEO was evident at 50-53°C. As the temperature was

increased, another melting endotherm appears at ~165°C due to crystalline PLLA in the L-series (Figure 3.5). This data confirmed that PLLA crystallizes in the bulk. In contrast, the R-series did not show a melting endotherm (besides that of PEO), indicating that in the bulk they are amorphous.

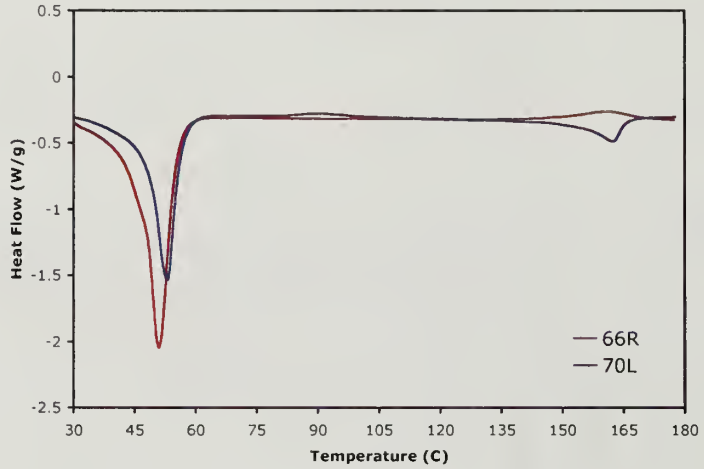

Figure 3.5. DSC of L- and R-series PLA-PEO-PLA triblock copolymers.

The samples were further probed using powder X-Ray diffraction, as this technique can be used on both the bulk polymers (in the dried powder form) and the hydrated polymer hydrogels. Figure 3.6a shows the scattering of both L- and R-series dry powder samples. The peaks at $2\theta \approx 19°$ and 23° are characteristic of crystalline PEO,[115] and overlapped with the peaks at $2\theta \approx 19°$ and 22° corresponding to crystalline PLLA. However, the peak at $2\theta \approx 17°$ is solely due to crystalline PLLA[115, 127-129] and confirms the presence of crystalline PLLA in the L-series and the absence of crystalline PLLA in the R-series in agreement with the DSC data. When the samples were hydrated to form gels, the crystalline PEO peaks were suppressed since these chains became solvated, but the crystalline PLLA peaks appeared to sharpen for the L-series (Figure 3.6b). This data confirmed the presence of crystalline domains within the stereoregular

polymer hydrogels and suggested that they impacted the overall structure to result in a stiffer hydrogel.[130]

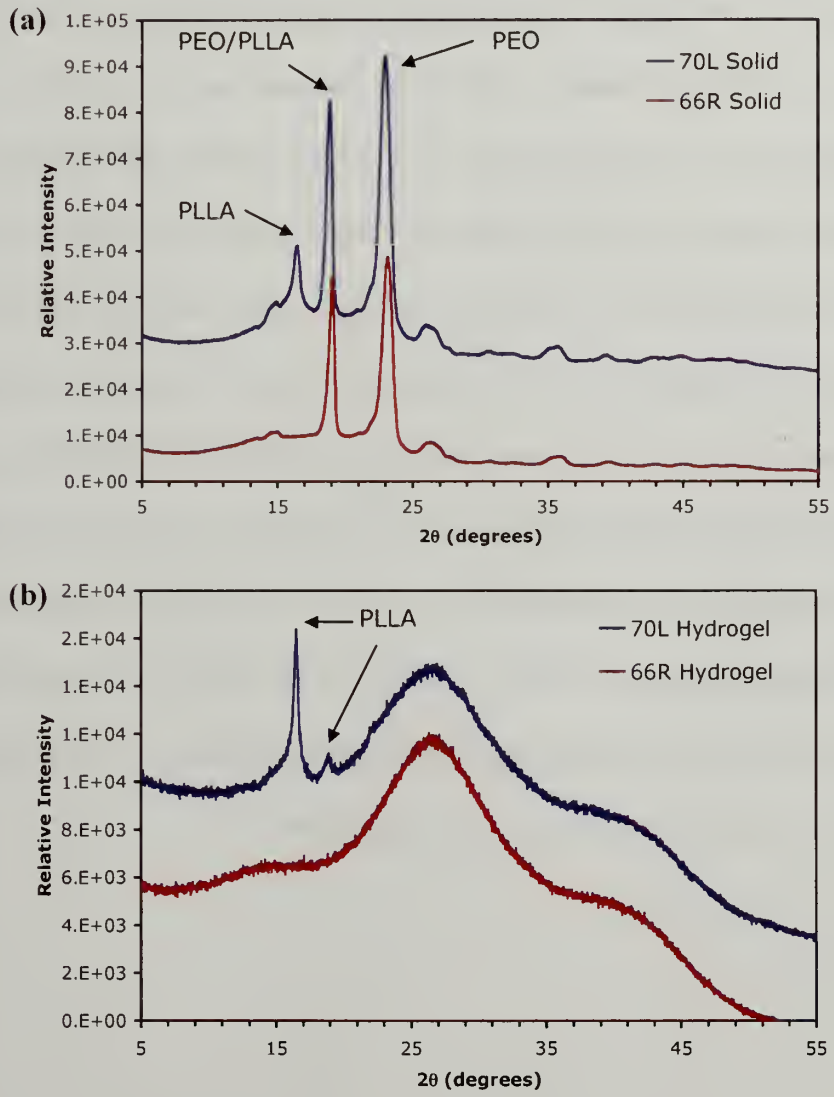

Figure 3.6. XRD of bulk and hydrogel samples. (**a**) XRD of powdered solids of 70L and 66R. (**b**) XRD of 25 wt% samples of 70L and 66R.

To gain greater insight into the assembly PLA-PEO-PLA in water, the nano-scale structure of L- and R-series was further probed used Small Angle Neutron Scattering (SANS) in collaboration with Sarvesh K. Agrawal of the Surita Bhatia group in chemical engineering.[131] At low concentrations PLA-PEO-PLA is expected to form flower-like micelles, but as the concentration is increased micelles crowd and bridging may occur.

As the micelles were crowded a correlation peak was evident for the amorphous triblock copolymers and a shoulder was evident for the crystalline triblock copolymers (Figure 3.7a and b, respectively). The correlation peak for 72R indicated the inter-micellar spacing and shifted to larger q (smaller length-scales) as the concentration was increased, as expected. The shoulder seen for 72L indicates a broader polydispersity in the inter-aggregate spacing. Further experiments using contrast matching demonstrated that the L-series polymers formed 2-dimensional micelle cores. This data, coupled with our XRD and work previously described for block copolymers with a semi-crystalline block[132-136] suggested the formation of "lamellar micelles" where the PEO chains align as brushes on crystalline PLLA lamellae (Figure 3.7c). The random orientation and possible polydispersity in size of the lamellae account for the broad correlation peak seen in the SANS spectrum for the L-series. Overall the differences in structure between L- and R-series reinforced the rheology and XRD data to show that crystalline domains within the junction points influenced the material properties.

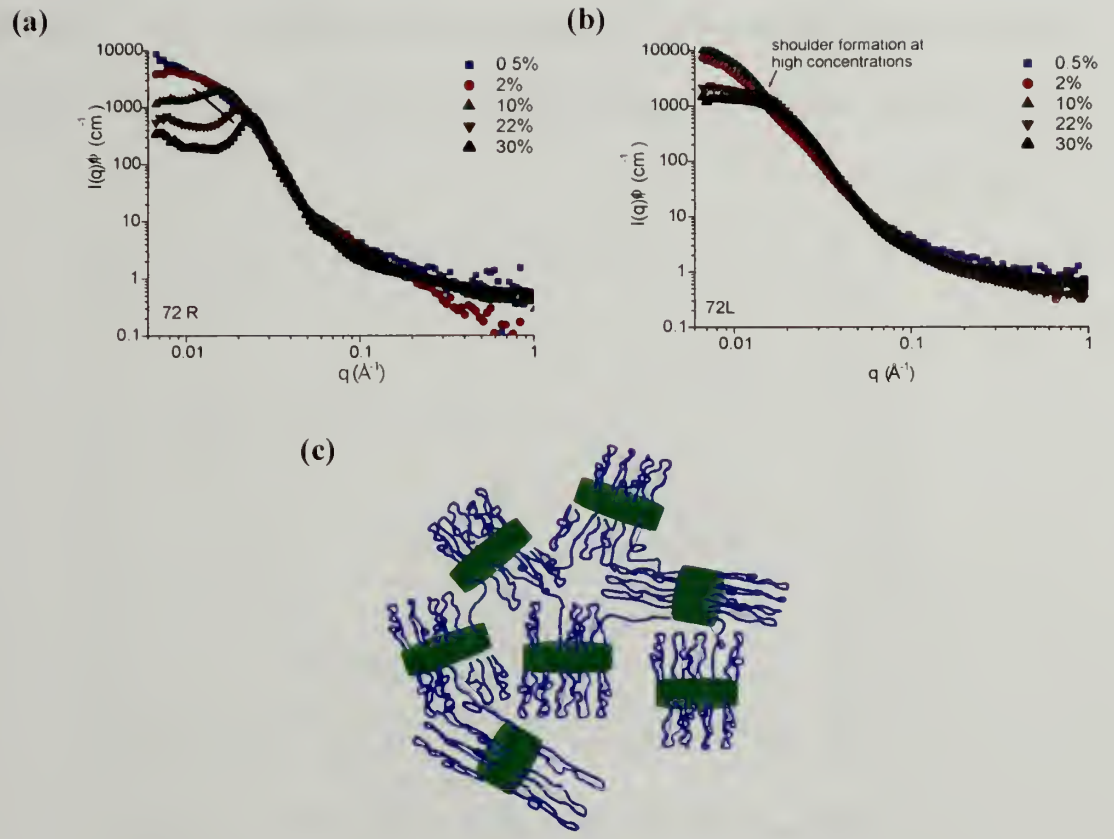

Figure 3.7. SANS spectra and lamellar micelle network (**a**) SANS spectrum of 72R at various concentrations. (**b**) SANS spectrum of 72L at various concentrations. (**c**) Schematic structure of lamellar micelle network formed by L-series polymers. (Reproduced from Agrawal et al., Macromol, 2008.)

Since the structure of the physical hydrogels is affected by crystallinity in the PLA block, we probed differences in the state of water using DSC. There are three known states of water in a hydrogel: free water, freezing bound water where the water weakly interacts with the polymer, and non-freezing bound water in which there are strong hydrogen bond interactions between the polymer and water causing it not to freeze. By freezing the hydrogel and watching the water melting endotherms, the relative amount of each state of water can be determined.[137-140] For PLA-PEO-PLA physical hydrogels, the melting endotherm for freezing bound water is present at approximately -15°C as shown in Figure 3.8. The freezing bound water melts first because the polymer-

water interaction is weaker than the hydrogen bonding interactions in ice (formed from the free water). At ~ 0°C a stronger endotherm is present corresponding to melting of ice or free water.

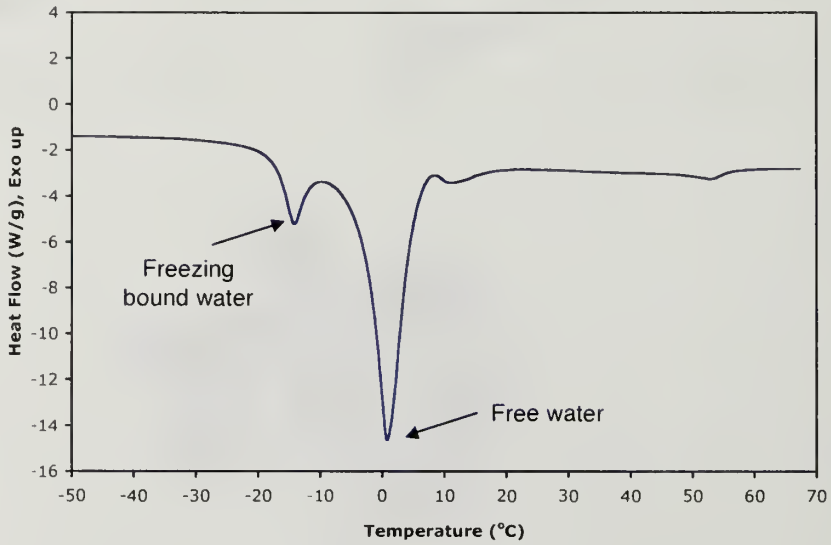

Figure 3.8. DSC of 20 wt% PLLA-PEO-PLLA hydrogel.

The total water content in the hydrogel is known (80 wt% water in this case) and is made up of all three states of water, as shown in the equation below, followed by a rearrangement of the variables:

$$W_t = W_f + W_{fb} + W_{nfb}$$
$$W_{nfb} = W_t - (W_f + W_{fb})$$

where W_t is the total water in the hydrogel, W_f is free water, W_{fb} is freezing bound water, and W_{nfb} is non-freezing bound water. The free and freezing bound water content can be approximated by comparing the heat of fusion of the melting endotherm, Q_{endo}, (determined by integrating the peak shown in Figure 3.8 from approximately -30°C to 5°C) to the heat of fusion of free water in the hydrogel, which we assume is the same as

that of ice (Q_f = 334 J/g). Using this relation the percentage of non-freezing to freezing water can be determined as shown in the equation below:

$$W_{nfb} = W_t - \left(\frac{Q_{endo}}{Q_f} \right)$$

Since previous work showed that the crosslinks in the R-series hydrogels were more dynamic than the L-series, we expected more water could penetrate the hydrophobic micelle core and bind to the amorphous PLA than the crystalline PLLA. The association of water and PLA would be weak leading to freezing bound water. We therefore expected the R-series to have a higher percentage of free and freezing bound water. We also believed that as the hydrogel aged and/or degraded, more water could weakly bind to polymer and increase the percentage of free and freezing bound water. However, as shown in Figure 3.9, there was little difference in the percentage of free and freezing bound water between L- and R-series polymer hydrogels, and there was little change with time. This is perhaps because the hypotheses above discussed the freezing bound water, which is actually only a very small percentage of the total amount of freezing water (refer back to the small endotherm at -15°C compared to the large endotherm at 0°C in Figure 3.8), and thus has little impact on the overall total amount of freezing water. So, while there were very obvious differences in the structure and mechanical properties of crystalline versus amorphous hydrogels, this did not have much impact on the states of water within the polymer hydrogels.

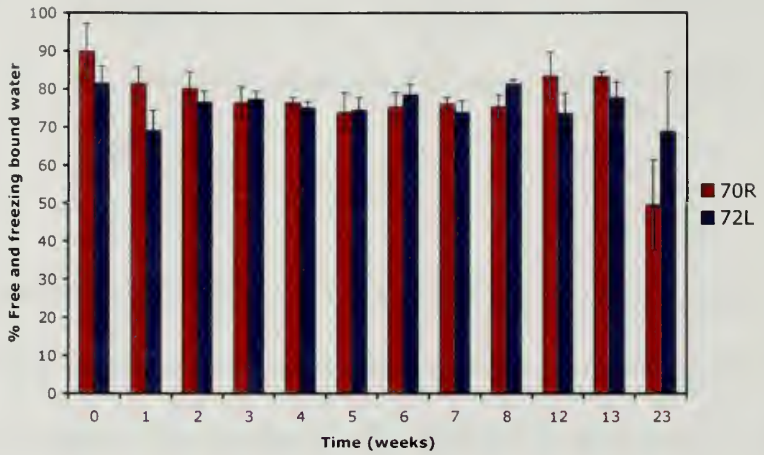

Figure 3.9. Percentage of free and freezing bound water in L- and R-series hydrogels with 80% water content over time (average of 4-5 samples for each data point).

3.4. Influence of Hydrophobic PLA Endblock Length

Since the formation of network junctions is dependent on the hydrophobic interaction of PLA endblocks, we explored how varying the PLA block length affected the mechanical properties of both L- and R-series polymer hydrogels. We expected longer PLA would have more hydrophobic character resulting in stronger interactions within the micelle core and stiffer materials. The experimental data showed the expected results for both semi-crystalline and amorphous materials (Figure 3.10).[122, 141] Therefore, varying the PLA block length is another chemical handle, in addition to crystallinity, to dial in the desired material properties. The rheology data was further analyzed by comparing the relaxation times of the networks. The relaxation time is related to the lifetime of the junction, or the time necessary for a chain to pull out from a hydrophobic core, and is estimated to be the inverse of the frequency where G' and G'' cross. In the crystalline hydrogels, the storage modulus was greater than the loss modulus over the entire frequency range, indicating that the crosslinks were permanent over the time scales explored during the experiment (relaxation time is greater than 10 seconds, corresponding

to the smallest frequency probed, 0.1 Hz).[142] This was consistent with the previously proposed network structure where the crosslinks are composed of longer-lived crystalline network junctions. However, the amorphous systems had finite relaxation times, in accordance with the reversibility of the network junctions, that linearly increased with the PLA block length. The increase indicated that longer PLA block lengths led to longer-lived junctions and stiffer materials. While, the longer relaxation times could be attributed to either an increase in chain entanglement within the cores or an increase in the hydrophobic effect, SANS experiments confirm that the aggregation number increased as the block length increased and confirms that hydrophobic interactions were enhanced.[131]

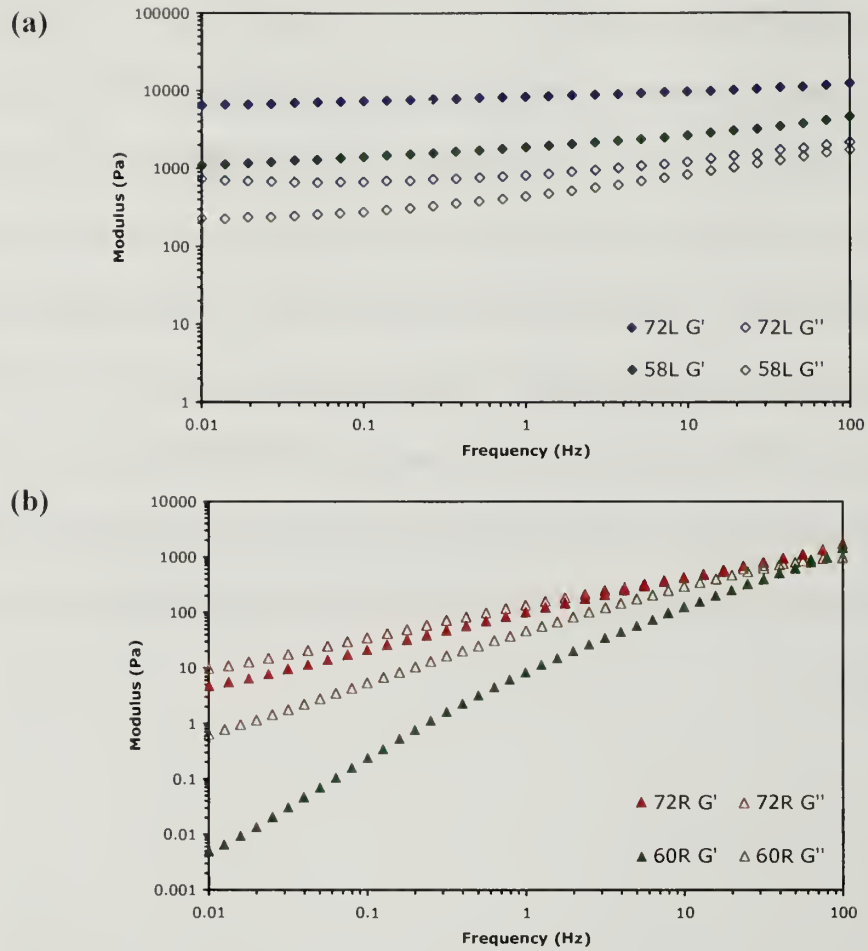

Figure 3.10. Rheology of L- and R-series with varying PLA length. **(a)** Storage and loss modulus of L-series at 25wt%. **(b)** Storage and loss modulus of R-series at 25wt%.

3.5. Conclusions

The mechanical properties of PLA-PEO-PLA hydrogels were strongly influenced by making very small chemical changes in PLA endblock stereoregularity and length. By polymerizing with either L- or DL-lactide monomer, the resulting triblock was either stereoregular (isotactic) or stereorandom (atactic), respectively. The PLA endblocks of the stereoregular triblock copolymer crystallized in the bulk, while the stereorandom triblock copolymer did not, as evidenced with both DSC and XRD techniques. When dispersed in water, the stereoregular triblock still had crystalline PLLA domains. These domains directly impacted the materials' stiffness by altering the structure and lifetime of

the network junctions as characterized using XRD, SANS, and rheology techniques and increased the storage modulus of the gel. However, the different structures (crystalline versus amorphous hydrogels) did not seem to affect the state of water in the hydrogels as characterized by DSC. This likely implies that the water primarily binds to PEO and not PLA, and since both types of gels have the same amount of PEO, the states of water are similar in each. Also, by lengthening the PLA block the lifetime of the network junctions were prolonged due to an increase in aggregation by the hydrophobic effect. In conclusion, we have used a variety of characterization techniques to gain insight into the structure of these hydrogels and to relate them to their overall properties and function. By utilizing differences in both block length and crystallinity, the dynamic moduli ranged over several orders of magnitude and can address a number of soft tissues.

CHAPTER 4

INFLUENCE OF SYNTHETIC TECHNIQUE AND CONTAMINANTS ON PLA-PEO-PLA HYDROGEL PROPERTIES

4.1. Introduction

In the previous chapter PLA-PEO-PLA hydrogels' mechanical properties were influenced by crystallinity. Those hydrogels with crystalline PLLA endblocks had a higher storage modulus (up to one order of magnitude) than the amorphous equivalents. While all the previous work was done with polymers synthesized in the bulk, we later modified the synthetic procedure to yield a polymer with a narrower molecular weight distribution. Analysis of gels formed with the newer solution-synthesized polymers showed differing mechanical properties than our initial experiments. More specifically, solution-synthesized polymers consistently formed stiffer hydrogels than bulk-synthesized polymers. This suggested that the synthetic conditions, either bulk-polymerization or solution-polymerization, also affected the mechanical properties. In this chapter we explored the characterizable differences between the two polymerization techniques to account for the changes in modulus. Based on the observed differences in the mean crystallite length of PLLA, we proposed a model explaining the cause for the changes in mechanical properties in the crystalline polymers. However with further testing, the modulus of the amorphous systems was even more greatly affected by the synthetic technique. Since the proposed model was only valid for crystalline systems, we also studied the influence of polydispersity as the source of the discrepancy.

We also considered the assembly of PLA-PEO-PLA hydrogels to identify other possible causes for changes in hydrogel stiffness. We know network junctions can only

be made by bridging two micelle cores, and this association is only possible with an ABA triblock copolymer. We also know that the lifetime of the junctions is decreased when the PLA block length is shortened and can cause a transition from a gel-like material to a more fluid-like material (Section 3.4). Taking these findings into consideration, it appeared likely that a contaminant in the bulk-synthesized polymers interfered with either or both of the two described processes to lower the material's stiffness. Therefore, we also considered the possible contaminants in PLA-PEO-PLA polymerizations and how they affect the overall mechanical properties of the physical hydrogels.

4.2. Methodologies: Synthesis and Characterization

Bulk-synthesized and solution-synthesized polymers were prepared as already described in Chapter 2. A poly(ethylene glycol)-monomethyl ether (M_n = 9 kDa, Polymer Source, PDI = 1.18) with similar molecular weight to the telechelic PEO used for triblock copolymer synthesis was used without further purification to synthesize PLA-PEO diblock copolymer. Poly(ethylene glycol)-monomethyl ether macroinitiator (1 equiv) was weighed into a dry 3-neck round bottom flask with a stir bar and attached to a condenser. The PEO was stirred and heated at 130°C under nitrogen flow. Tin (II) 2-ethylhexanoate (0.25 equiv) was added to the PEO, followed by the immediate addition of lactide (17.5 equiv). The targeted degree of polymerization of PLA was half of the total of the triblock copolymer since the total accounted for *two* PLA endblocks in the triblock copolymer, while the diblock copolymer only had *one* PLA endblock. The condenser was turned on and toluene was added to the reaction mixture (approximately [PEO] = 28 mM). The mixture reacted at 130°C for 24 hours under nitrogen flow, was cooled then diluted with THF, and precipitated using hexanes. The recovered white

powder was separated with a filter funnel, collected, and dried under vacuum at room temperature. The yield was approximately 60% and the PDI = 1.27 (broadness due to the PEG-monomethyl ether macroinitiator). ^{1}H NMR (300 MHz, $CDCl_3$) δ 5.15-5.20 (quartet when polymerizing with L-lactide, multiplet when polymerizing with DL-lactide), δ 3.64 (s), δ 1.48-1.60 (d), M_n = 11,800.

PLA homopolymers were synthesized using benzyl-alcohol (Aldrich, anhydrous 99.8%) as an initiator. Benzyl-alcohol (1 equiv) was measured into a 2-neck round bottom flask attached to a condenser. About 17 mL of anhydrous toluene was added to the flask, the condenser was turned on, and the flask was placed in an oil bath to reflux. Tin (II) 2-ethylhexanoate (0.5 equiv) was added to the reaction, followed by the immediate addition of either L- or DL-lactide (35 equiv). The reaction mixture was refluxed for 4 hours, quenched with methanol, diluted with THF, and precipitated in cold hexanes. The white precipitate was collected and dried under vacuum. For the semi-crystalline PLLA: yield ≈ 80%, DP = 43, and PDI = 1.17. For amorphous PRLA: yield ≈ 67%, DP = 70, PDI = 1.40. The degree of polymerization was determined by comparing the benzyl-protons from the initiator to the methyne protons of PLA. The chemical structures for PLA-PEO diblock copolymer and PLLA and PRLA homopolymers are shown in Figure 4.1. ^{1}H NMR (300 MHz, $CDCl_3$) δ 7.3-7.4 (benzyl protons), δ 5.11-5.24 (quartet when polymerizing with L-lactide, multiplet when polymerizing with DL-lactide), δ 1.40-1.60 (d). All other techniques (i.e. ^{1}H NMR, GPC, hydrogel preparation, and rheology) are already described in Chapter 2.

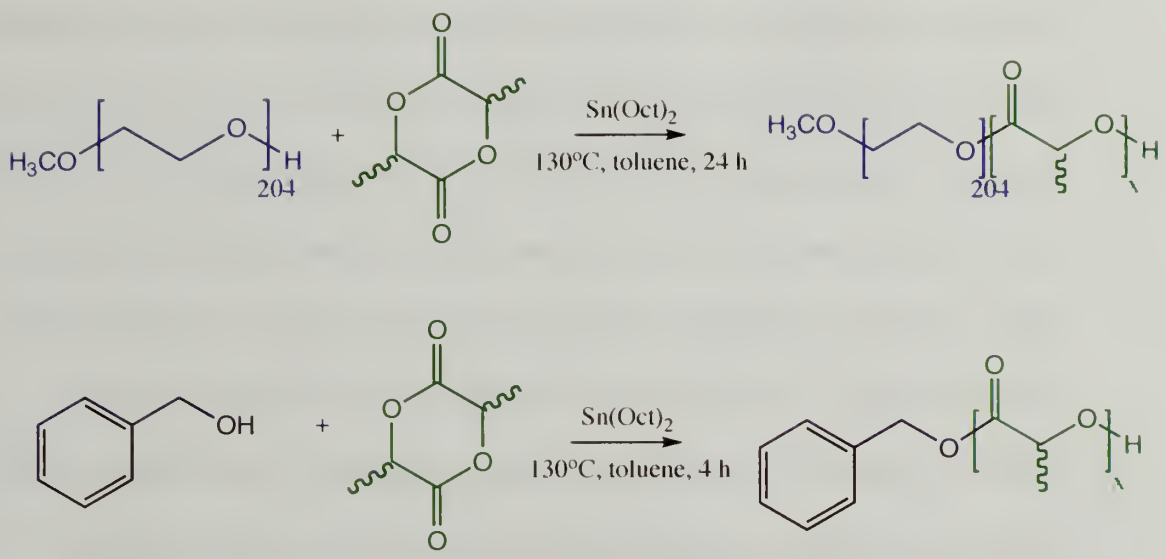

Figure 4.1. PLA-PEO diblock copolymer and PLA homopolymer syntheses.

4.3. Bulk- versus Solution-Synthesized Polymer Hydrogels

4.3.1. Modification of PLA-PEO-PLA Synthetic Conditions

PLA-PEO-PLA triblock copolymers were synthesized via two different synthetic methods – bulk or solution polymerization. The previously established sample nomenclature remained consistent with a slight modification to denote which polymerization method was used. For example, b-72L means the total DP of lactic acid units is 72, the preceding letter signifies the synthetic method used (b = bulk synthesis and s = solution synthesis), and the following letter still signifies the stereochemistry of the PLA end block (L = semicrystalline PLLA and R = amorphous or stereorandom PRLA), while the PEO midblock was still held constant (M_n = 8800 Da). Initially the bulk polymerizations were well controlled with high yield and narrow PDI, but with time the reaction led to polymers with significant lower molecular weight tailing (by GPC) and sometimes bimodal distributions (see Section 2.2). For this reason, the conditions were modified to a solution synthesis, as it also resulted in controllable DP, complete

conversion, and high yields. However, the solution synthesis showed no problematic tailing in the GPC chromatograms and consistently displayed an even narrower molecular weight distribution than the bulk synthesis (PDI $\leq$ 1.1 for solution-synthesized and PDI $\leq$ 1.2 for bulk-synthesized). Figure 4.2 shows typical chromatograms for two polymers, bulk- and solution-synthesized, with similar molecular weights (as characterized by ^{1}H NMR) but slightly different PDI's (PDI $\approx$ 1.16 for bulk-synthesized and 1.07 for solution-synthesized PLA-PEO-PLA). Because of the narrower molecular weight distributions, the solution-synthesis method was adopted to make PLA-PEO-PLA triblock copolymers.

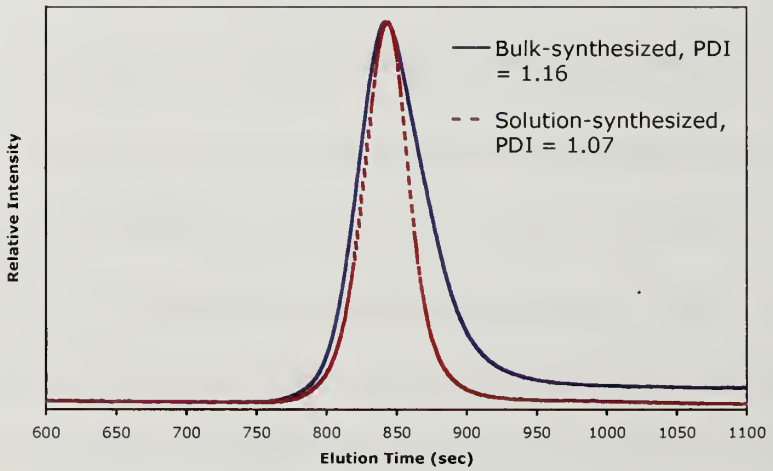

Figure 4.2. GPC of bulk-synthesized and solution-synthesized PLA-PEO-PLA.

4.3.2. Impact of Crystallinity on Hydrogel Properties

Hydrogels from solution-synthesized L-polymers were prepared and evaluated. Qualitatively the hydrogels from the solution-synthesized L-polymers appeared slightly different. Before the gels from bulk-synthesized polymers were white in color and fairly homogeneous, but the gels synthesized from solution, while also white, appeared to be more granular. We attempted to characterize the solution-synthesized hydrogels with rheology at the same concentration as studied prior (25 wt%), but the material was stiff

enough that the rheometer was not able to compress the sample with the cone geometry to the proper sample gap spacing. Therefore, to make the sample more compressible and measurable using the rheometer, the concentration was decreased to 20 wt% polymer in water and compared to the bulk-synthesized hydrogels at 25 wt%. Knowing that both samples had similar molecular weights and they both had semi-crystalline PLLA endblocks but different concentrations, one would expect that the less concentrated hydrogel (solution-synthesized) would have lowered stiffness since the modulus is concentration dependent, but this proved not to be the case. Interestingly, as shown in Figure 4.3a, the solution-synthesized polymers generated materials with slightly higher moduli (both storage and loss modulus) than the corresponding bulk-synthesized polymer hydrogels despite being less concentrated. Furthermore, both materials formed hydrogels as defined by Chambon and Winter, in which $\tan\delta = (G''/G')$ is frequency independent (Figure 4.3b) and the slopes of G' and G'' are parallel.[143, 144] Keeping in mind that crystallinity can greatly affect the mechanical properties of these hydrogels, we suspected that solution-synthesized L-polymers had a higher degree of crystallinity.

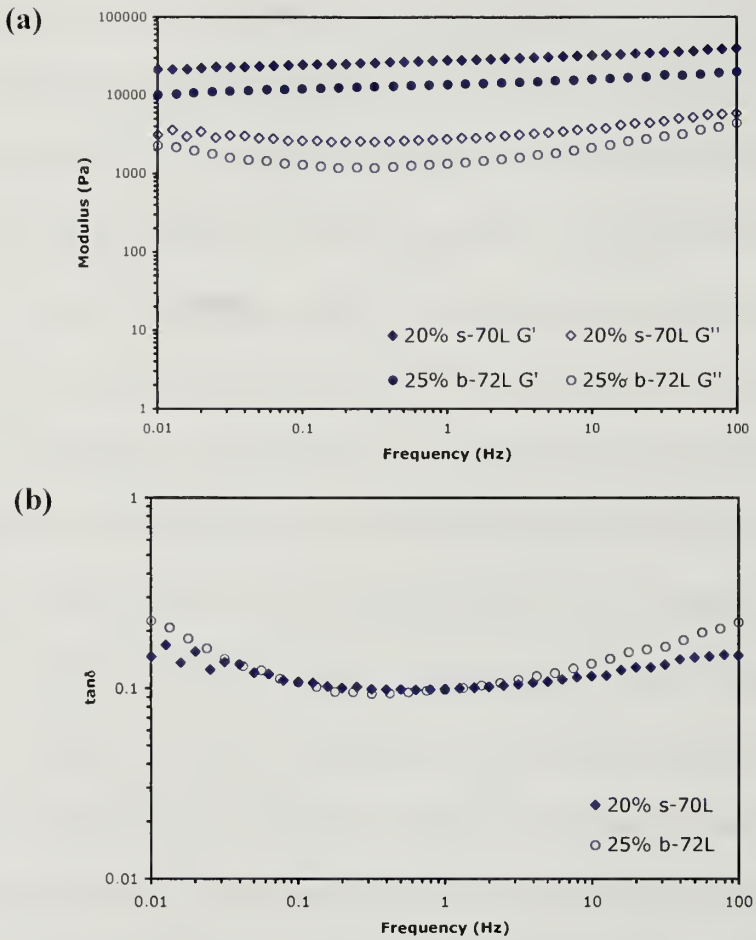

Figure 4.3. Rheology of bulk- and solution-synthesized L-polymer hydrogels. **(a)** G' and G'' versus frequency. **(b)** tanδ versus frequency.

To better understand the impact of crystallinity in the two different hydrogels, we investigated the PLLA crystalline microstructure of the triblock copolymer both before and after hydrogel formation with powder XRD. Figure 4.4 shows the XRD patterns of the bulk- and solution-synthesized polymers in the dried powder form. It was apparent that the two polymers had differences at $2\theta \approx 17°$, which is solely attributed to crystalline PLLA,[127-129] since the bulk-synthesized polymers had a much sharper peak than the

solution-synthesized polymers. The sharpness or broadness of a peak is caused by the size of the scattering crystallites and can be calculated using the Scherrer equation:[145]

$$L_{hkl} = (K\lambda/\beta_o)\cos\theta$$

where L_{hkl} is defined as the mean crystallite length, K is a constant (K = 1 is commonly used and is the value that we have used), λ is the X-ray wavelength (1.54Å), β_o is the full width at half-maximum of the peak, and θ is the Bragg angle of the reflection. Using the Scherrer equation, we determined that the bulk-synthesized polymers consistently had a larger mean crystallite length than the solution-synthesized polymers, L_{hkl} = 12.0 nm and 5.6 nm, respectively, for the polymers shown in Figure 4.4. We thought the differences in crystallite lengths of the dry samples may have affected the overall network structure of the corresponding hydrogels. Assuming this was true, hydrogels formed from bulk-synthesized polymers would have longer crystallite lengths than hydrogels formed from solution-synthesized polymers. This assumption coupled with the rheology data suggested that shorter crystallite lengths lead to stiffer materials.

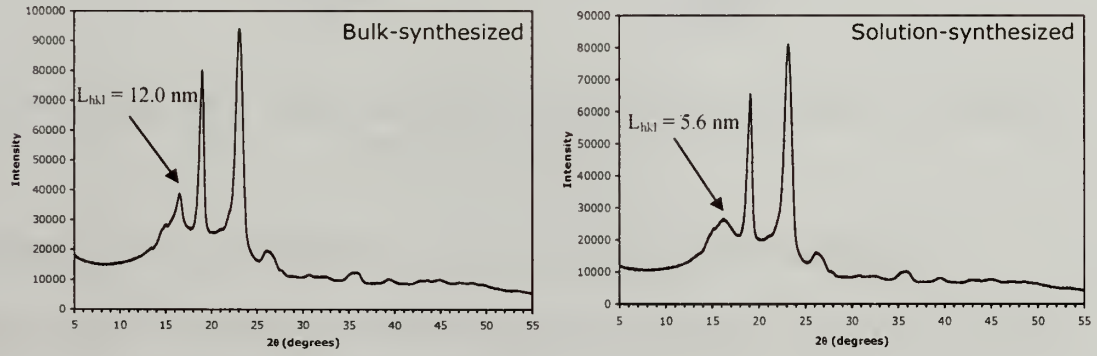

Figure 4.4. XRD of bulk- and solution-synthesized dry polymers.

To better evaluate whether the PLLA crystallite length should influence the hydrogel properties, we again considered the physical network structure. The junction points are formed through hydrophobic interactions of the PLLA endblocks, and these

junction points are further stabilized by the crystallization of PLLA within the hydrophobic lamellar micelle core.[130, 131] If the crystallite lengths within the micelle core were smaller (as was measured with solution-synthesized polymer gels), this could suggest that less PLLA chain ends were associated within a given lamellar micelle. Assuming that less chain ends were associated per lamellar micelle and the total number of PLLA chain ends was held constant (concentration was fixed), more network junctions must have been formed to account for the hydrophobic chain ends. This increase in crosslink density could have accounted for the stiffening of the hydrogel. Figure 4.5 illustrates the proposed structural differences in network structure with shorter and longer mean crystallite lengths.

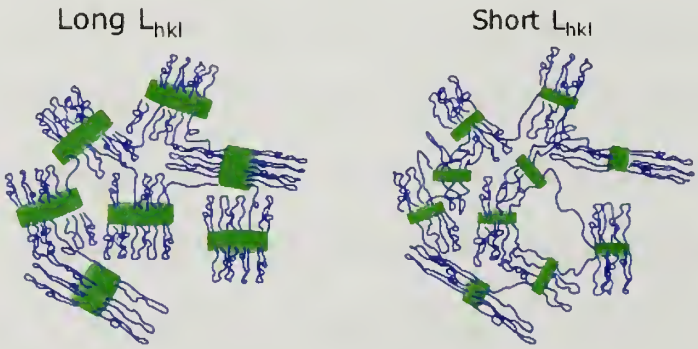

Figure 4.5. Proposed structures of PLLA-PEO-PLLA physical hydrogels with varying mean crystallite length.

The hypothesis for the correlation between crystallite length and gel properties described above was evaluated by forming hydrogels with polymers of various crystallite lengths. To vary the crystallite length one bulk-synthesized polymer (b-62L) and one solution-synthesized polymer (s-68L) were subjected to various processing conditions including precipitation from a refluxed solution of toluene, or annealing at 180°C for 3 hours and quenching with liquid nitrogen, ice water, water, or room temperature air. We

expected that precipitation from solution and quenching at low temperatures would suppress crystallization leading to shorter L_{hkl}, while quenching at higher temperatures would lead to longer L_{hkl}. However, the mean crystallite length stayed fairly constant for solution-synthesized polymers, and there was no direct correlation between L_{hkl} and quenching temperature for bulk-synthesized polymers. Nevertheless, we did achieve a range of L_{hkl} from ~ 5.6 nm to 13.9 nm. These polymers were used to form hydrogels and their relevant parameters are listed in Table 4.1 (L_{hkl} before and after gel formation and G' of the gel at 100 Hz). Of note is that the L_{hkl} of the gels are larger than the powder forms suggesting an evolution of the PLLA crystal during hydrogel formation. The reason for this evolution still remains in question since the melting temperature of PLLA (T_m ~ 160°C) is much higher than the preparation temperature.

Table 4.1. Crystallite lengths and rheological properties.

Bulk-synthesized polymers				*Solution-synthesized polymers*				
Sample*	**L_{hkl} powder (nm)**	**L_{hkl} gel (nm)**	**G' (kPa)**	**Sample***	**L_{hkl} powder (nm)**	**L_{hkl} gel (nm)**	**G' (kPa)**	Increasing modulus
b-62L	13.9	12.8	6.5	**s-68L**	5.56	12.6	17.8	
b-62L	13.0	16.2	17.4	**s-68L**	5.56	18.6	19.4	
b-62L	12.0	23.0	21.0	**s-68L**	5.67	9.3	24.9	
b-62L	8.6	25.7	21.2	**s-68L**	5.63	20.3	27.8	
b-62L	10.3	24.2	32.5	**s-68L**	5.63	19.8	29.9	

*The same triblock copolymer was used for the bulk- and solution-synthesized polymers, respectively, but melted and quenched at various temperatures to achieve various mean crystallite lengths.

Contrary to our expectations, there was no correlation between the crystallite length of the polymer, or hydrogel, and the resulting hydrogel modulus. Therefore, the difference in crystallite lengths for the bulk- and solution-synthesize polymers most likely did not account for the discrepancies in the observed mechanical properties. Furthermore, in almost all cases, the mean crystallite length increased once the powder

was used to form the hydrogel, suggesting further crystallization during the network formation process. Because crystallization was induced when forming the hydrogel, the resulting mean crystallite lengths of both solution- and bulk-synthesized polymer hydrogels were much more similar (refer to Figure 4.6 and Table 4.1). Taking this data into account, the mean crystallite length of the neat powder was not the dominant factor influencing the mechanical properties of the hydrogels, and the proposed model in Figure 4.5 was invalidated.

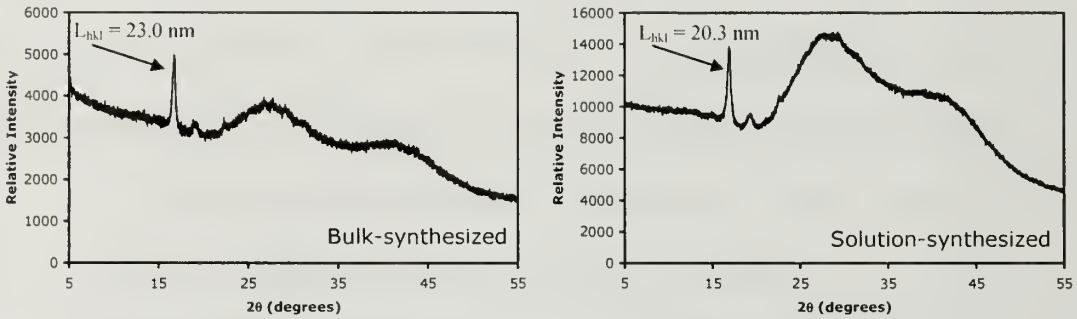

Figure 4.6. XRD of bulk- and solution-synthesized polymer hydrogels.

4.3.3. Impact of Polydispersity

Since the crystallite size was not the dominant factor accounting for the differences between bulk- and solution-synthesized polymer hydrogels, the amorphous R-series polymer hydrogels were prepared and tested with rheology to see if they were also influenced by the synthetic technique. As was seen with the L-series, the newer solution-synthesized polymer dispersions led to stiffer materials than the bulk-synthesized equivalents. Furthermore, while the L-series bulk- and solution-synthesized polymer hydrogels both showed the same characteristic behavior (G'> G'', and little frequency dependence), the solution-synthesized R-series dispersions displayed drastically different rheological behavior than the bulk-synthesized materials (Figure 4.7a). Previously, the

R-series showed typical viscoelastic liquid behavior, where G' and G'' were frequency dependent, but the newer solution-synthesized materials had more gel-like properties with G' > G'' over the entire frequency range and were much less frequency dependent despite being less concentrated. However, tanδ decreased with frequency (Figure 4.7b) and the slopes of G' and G'' were not parallel for all R-series materials and thus do not pass the Chambon-Winter definition of a gel.[143, 144] Nevertheless, there is a marked difference in the rheological properties between bulk- and solution-synthesized polymer materials, and the results with the amorphous R-series polymers confirmed that variations in crystallinity alone do not explain these differences. The only other measured change between the two techniques, besides the crystallite size, was polydispersity. Solution-synthesized polymers consistently had narrower molecular weight distributions than bulk-synthesized polymers (refer back to Figure 4.2), and so the impact of PDI was further explored.

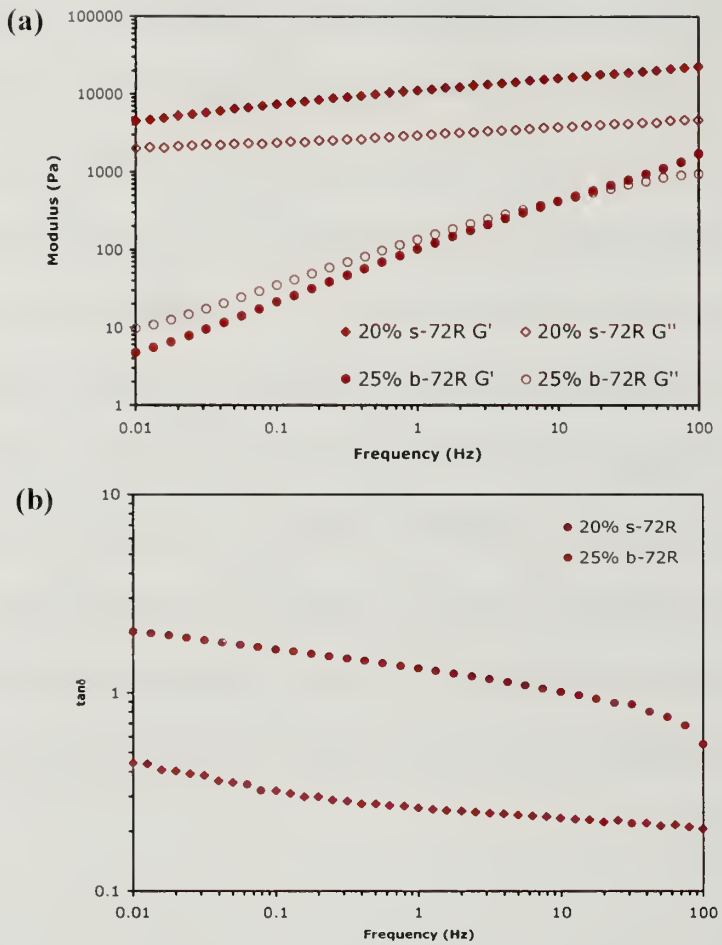

Figure 4.7. Rheology of bulk- versus solution-synthesized polymer hydrogels. **(a)** G' and G'' versus frequency. **(b)** tanδ versus frequency.

To vary the polydispersity of PLA-PEO-PLA triblock copolymers we mixed solution-synthesized polymers with differing molecular weights. More specifically, a s-69R sample and a s-57R sample were combined at different proportions by weight (100:0, 75:25, 50:50, 25:75, and 0:100), dissolved in THF, and precipitated in hexanes. By combining in the solution state we ensured good mixing, and R-series polymer was used because the mechanical properties were more significantly impacted than the L-series. The mixed polymer systems gave a range of PDI's, and these polymers were used

to form hydrogels at 20 wt% polymer. The rheological data for these gels are shown in Figure 4.8a (Figure 4.8b only shows G' for clarity and lists the measured PDI's) and again displayed the typical dependence on the PLA hydrophobe block length.[122, 141] As more s-57R was added, the storage modulus decreased and there was a transition from gel-like to viscoelastic fluid-like behavior. However, it appeared that polydispersity did not directly play a role in the mechanical properties when looking specifically at samples 100% 69R and 75% 69R:25% 57R (highlighted in Figure 4.8b). The PDI's for these polymers are 1.07 and 1.14, respectively, but they displayed almost identical rheological responses over the frequency range probed. So, in this case, two systems with different PDI's produced materials with very similar mechanical properties. What appeared to be more important to these results was the PLA block length as has been previously discussed.[141]

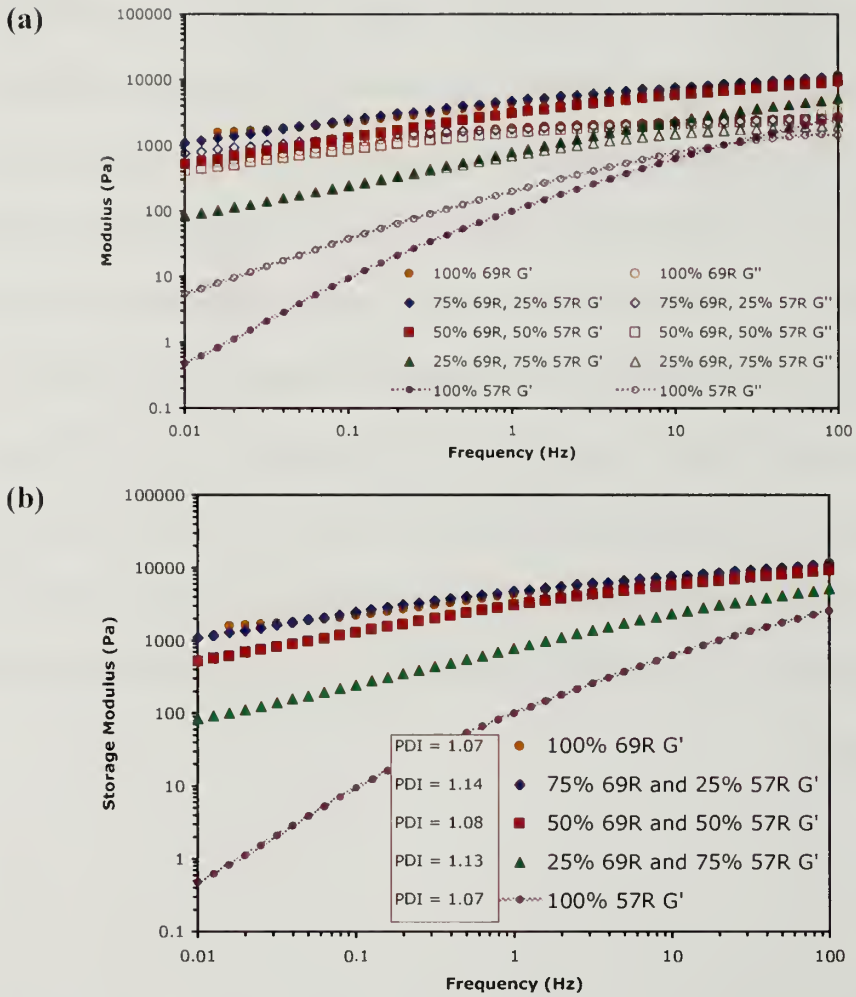

Figure 4.8. Rheology of mixed molecular weight systems. (**a**) Storage and loss modulus versus frequency. (**b**) Just G' is shown for clarity and the corresponding PDI's.

4.4. Contaminants in PLA-PEO-PLA Triblock Copolymer Hydrogels

4.4.1. Asymmetric Triblock and Diblock Copolymer Contaminants

Since crystallinity and PDI do not directly impact gel stiffness, it was much more likely that a contaminant was affecting the assembly of the associative network structure. We surmised this contaminant was an asymmetric triblock copolymer in which one PLA endblock was significantly shorter than the other. Highly asymmetric triblock copolymers with very short PLA could lower the hydrogel's modulus since, as already

discussed in Chapter 3, shorter PLA endblocks lead to shorter junction lifetimes that weaken the network structure. In the most extreme case a triblock copolymer with a very short PLA endblock may not be hydrophobic enough to drive association with a neighboring micelle, ultimately acting as an "effective" diblock copolymer. These types of polymers would not contribute to the network structure and would lower the overall stiffness by increasing the number of dangling ends as illustrated in Figure 4.9. Having asymmetric triblock copolymers in the system would affect the mechanical properties of both amorphous and semi-crystalline polymer hydrogels, and their presence would also broaden the PDI. The data presented in Sections 4.3.1 through 4.3.3 is in good agreement with these predictions and suggested that there was a side-reaction in the bulk-synthesized polymers that led to highly asymmetric triblocks or effective diblocks, while in the solution-synthesis these reactions were suppressed giving lower PDI's and stiffer gels. We speculated that asymmetric triblock copolymers were synthesized via chain transfer reactions in which growing PLA chain ends attacked a neighboring PLA to give two triblock copolymers with one shorter and one longer PLA chain end (Figure 4.10). This type of reaction is consistent with previous work showing that both inter- and intramolecular chain trans-esterification can occur when polymerizing PLA homopolymer using tin catalysts. These side reactions led to partial degradation/depolymerization and cyclic lactide oligomers from chain backbiting at elevated temperatures.[146-149]

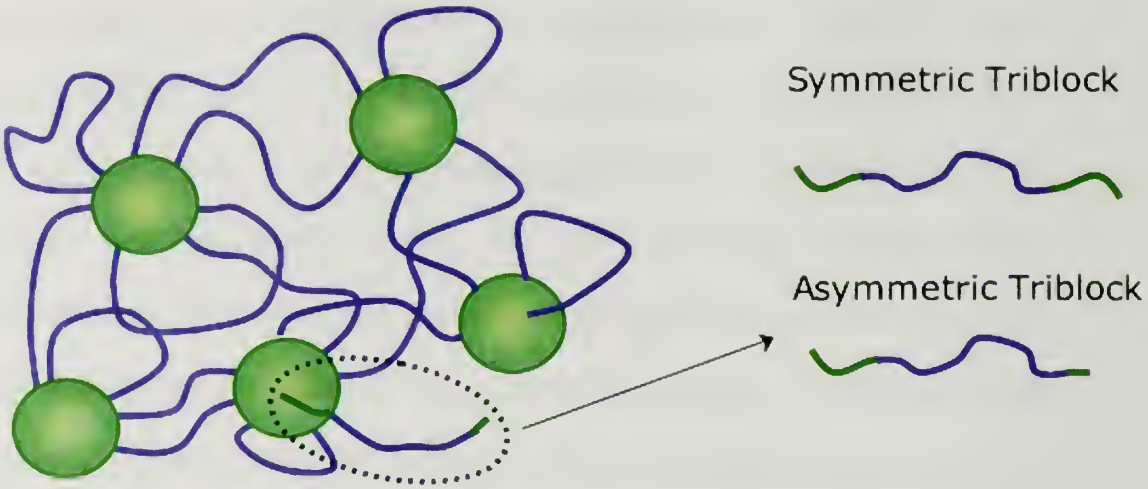

Figure 4.9. Schematic of network with asymmetric triblock copolymer contaminants.

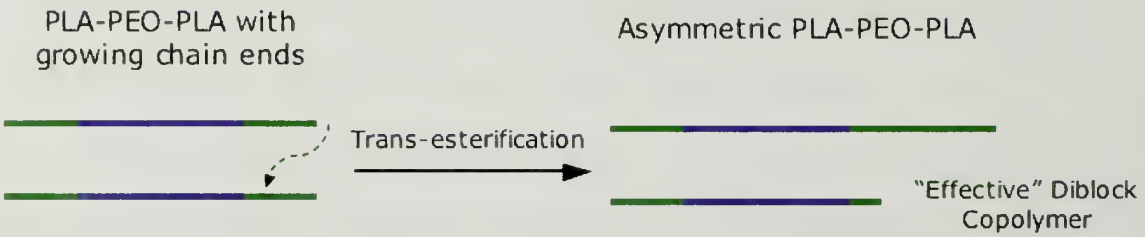

Figure 4.10. Formation of asymmetric triblock copolymer.

Further work by Chang and co-workers described "non-ideal" chain growth in PLA-PEO diblock and PLA-PEO-PLA triblock copolymers.[150-152] By using liquid chromatography at the critical condition (LCCC), the solvent conditions were tuned so the chromatography column did not interact with PEO. In this way, copolymers were solely separated by their PLA content. Various fractions were eluted, collected, and the molecular weight was characterized using MALDI-Tof. Using this technique they first found that PLA blocks can have an odd number of lactic acid units.[151] This finding was unexpected since PLA is polymerized by using a cyclic dimer (lactide) and should ideally only produce copolymers with an even number of lactic acid residues. These results suggested that ester bonds in the polymer backbone could be broken during the

polymerization process. Also using LCCC, they found that although PLA-PEO-PLA triblocks are commonly assumed to be symmetric, meaning there are the same number of residues on each PLA endblock, they can be asymmetric.[150, 152] They came to this conclusion because triblock copolymers with the same molecular weight (MALDI-Tof analysis) were eluted at different times, and they believed the imbalance in the PLA chains ends caused different interactions with the column. All of this work gives credence to the possibility of asymmetric triblock copolymers contaminants within our own system.

Unfortunately, it is very difficult to prove the presence of asymmetric triblock copolymers. The previous work was done with triblock copolymers with lower molecular weights, and as the molecular weight grows larger, as in our case, it is harder to determine the critical point and the data is more difficult to analyze and interpret. In fact, the Chang group attempted to use the LCCC technique on our own PLA-PEO-PLA samples (Figure 4.11). Both the bulk- and solution-synthesized polymers had some small amount of lower molecular weight polymer that could possibly be attributed to diblock copolymer, and it appeared that there was a greater fraction of low molecular weight polymer in the bulk-synthesized polymer. Furthermore, the bulk-synthesized polymer had a higher molecular weight fraction as well. However, overall the results were inconclusive.

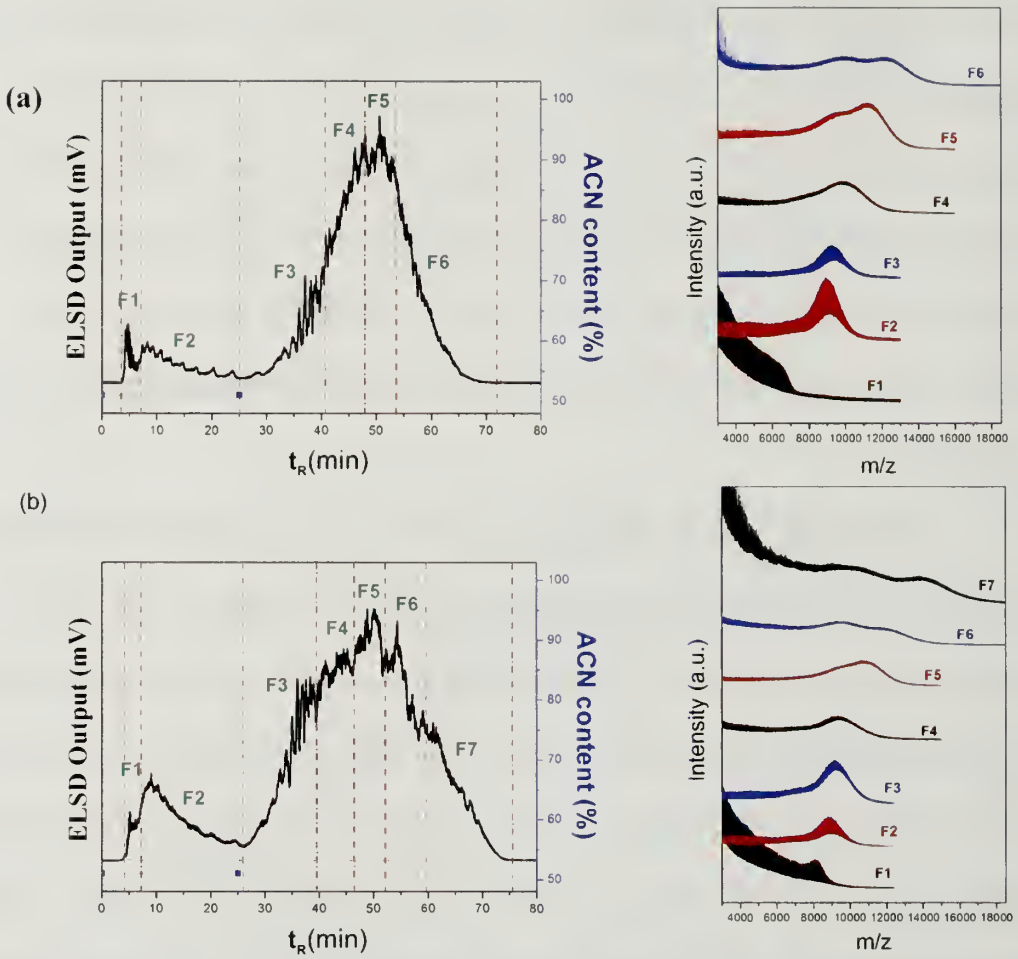

Figure 4.11. LCCC analysis on left and MALDI-Tof analysis on right. **(a)** Solution-synthesized PLA-PEO-PLA. **(b)** Bulk-synthesized PLA-PEO-PLA.

Since we can neither prove asymmetric triblock copolymers are present, nor can we directly synthesize them, we chose to model the most extreme case of a highly asymmetric triblock (effective diblock copolymer) with actual diblock copolymer. Both PLLA-PEO and PRLA-PEO diblock copolymers were synthesized using a poly(ethylene glycol) monomethyl ether and were then combined with a solution-synthesized triblock copolymer by dissolving in THF to ensure good mixing and precipitation in hexanes. We expected the percentage of effective diblock copolymers contaminants to be small so the

mixtures were prepared with small amounts of diblock content (5 wt% diblock: 95 wt% triblock and 10 wt% diblock: 90 wt% triblock). The molecular weight distributions of the mixtures were evaluated with GPC, and although one might expect to see a bimodal distribution because two polymers with different molecular weights were present, that was not the case as evidenced in Figure 4.12. The actual difference in molecular weight between diblock and triblock copolymer was approximately 2.5 kDa and was not significant within the resolution of our GPC setup. So, although there was a slight broadening in the distribution on the lower molecular weight side of the peak, the PDI was still narrow (PDI = 1.10). The broadening on the lower molecular weight side was consistent with the broadening seen in the bulk-synthesized polymers and supported the thought that effective diblock copolymers were present (Figure 4.2). However, there was also some broadening on the higher molecular weight end of the bulk-synthesized polymers as compared to the solution-synthesized polymers. This may suggest that in addition to chain trans-esterification reactions that shorten PLA endblocks, there may also be some reactions that lengthen PLA endblocks as was shown in the illustration in Figure 4.10, in which one chain end is lengthened while the other is shortened. The higher molecular weight broadening was much slighter than the lower molecular weight broadening, and thus we mainly focused on the presence of effective diblock copolymers.

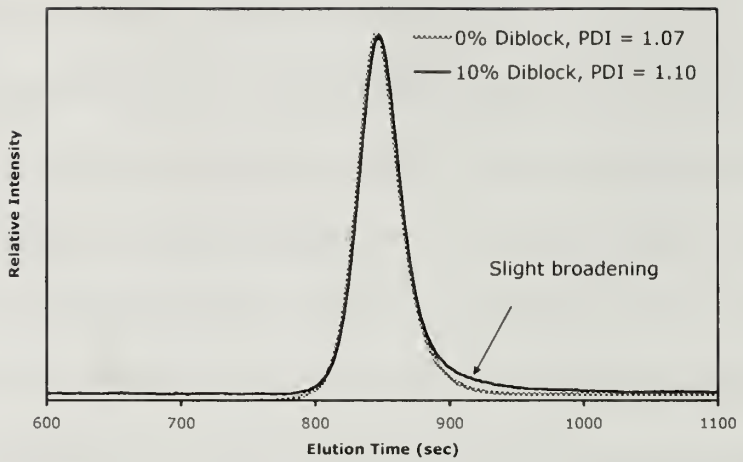

Figure 4.12. GPC chromatogram of R-triblock and mixed R-triblock/diblock copolymers.

The mixed diblock/triblock copolymers were used to form 20 wt% hydrogels, and the mechanical properties were probed with rheology. Results for the semi-crystalline L-polymer gels are in Figure 4.13, while the amorphous R-polymer gels are in Figure 4.14. For both sets of polymers, as diblock copolymer was added the moduli decreased, as expected. More specifically, the storage modulus at 100 Hz decreased from 39.3 to 23.7 kPa when 10% diblock was added in the L-series, and the decrease in the R-series was much more dramatic starting at 22.4 kPa and decreasing to 5.4 kPa when 10% diblock was added. While there was only a slight measured effect on modulus with increasing diblock in the L-series, we believe this is in agreement with our previous work that crystallization within the hydrophobic micelle cores increases the network stability. So, while the lifetime of the junctions or the number of junctions may have slightly decreased, the strength of the associated crystallites counteracted this to ultimately maintain longer relaxation times. The two opposing forces led to a slightly softened hydrogel, but the storage modulus still remained greater than the loss modulus over the entire frequency range and the moduli remained fairly frequency independent.

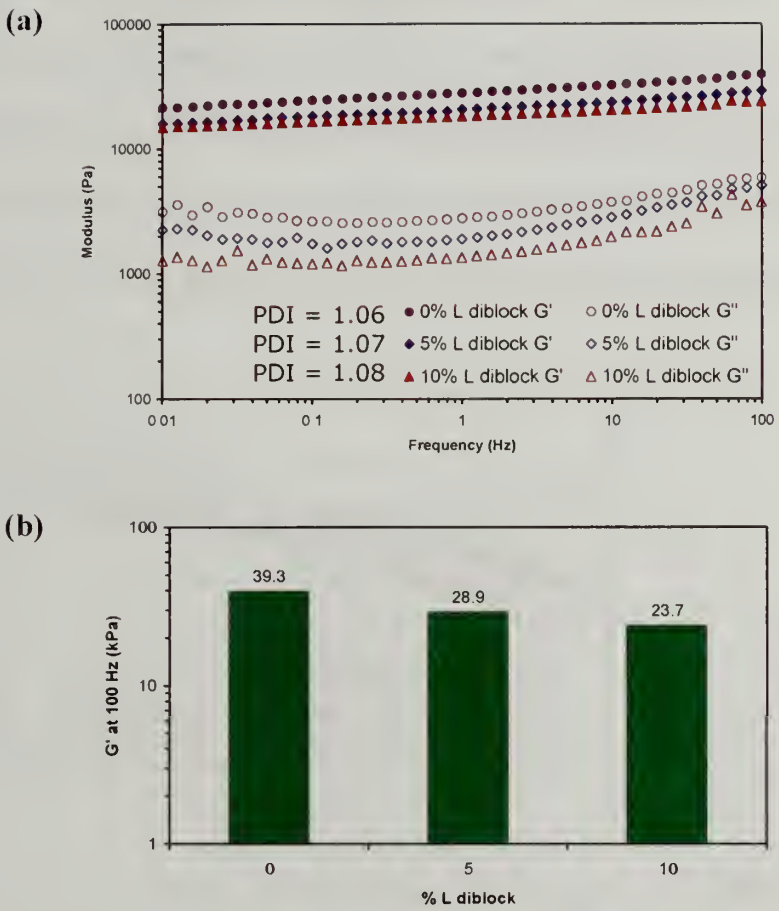

Figure 4.13. Mechanical properties of L triblock/diblock mixed systems. (**a**) Rheology of L-gel with 5 and 10 wt% diblock added. (**b**) Comparison of G' at 100 Hz.

In contrast, the amorphous R-polymer hydrogels were greatly affected by the incorporation of diblock copolymer. The storage modulus was reduced by almost an order of magnitude when going from 0% added diblock to 10% added diblock (G' at 100 Hz was 22.4 and 5.4 kPa, respectively). Furthermore, the system transitioned from a gel-like material to a viscoelastic fluid-like material with a crossover between G' and G'' in the mid-frequency range as diblock copolymer was added. These findings confirmed that diblock copolymer or effective diblock copolymer within an associative triblock copolymer hydrogel directly impacted the average relaxation time of the network

junctions. Interestingly, the observed mechanical changes for systems with added diblock were very similar to those seen in the bulk-synthesized polymer hydrogels. Overall the data supported that the most likely cause for the observed differences between bulk- and solution-synthesized triblock copolymers was caused by highly asymmetric triblock copolymers that may act as effective diblock copolymers.[130]

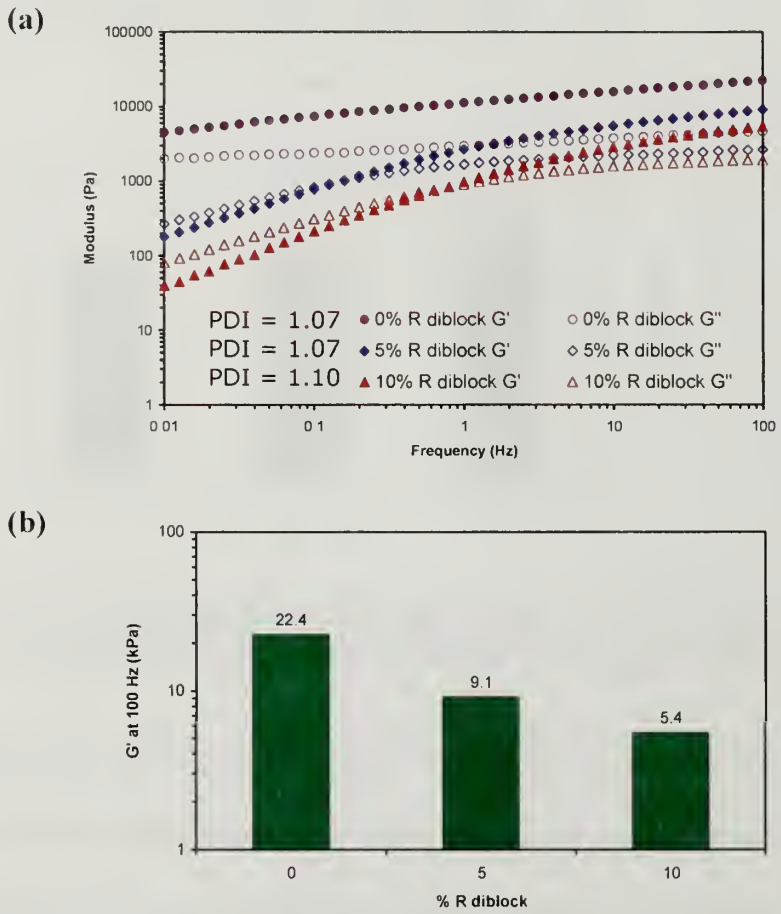

Figure 4.14. Mechanical properties of R triblock/diblock mixed systems. (**a**) Rheology of R-systems with 5 and 10 wt% added diblock. (**b**) Comparison of G' at 100 Hz.

The PDI's for the mixed systems are also listed in Figures 4.13 and 4.14 and even when 10% diblock copolymer was added, the PDI remained relatively narrow (PDI ≤ 1.10) compared to polymers synthesized by bulk polymerization indicating that the bulk-

synthesized samples may have had even greater amounts of effective diblock copolymer than was studied. To consider this possibility, higher concentrations of diblock copolymer contaminants were explored. We also wished to see if additional diblock copolymer would affect the overall crystallinity in the L-polymers. Both crystalline and amorphous diblock/triblock copolymer mixtures were made with the following incorporation of diblock (by weight): 10%, 20%, 30%, and 40%. The mixed systems' polydispersity was probed with GPC for both crystalline and amorphous systems, and despite having a large amount of diblock copolymer, the PDI's still remained relatively low (PDI $\leq$ 1.15). This again demonstrated that GPC could not help to determine if these types of contaminants were present. The mixed polymers were then used to form hydrogels and tested with rheology and XRD where applicable.

It was originally hypothesized that diblock copolymer mixed within triblock copolymer would lead to greater chain mobility, faster crystallization, and longer PLLA mean crystallite lengths. This explanation would account for the different crystallite lengths measured between the bulk- and solution-synthesized polymers (refer back to Figure 4.4). However, the XRD of the crystalline mixed systems in Figure 4.15 showed there was little change in the mean crystallite length as more diblock copolymer was added and that the solution-synthesized mixed systems still had a much shorter crystallite length than the bulk-synthesized polymers, discrediting our original hypothesis. Rather, we believe that after polymerization from the bulk when the polymer was dissolved in THF not all of the crystalline PLLA aggregates were fully dissolved. This is more likely the reason why bulk-synthesized polymers have a sharper PLLA peak. Rheology of the crystalline diblock/triblock mixtures showed that incorporating diblock copolymer in the

triblock had little effect on the mechanical properties of the hydrogel (Figure 4.16a). This again demonstrated that the crystallinity within the system helped to make more permanent crosslink points to make a stiff hydrogel. It was expected that by incorporating more diblock into the amorphous triblock copolymer systems, the effects would be much greater. While the results in Figure 4.16b showed that the lifetime of the network decreased with increasing amount of diblock, the new experiments took higher incorporation of diblock (30% and 40%) to show the same properties as the first tests (at 5% and 10% diblock, Figures 4.13 and 4.14). This indicated that there was variability between measurements and hydrogel processing conditions but was expected due to the transient nature of the network.

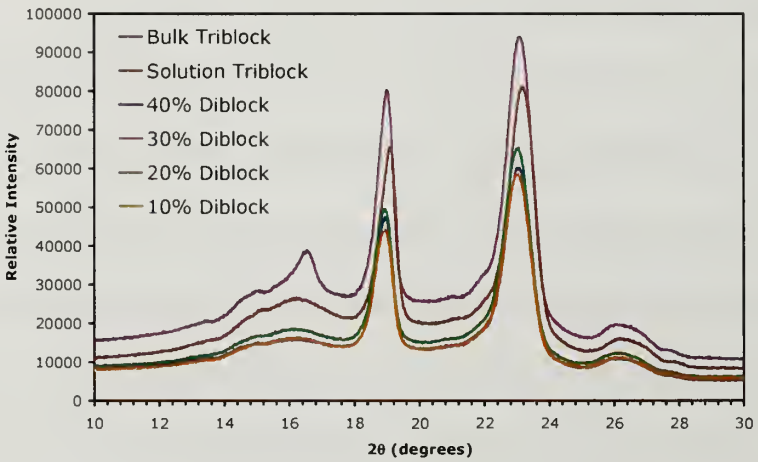

Figure 4.15. XRD of mixed bulk-synthesized triblock, solution-synthesized triblock, and mixed L-diblock/triblock systems.

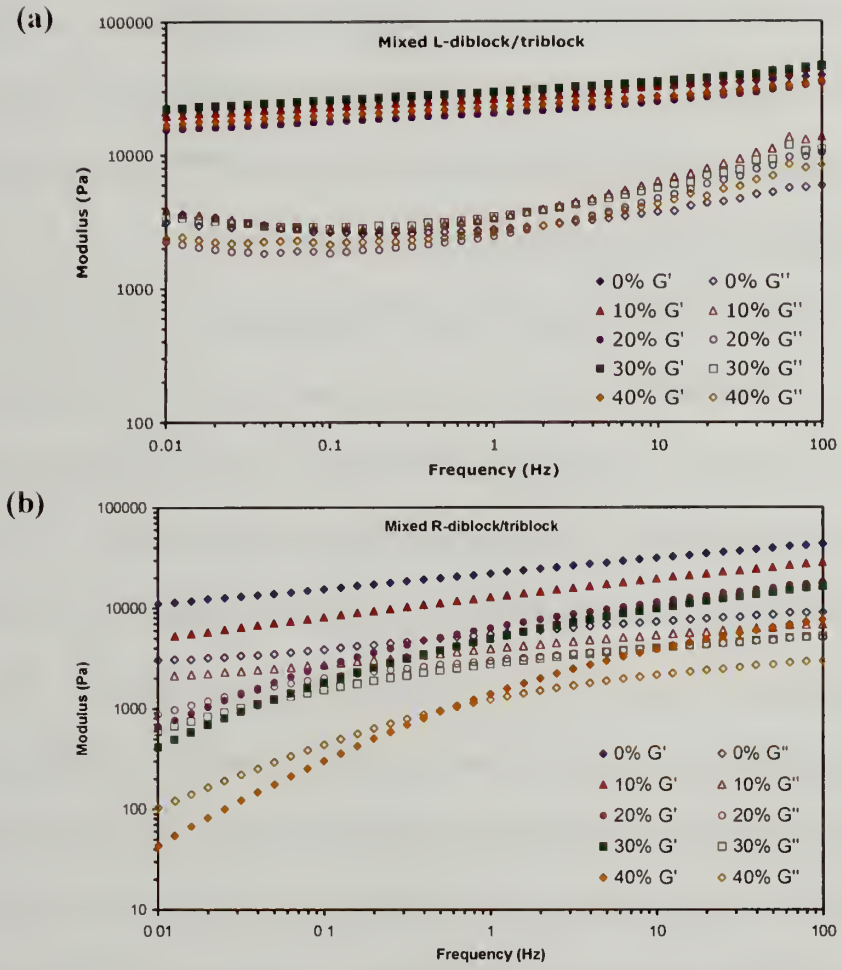

Figure 4.16. Rheology of mixed systems with higher diblock incorporation. (**a**) Mixed L-diblock/triblock. (**b**) Mixed R-diblock/triblock.

4.4.2. Homopolymer Contaminants – PEO and PLA

Although the presence of asymmetric triblock copolymers was the most likely cause for the change in mechanical properties when comparing bulk- to solution-synthesized polymers, we did not have the means to prove that this contaminant was present. Therefore other possible contaminants were investigated to see if they could account for the differences between the two polymerization methods. Some other possible contaminants besides effective diblock copolymer include PEO and PLA homopolymers. PEO may be present due to insufficient initiation, trans-esterification reactions on both ends of the growing polymer leaving very short PLA chain ends to give

"effective" PEO homopolymer, or PLA degradation/depolymerization can lead to "effective" PEO homopolymer. PLA homopolymer and/or cyclic oligomers may be present if there was degradation of the PLA chain ends[146-149] or if any water was present in the reaction mixture to initiate lactide polymerization.

The effects when incorporating PEO homopolymer within the triblock copolymer systems were studied first. Again, because crosslinks can only form through bridging of triblock copolymers, it was expected that adding PEO homopolymer would decrease the amount of these junctions and hence the stiffness of the hydrogel. PEO was mixed with both crystalline and amorphous triblock copolymer at 5 and 10 wt%, and the corresponding hydrogel (20 wt% solids) was probed using rheology. The data in Figure 4.17 showed that, as expected, the addition of PEO lowered the overall mechanical properties for both the crystalline and amorphous systems. However the effects were very small – the biggest change in modulus being a factor of 3. Perhaps if a greater amount of PEO were incorporated the effects would be greater. Of note, the amorphous systems began to display a crossover point (where $G' \approx G''$) when 10% PEO was incorporated, suggesting the lifetime of the network junctions was affected.

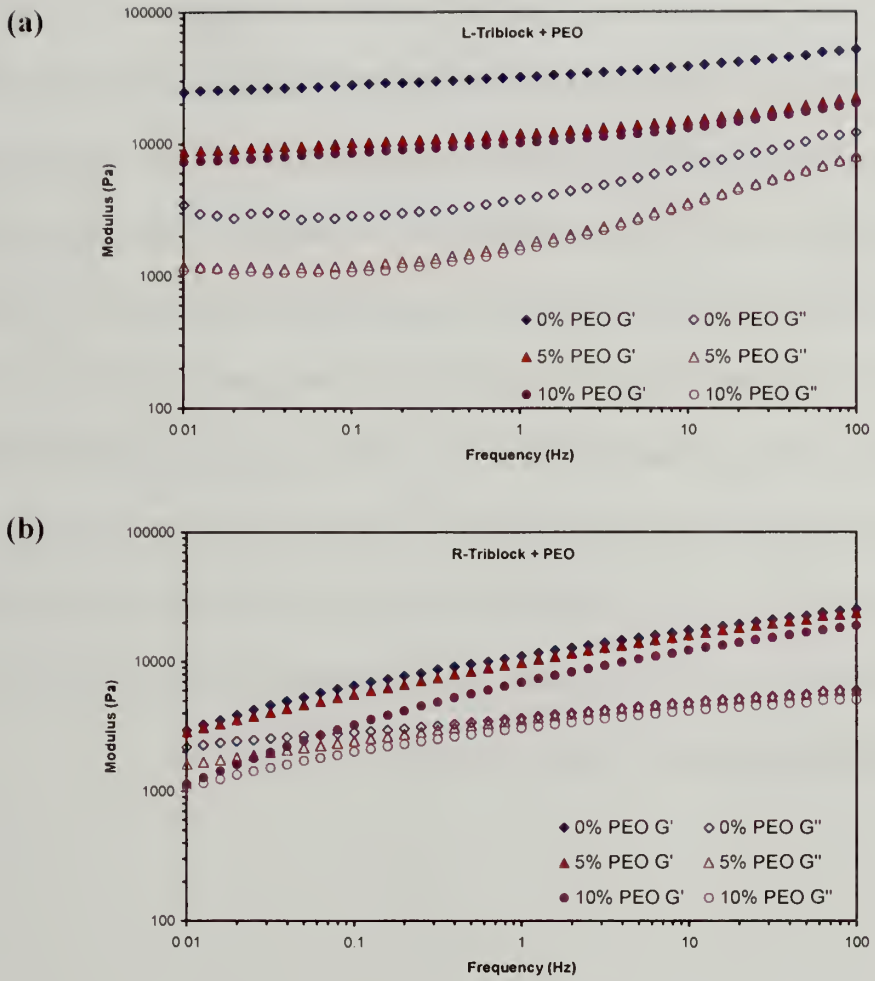

Figure 4.17. Rheology of mixed triblock/PEO Systems (**a**) L-triblock + PEO (**b**) R-triblock + PEO.

Finally, we explored the effects on properties when PLA homopolymer was mixed with PLA-PEO-PLA triblock copolymers. Low molecular weight amorphous PLA (M_n = 5100) and semi-crystalline PLLA (M_n = 3200) were synthesized and mixed with the corresponding triblock copolymer at 5 and 10 wt%. By adding PLA homopolymer we again expected fewer crosslinks in the network structure lowering the hydrogel's modulus. Figure 4.18 shows results for both the semi-crystalline and amorphous hydrogels at 20 wt%. In the crystalline gels, adding PLLA homopolymer had

little effect on the mechanical properties. Although the number of crosslinks lowered, the PLLA homopolymers likely could also crystallize within the micelle cores to stabilize the junctions and help maintain long-lived crosslinks and a stiff gel. For the amorphous hydrogels the overall stiffness decreased and the relaxation times appeared to decrease. These results were similar to what was measured when adding PEO homopolymer, again reinforcing the thought that the crosslink density decreased. Interestingly, the amorphous mixed PLA homopolymer/PLA-PEO-PLA triblock copolymer systems formed hydrogels that were white and opaque, where those without PLA homopolymer were fairly transparent. This color change was likely due to the increased amount of hydrophobic polymer in the system and indicated that the PLA polymer was not fully soluble in water causing large aggregates to phase separate and scatter light.

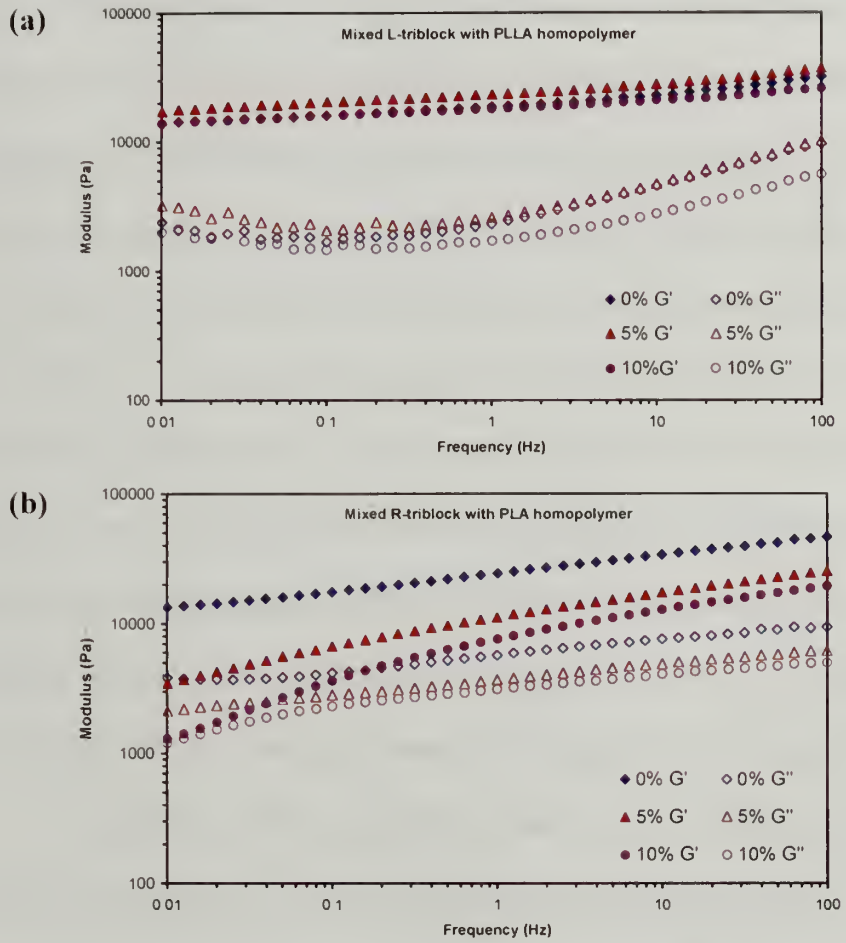

Figure 4.18. Rheology of triblock/PLA polymer hydrogels. (**a**) L-triblock + PLLA. (**b**) R-triblock + PLA.

4.5. Conclusions

PLA-PEO-PLA hydrogels' mechanical properties were influenced by the polymer synthetic technique. Initial experiments on mechanical properties of bulk-synthesized polymer hydrogels showed a dependence on crystallinity and hydrophobic PLA length. The newer solution-synthesized polymer hydrogels displayed the same tendencies, but overall had higher moduli than the bulk-synthesized counter-parts. Investigations using XRD showed that bulk-synthesized L-polymers had longer crystallite lengths than solution-synthesized polymers. This observation led to the hypothesis that solution-synthesized polymer hydrogels had shorter crystallite lengths and correspondingly a

greater number of network junctions and higher modulus. After further exploration, we found there was no such correlation between mean crystallite length and hydrogel modulus. Furthermore, the observed differences between the two synthetic techniques was consistent with the amorphous triblock copolymers, confirming that changes in crystallization was not the underlying cause of mechanical discrepancies. Differences in PDI were the only other measurable changes between the two synthetic techniques. To better understand the effects of the molecular weight distribution, polymers with different molecular weights were mixed and used to form hydrogels. These experiments illustrated that two systems with different PDI's displayed the same mechanical properties. So, neither crystallinity nor variations in the molecular weight distribution alone accounted for the increased mechanical properties of the solution-synthesized polymer hydrogels versus the bulk-synthesized polymer hydrogels.

We thus studied how contaminants within an associative network can influence the mechanical properties and how the contaminants may relate to the measured differences between bulk- and solution-synthesized polymers. We believe highly asymmetric triblock copolymers were present in the bulk-synthesized polymers because of more prevalent side reactions at elevated temperatures. These asymmetric triblock copolymers may effectively act as diblock copolymers to reduce the number of physical crosslinks, lower the lifetime of the crosslink, or both. The presence of asymmetric triblock copolymers was modeled with diblock copolymers and the most significant effects on mechanical properties were seen in the amorphous systems – even a small amount of diblock contaminant greatly changed the modulus of the physical hydrogel. Other possible contaminants that would lead to fewer bridges in the network were also

studied, including PEO and PLA homopolymer. Similar to the systems incorporating diblock copolymer, the gel stiffness and junction lifetime lowered with the addition of the homopolymers contaminants for the amorphous systems, as expected. However, in general, the stiffness of the semi-crystalline systems was only slightly affected by all three different types of contaminants, which again emphasizes that crystalline regions in the micelle core have a large impact on mechanical properties. Ultimately, there could possibly be a mixture of all three possible contaminants due to side-reactions, but current characterization techniques are incapable of distinguishing them from triblock copolymer. Finally, this work highlights the limitations of GPC as a characterization technique for purity. Although we mixed two different polymers (triblock and diblock), the molecular weight differences were small enough that a low PDI was measured. So, even though the bulk-synthesized polymers had narrow distributions, a contaminant was likely present and affecting the hydrogel properties. This motivates the exploration of more sophisticated polymer characterization methods so that one can better design the desired material properties.

CHAPTER 5

PHOTOCROSSLINKED PLA-PEO-PLA HYDROGELS

5.1. Introduction

We have demonstrated that physically crosslinked PLA-PEO-PLA hydrogel stiffness can be influenced by varying PLA block length, PLA crystallinity, synthetic technique, and by incorporating contaminants. Using these chemical modifications, the storage modulus was tuned from 0.3 to 50 kPa, and this range addresses a number of soft tissues including bovine brain and retinae,[34] some cardiovascular tissue,[35, 37] canine lung tissue,[40] and pig kidney tissue.[41] However, the crosslinks in these systems are brought about by hydrophobic interactions and are purely physical. The corresponding micellar network structure is dynamic, and the crosslinks are reversible because there are no covalently tethered junction points. Since the crosslinks are reversible, when PLA-PEO-PLA physical hydrogels are introduced to a highly aqueous environment they can continue to swell until they convert from a gel to a sol, or they precipitate out of solution. At this point, the gels lose their mechanical integrity and can no longer act as a cellular support.

To address the problem of reversible crosslinks, we have modified PLA-PEO-PLA triblock copolymer endgroups with a chemically crosslinkable moiety. The modified triblock copolymer was self-assembled into a physical hydrogel, and Ultra-Violet (UV) radiation initiated a photocrosslinking reaction within the PLA micellar cores, converting physical crosslinks to chemical crosslinks. By using this technique we hoped to maintain the self-assembled structure, but lock the structure in place so that the crosslinks remained intact when swollen in excess solvent. This chapter describes the

swelling, degradation, and mechanical properties of the photocrosslinked hydrogels, and discusses important considerations in data analysis methods.

5.2. Synthetic Methodology

Amorphous PLA-PEO-PLA (R triblock) was solution-synthesized as previously described in Section 2.3 and reacted with excess acryloyl chloride using excess triethyl amine as a basic catalyst to ensure quantitative end-group conversion. The calculated conversion initially was well over 100% (determined by comparing the ^{1}H NMR integration of acrylate protons to the methylene protons of the PEO midblock). We believe PLA partially hydrolyzed and small PLA oligomers were functionalized with the acrylate moiety, accounting for the large calculated conversion. Also, comparing the integrations of acrylate protons on the endgroups to the methylene PEO protons in the main chain can lead to large inaccuracies, since this compares a very small number to a very large number. To account for these issues, the synthesis and characterization were modified as described below.

PLA-PEO-PLA (1 equiv) was dissolved in toluene and attached to a Dean-Stark trap with a condenser. The solution was then azeotropically distilled to remove water and prevent ester hydrolysis. The solution was cooled to room temperature and placed in an ice bath. Triethylamine (10 equiv) was added dropwise to the solution, followed by dropwise addition of acryloyl chloride (10 equiv), and the reaction was stirred overnight. Triethylamine/hydrochloric acid salt was removed by filtration, and the toluene was evaporated. The resulting product was dissolved in tetrahydrofuran, passed through a plug of basic alumina, precipitated in hexanes, and dried under vacuum. Conversion was determined by comparing the integration of the acrylate protons to the methylene protons

closest to the ester (protons a and c as labeled in Figure 5.1) since the number of protons is much more comparable (6:4). The calculated conversion was just slightly over 100% and the calculated degree of polymerization for PLA (comparing PLA methyne protons to PEO methylene protons) slightly decreased from that of the initial triblock copolymer. Both calculations suggested that there was still some hydrolysis that occurred during reaction, but all the polymer was end-functionalized and the polydispersity index remained very narrow.

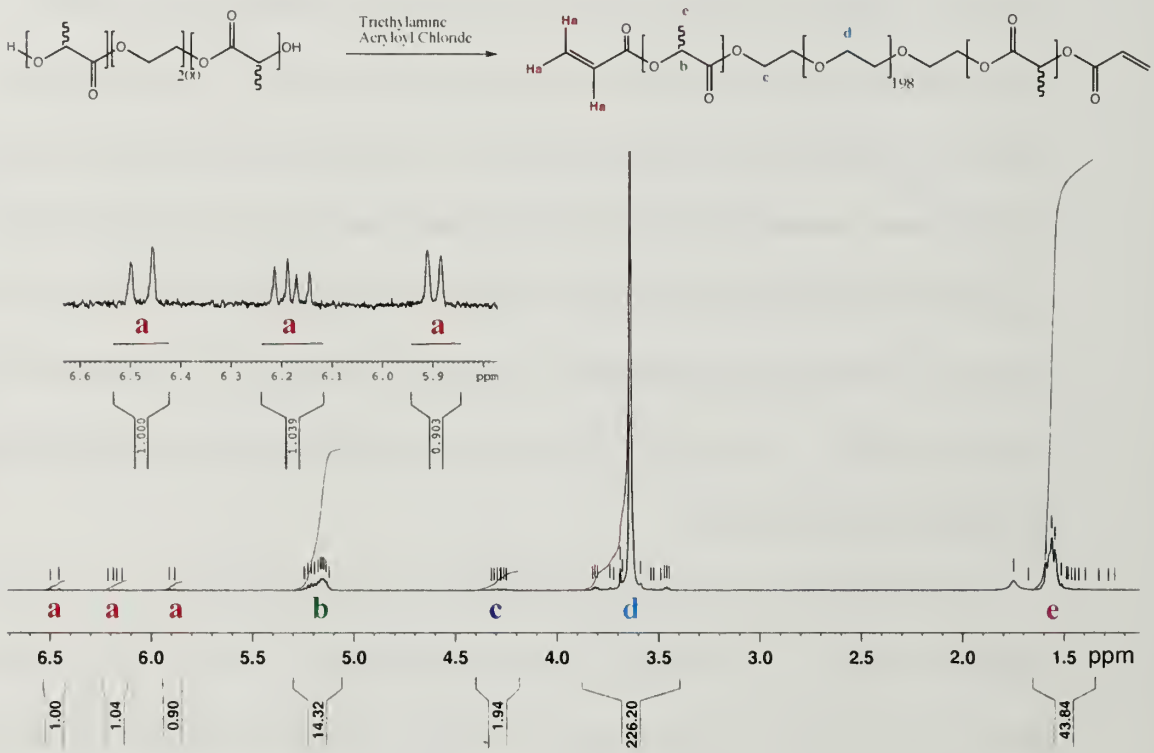

Figure 5.1. ^{1}H NMR of acrylate functionalized PLA-PEO-PLA. All appropriate protons are labeled.

To prepare photocrosslinked hydrogels, end-functionalized PLA-PEO-PLA was weighed into the wells of a 48-well cell culture plate, heated to 80°C under vacuum for 1.5 hours to melt a film, and then cooled to room temperature. The photoinitiator solution was prepared by dissolving Irgacure 2959 (Ciba) in phosphate buffered saline

(PBS) solution (pH = 7.4) to a final concentration of 0.05% (w/v). The initiator solution was added on top of the polymer film and allowed to swell into a physical hydrogel for 3 to 4 days. Once fully swollen, the plate was irradiated with long-wave UV (~365nm) for 5 minutes to initiate the photocrosslinking reaction. The plate was then flipped upside-down and irradiated for 5 more minutes (height of the gel was approximately 10 mm). The hydrogel concentrations were varied (10, 15, 25, 35, 45% w/v) by adjusting the amount of polymer added to the well and maintaining a constant volume of added photoinitiator solution.

5.3. Physical Characterization of Photocrosslinked PLA-PEO-PLA Hydrogels

5.3.1. Degradation and Swelling

The photocrosslinked hydrogels were removed from the 48-well plate, transferred to a 24-well plate, immersed in PBS at 37°C, and swollen for extended periods of time. The wet weight (W_w) and dry weight (W_d, after drying in a vacuum oven to remove all water) were measured at various time points and used to calculate the swelling ratio, Q:

$$Q = \frac{W_w - W_d}{W_d}$$

Degradation was characterized by measuring the initial weight of the dry polymer before degradation (m_{pi}) and the mass of the dried hydrogel after a defined swelling/degradation time (m_p) to determine mass loss:

$$Mass\ Loss = \frac{m_{pi} - m_p}{m_{pi}}$$

The swelling solution was exchanged with fresh PBS every 3-4 days to remove degradation products (lactic acid, PLA oligomers, PEO, and polyacrylic acid) and

maintain a constant pH of ~7. The photocrosslinked hydrogels remained mechanically intact when initially swollen and for extended periods of time; conversely, physical hydrogels swelled the excess solution and converted from a gel to a sol within an hour, making Q and mass loss measurements impossible.

The swelling ratio of the photocrosslinked PLA-PEO-PLA gel was initially ~ 3.5 (prepared at 25% w/v) and increased exponentially with time to ~ 25, as shown in Figure 5.2. After approximately 52 days, the gels were very swollen and soft, difficult to handle, and Q could no longer be accurately measured. The cleavage of ester bonds in PLA can be described by a pseudo-first order equation, since the water content and pH remain approximately constant with time, leading to an exponential decay of ester concentration versus time.[153, 154] Since crosslinks could only be broken by degradation of ester bonds, as the ester was hydrolyzed, the cross-link density (ρ_c) also decreased exponentially. The exponential decrease in ρ_c was reflected well in the swelling data, as Q is inversely proportional to ρ_c and corroborates the assumption of first order kinetics.[155]

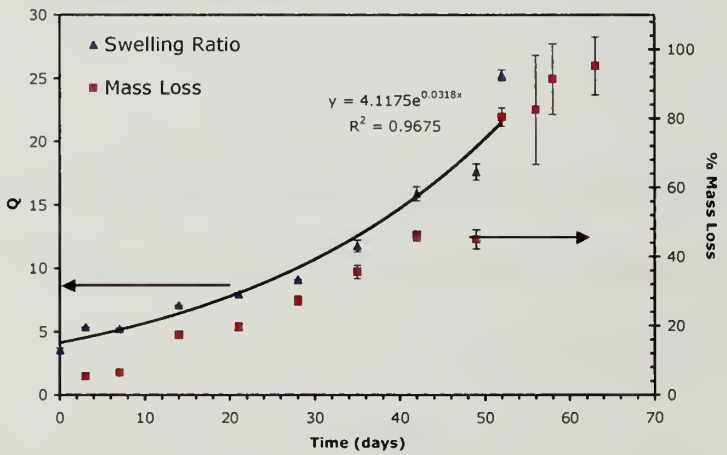

Figure 5.2. Swelling and degradation of photocrosslinked 25% w/v PLA-PEO-PLA in PBS. Changes in swelling ratio (Q) and % mass loss were measured. Q increases exponentially with time as shown by the black fitted line.

The mass loss also increased with degradation time as expected. However, the kinetics were not as easily explained as with the swelling ratio. While the ester hydrolysis increased exponentially, as already described, this was not directly reflected in the mass loss data since the hydrolysis of an ester bond does not necessarily release a molecule from the network. When describing Q, a broken ester bond breaks a crosslink point (or breaks an ineffective loop in the system), making hydrolysis and Q proportional. But in order to lose mass, hydrolysis needs to occur at two sites on the same chain - only in this way can PLA oligomer, lactic acid, or PEO be released. Therefore, the kinetics were much more complicated and showed variation from an exponential function. Also, the rate of mass loss sharply increased after approximately 52 days of degradation. This was attributed to the release of polyacrylic acid. As the system was photocrosslinked, a polyacrylate was polymerized with pendant PLA chains, leading to several crosslink sites on the polyacrylate backbone. Before the polyacrylate can be released all of these sites must be hydrolyzed, and this only occured when most of the ester linkages were hydrolyzed. At this point the polyacrylate was released and likely accounts for the sharp increase in mass loss.

The time for full degradation (63 days) was longer than reports of similarly crosslinked PLA-PEO-PLA hydrogels.[71, 73] This extended degradation time was likely due to differences in molecular weight and possibly due to the network structure. Most commonly, photocrosslinked hydrogels are made by crosslinking macromers that are fully soluble in water, leading to a random network structure. In our case, the polymer first self-assembled into a physical hydrogel with a micellar network structure where a PEO shell surrounds a hydrophobic PLA core. It is possible that water cannot as easily

access the ester linkages within this core as in a random network and the overall rate of hydrolysis would thus be slowed. While, this hypothesis was not quantitatively tested, the random network versus self-assembled network led to very different gels qualitatively. In Figure 5.3a PLA-PEO-PLA was photocrosslinked from a physical hydrogel, while in Figure 5.3b it was photocrosslinked from a solution of THF, dried down, and then soaked in PBS solution. The former led to a rubbery material while the latter led to stiff particulates that did not swell in water. Regardless of the cause, the extended degradation time is advantageous for tissue engineering, as this can allow the cells longer time to develop into functional tissue.

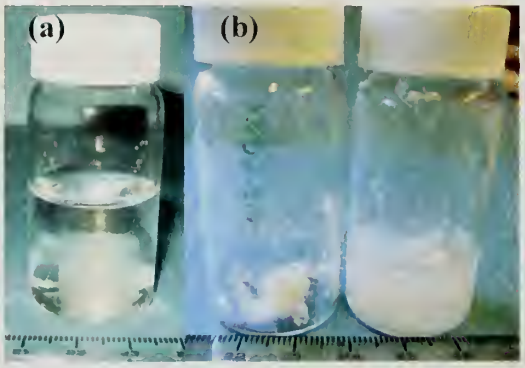

Figure 5.3. Photocrosslinked PLA-PEO-PLA hydrogels. (**a**) Photocrosslinked after self-assembled into physical hydrogel. (**b**) Photocrosslinked from THF solution, dried network is on the left and the network with very little swelling and large amounts of particles on the right.

5.3.2. Mechanical Properties of Photocrosslinked Hydrogels in Compression

Since the success of tissue engineering scaffolds is influenced by their mechanical properties, the photocrosslinked PLA-PEO-PLA hydrogels were evaluated in compression as a function of degradation time and hydrogel concentration. The rough top surface of the gels was cut with a razor blade to give a cylinder approximately 7.9 mm in height and 9.5 mm in diameter (all sample dimensions were measured prior to

compression testing). The gels were compressed using an Instron with flat plates at a rate of 1 mm/min (unless otherwise noted). Raw data (force vs. displacement) was converted to engineering stress and strain (or extension ratio) by using the initial dimensions of the gel. The stress versus strain curves showed the typical non-linear behavior exhibited by soft rubbery materials[156] and sample data is shown in Figure 5.4 for changes in degradation time, while Figure 5.5 shows changes with varying the concentration (the insets zoom in to a lower stress region).

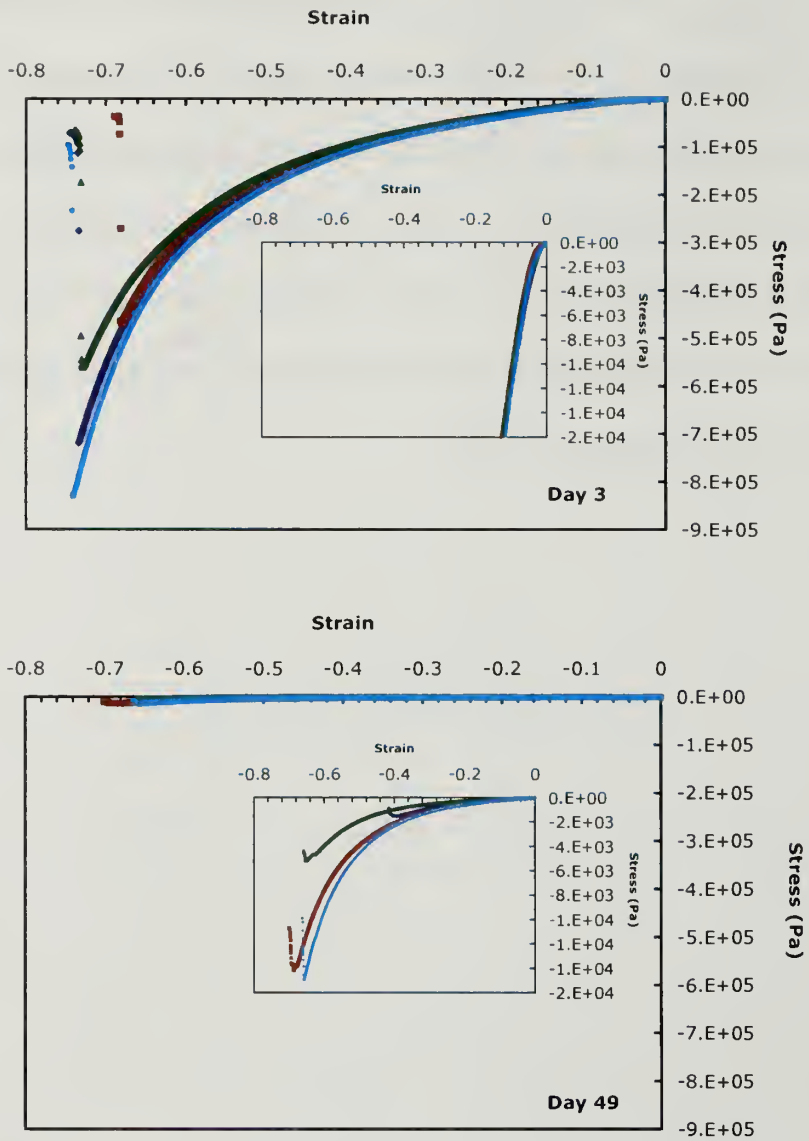

Figure 5.4. Stress versus strain for degraded photocrosslinked PLA-PEO-PLA hydrogels. (**a**) After 3 days of degradation. (**b**) After 49 days of degradation. Insets highlight a smaller stress region.

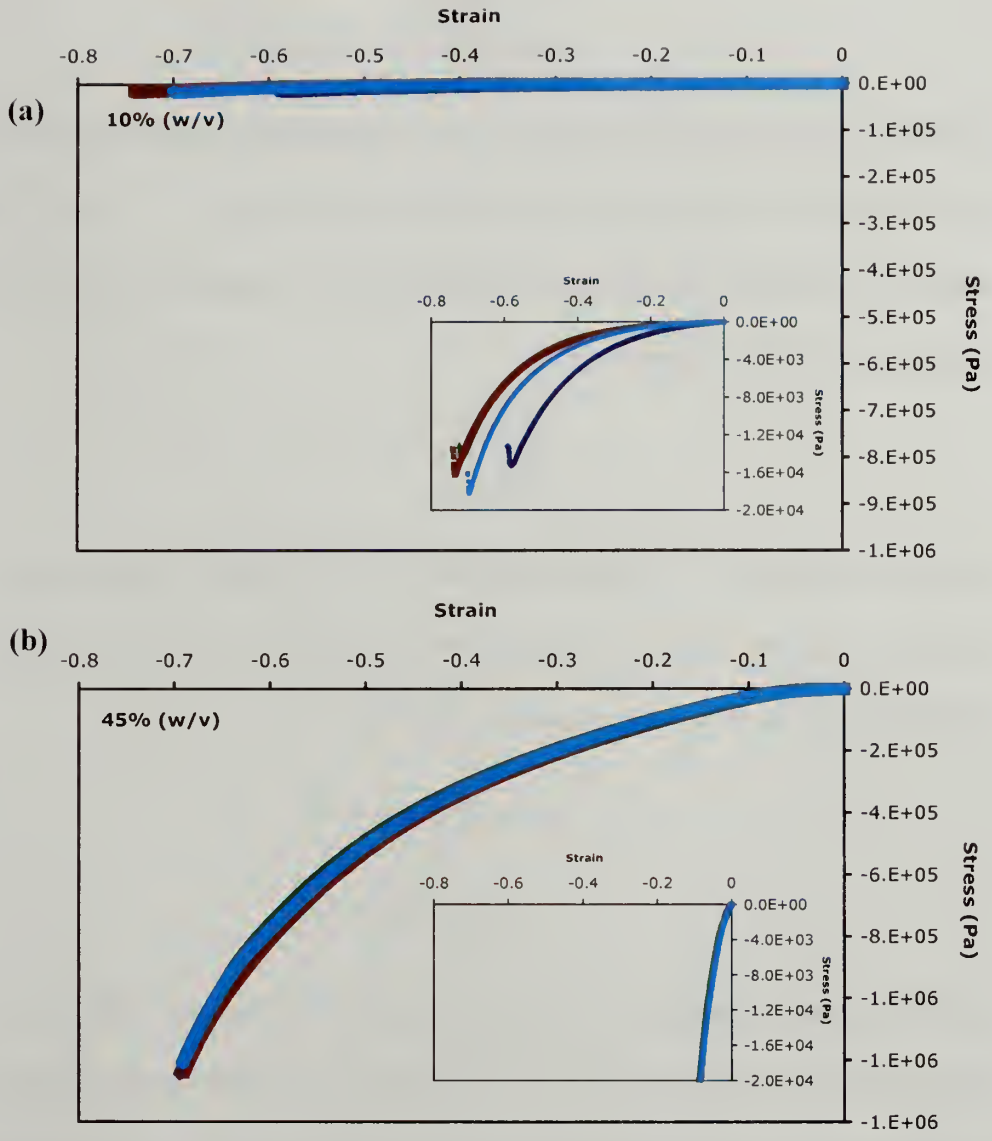

Figure 5.5. Stress versus strain for varying concentrations of photocrosslinked PLA-PEO-PLA hydrogels. (**a**) 10 wt% PLA-PEO-PLA. (**b**) 45 wt% PLA-PEO-PLA.

Qualitatively, the hydrogels softened as they degraded or as the concentration was decreased, but to quantitatively describe these effects a Neo-Hookean constitutive relationship for rubbers was used. In this model, the specific form of the strain energy function (U) is dependent on the first invariant of the deformation tensor (I_1) by a factor of C_1:

$$U = C_1(I_1 - 3)$$
$$U = C_1\left(\lambda_1^2 + \lambda_2^2 + \lambda_3^2 - 3\right)$$

where λ_i is the extension ratio in the i-direction (length over initial pre-stressed length) and is related to the strain (ε) with the following relation $\lambda = \varepsilon + 1$. For the case of uniaxial compression and assuming the material is incompressible the following simplifications can be made:

$$\lambda_1^2 = \lambda^2,\ \lambda_2^2 = \lambda_3^2 = \lambda^{-1}$$
$$\lambda_1^2\lambda_2^2\lambda_3^2 = 1$$

By substituting the above simplifications into the strain energy function and differentiating with respect to the extension ratio, the Neo-Hookean Constitutive relationship for stress (σ) is expressed as follows:

$$U = C_1\left(\lambda^2 + \frac{2}{\lambda} - 3\right)$$
$$\sigma = \frac{\partial U}{\partial \lambda} = 2C_1\left(\lambda - \frac{1}{\lambda^2}\right)$$

Where the single parameter C_1 is defined as the half of the shear modulus, G ($G = 2C_1$). This relationship can also be derived using a statistical thermodynamic approach in which the distribution of end-to-end distances between crosslinks is assumed to be Gaussian.[157-159] A typical stress versus strain curve and a fit for the data using the Neo-Hookean relationship is shown in Figure 5.6. The fit described the non-linear behavior of the hydrogel very well even at large strains and implied that the distribution of chains in the network was Gaussian and that engtanglements and loops had little contribution to the overall network.

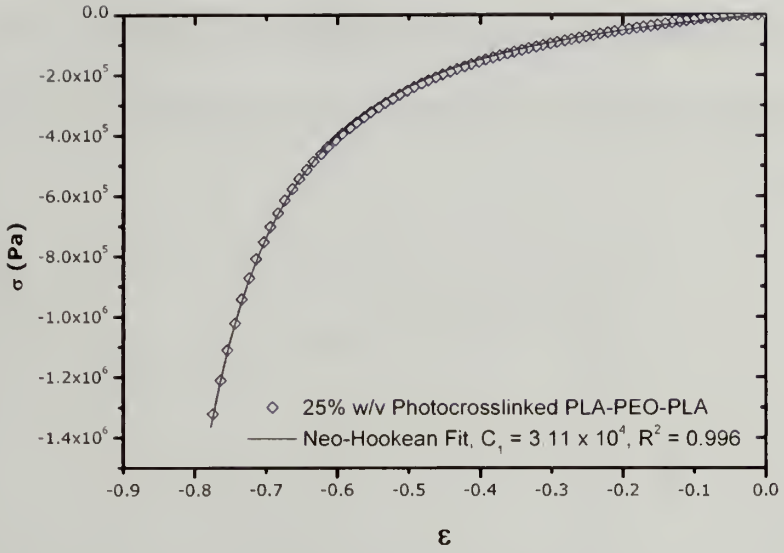

Figure 5.6. Stress vs. strain for 25 wt% photocrosslinked PLA-PEO-PLA hydrogel.

By using the Neo-Hookean fit, we observed the change in shear modulus as the hydrogels were degraded in PBS at 37°C in Figure 5.7. Before degradation the 25% (w/v) hydrogel had a modulus of approximately 64 kPa, but this value exponentially decreased with degradation time until a sharp decrease in modulus was observed after approximately 35 days. As already discussed, the hydrolysis of ester linkages leads to an exponential decrease in ρ_c and an increase in Q as they are inversely proportional; conversely, the modulus is directly proportional to ρ_c ($G \sim \rho_c v^{1/3}$).[155] Therefore, the exponential decrease of the shear modulus shown in the data corroborated the swelling data and again confirmed pseudo-first order kinetics for PLA hydrolysis. However, at a critical time point (in this case ~35 days) there was a sharp decrease in modulus from approximately 7 kPa to 0.15 kPa which would imply a loss of network percolation. However, swelling ratios were measured well past 35 days, and the materials, while very soft, could be handled and still appeared to be crosslinked hydrogel networks that had not

lost percolation. These combined observations suggest that at the time point of 42 days, we may have been probing a different mechanical parameter other than modulus while subjecting the materials to compression, such as a fracture toughness or strength of the hydrogel.

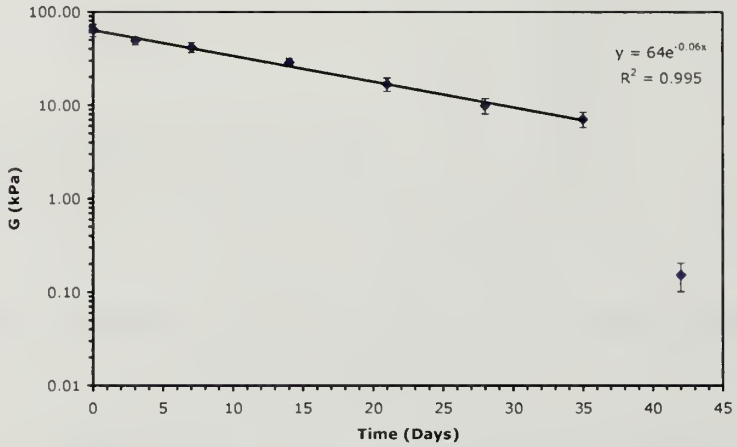

Figure 5.7. Shear modulus as a function of degradation time.

The attainable range of gel stiffness was probed by varying the concentration of the polymer hydrogels. Below 10% the material did not gel, and higher than 45% produced very brittle materials; we thus tested the following concentrations: 10, 15, 25, 35, and 45% w/v. With these gels the shear modulus was as low as 1.6 kPa and as high as 133 kPa, and we observed a linear dependence of modulus on concentration (Figure 5.8). The linear dependence was anticipated because of the micellar network structure. When forming the physical hydrogel, the network junctions were formed through hydrophobic interactions within the micelle cores; therefore, the number of network junctions was the same as the number of micelles. For these micelles to form, a critical aggregation number (N_{agg}) of polymer chains was necessary. Assuming the critical N_{agg} remained constant, as the concentration and number of chains increased linearly, so did

the micellar junction points and the crosslink density. Since the modulus is proportional to ρ_c, as ρ_c increased linearly so should the modulus (assuming that the volume fraction component of modulus had little impact on the modulus). The agreement between the data and the theory based on the argument above implied that the photocrosslinking process did effectively lock the self-assembled physical hydrogel structure in place.

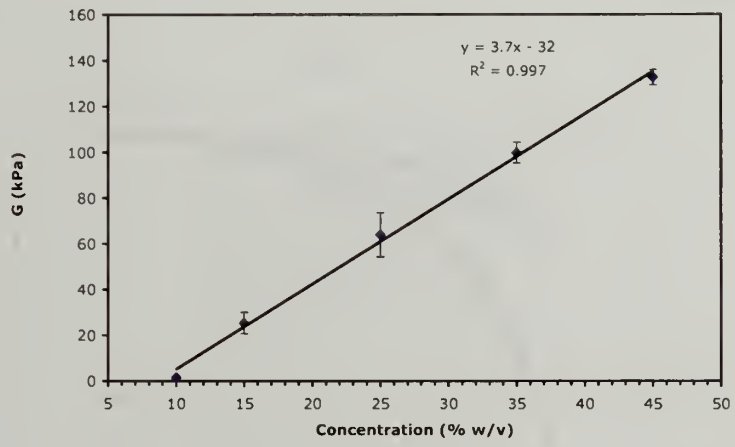

Figure 5.8. Shear modulus with varied polymer hydrogel concentration.

We revisited the impact of first forming a physical hydrogel before photocrosslinking versus photocrosslinking in a solvent in which PLA-PEO-PLA was soluble. Previously, an unstructured gel crosslinked in THF was qualitatively compared to a self-assembled physical hydrogel in PBS that was photocrosslinked. Since THF may have acted as a solvent for the well-plates in that case, PLA-PEO-PLA was photocrosslinked in a solution of N,N-dimethyl formamide (DMF) in a glass vial. This sample was then swollen in PBS for three days and compared to a hydrogel that was first formed into a physical gel before photocrosslinking. Figure 5.9 shows the stress-strain curves of each hydrogel while under compression. By fitting these with a Neo-Hookean model, the gel crosslinked in DMF had G = 13.9 kPa, while the self-assembled hydrogel

crosslinked in PBS had G = 55 kPa. So, the self-assembled structure has a modulus that is an order of magnitude greater than the unstructured gel. Furthermore, the hydrogel crosslinked in DMF had Q = 7.5 after swelling in PBS for 3 days, while the self-assembled photocrosslinked gel had Q = 5.3. These differences in stiffness and Q are likely directly caused by the differences in structure and leads to the increased degradation time.

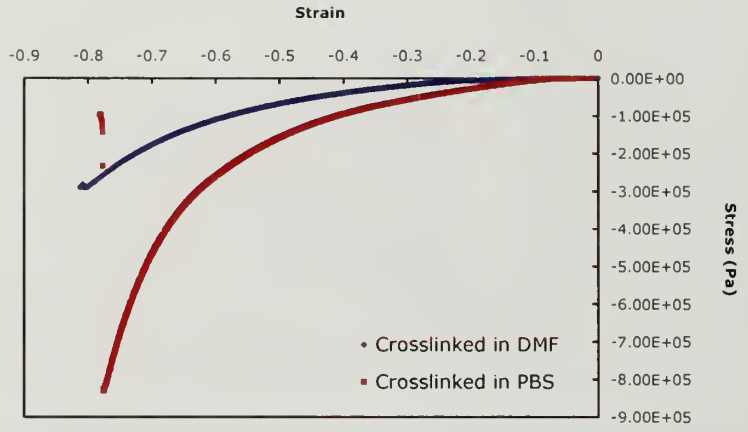

Figure 5.9. Comparing strain-stress curves for hydrogels crosslinked in DMF and PBS.

5.4. Important Considerations for Data Analysis

5.4.1. Influence of Assumed Constitutive Equations on Mechanical Properties

All previous data was analyzed by applying a Neo-Hookean constitutive model for rubbers, but the data could also be fit using other models. The most commonly employed model is the Hookean constitutive relationship in which stress (σ) is related to strain (ε) by the elastic modulus (E) in the following manner: $\sigma = E\varepsilon$. Although this relation only holds for linear elastic materials at small strains, it is often used to fit the non-linear curves of hydrogels.[160, 161] Alternatively, a two-parameter Mooney-Rivlin constitutive relationship for rubbers can be used to fit hydrogel data.[162, 163] In this model,

the strain energy function is dependent on both the first and second invariants of the deformation tensor. As with the Neo-Hookean model, uniaxial compression and incompressibility is assumed to simplify the equation. By differentiating the strain energy function with respect to the extension ratio, an expression for stress can be derived as shown below:

$$U = C_1(I_1 - 3) + C_2(I_2 - 3)$$
$$U = C_1\left(\lambda_1^2 + \lambda_2^2 + \lambda_3^2 - 3\right) + C_2\left(\lambda_1^2\lambda_2^2 + \lambda_1^2\lambda_3^2 + \lambda_2^2\lambda_3^2 - 3\right)$$
$$\sigma = \frac{\partial U}{\partial \lambda} = 2\left(\lambda - \frac{1}{\lambda^2}\right)\left(C_1 + \frac{C_2}{\lambda}\right)$$

In this case, the shear modulus is defined as two times the sum of the fit parameters, $G = 2(C_1 + C_2)$. This model can fit the non-linear behavior of hydrogels well and the second parameter allows for better fits at more extreme extension ratios. In our case when fitting with the Mooney-Rivlin model, C_1 was set equal to the C_1 determined from a free-floating Neo-Hookean fit, while C_2 was allowed to float to best fit the data.

All three models were used to analyze the hydrogel behavior in compression, but only the Neo-Hookean and Mooney-Rivlin fits accounted for the non-linear stress curves. While the rubber fits accounted for the whole strain range, the Hookean fit only applied to the low strain region, and even at low strains the stress profile was non-linear (Figure 5.10). Furthermore, the calculated modulus value for the Hookean fit was dependent on the strain range used to fit the data. At lower strains, the slope was slighter, but at higher strains the linear fit took more of the steep downward turn of the stress curve into account and the overall measured modulus increased. The extent of these effects were measured by fitting a Hookean relationship at 5, 10, and 15% strain with varying hydrogel concentrations, and the results are shown in Figure 5.11. As shown with the Neo-

Hookean fit, the modulus increased linearly with concentration, as expected, but the modulus value also increased as the fitted strain range was broadened.

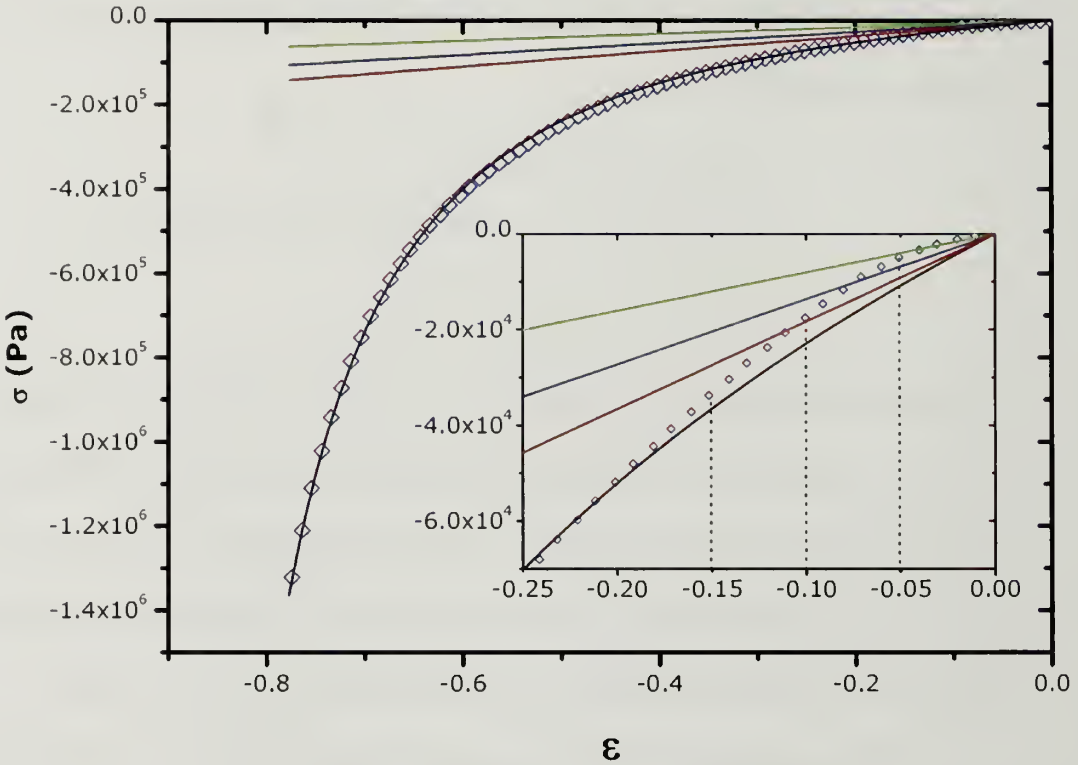

Figure 5.10. Typical stress versus strain curve with Hookean (green, blue, and red lines at 5, 10, and 15% strain range, respectively) and Neo-Hookean (black line) model fits. The inset zooms in on the small strain region and shows that even at low strains, the curve is non-linear.

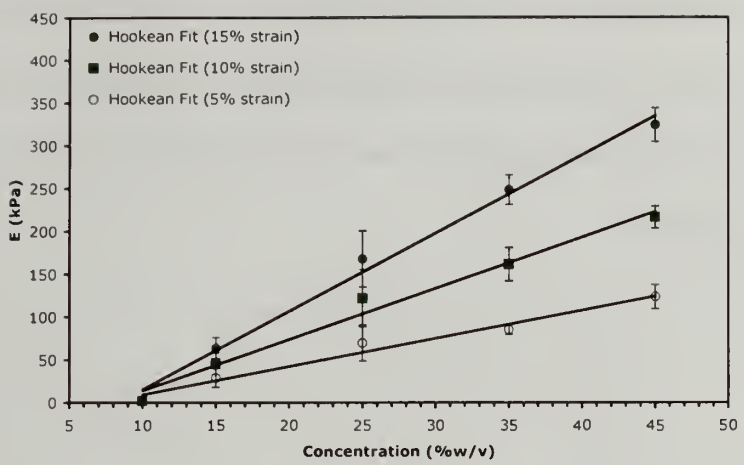

Figure 5.11. Elastic modulus vs. concentration using Hookean fits with various strain ranges.

To compare the values obtained from the rubber models to the Hookean model, the measured shear modulus was converted to an elastic modulus using the following relation: $E = 2G(1 + \nu)$, where ν is the Poisson's ratio defined as the ratio of the lateral tension to the longitudinal compression. Most commonly, rubbers and gels are assumed to be incompressible with a Poisson's ratio equal to 0.5, which was assumed for the Neo-Hookean and Mooney-Rivlin models. The results from both fits with varying concentration were converted to an elastic modulus in Figure 5.12. Again, all the fits showed a linear dependence on concentration, but the rubber fits calculated higher modulus values than the Hookean model. The difference in values was likely because the rubber models fit well for the high strain region. There was also no significant difference between the Neo-Hookean and Mooney-Rivlin fits, demonstrating that the stress-strain behavior of the gels is well described by using just one parameter fit. Furthermore, although a Poisson's ratio of 0.5 was assumed, significantly lower Poisson's ratios have been measured for several hydrogels.[67, 164, 165] For example, a Poisson's ratio as low as 0.33 has been reported for poly(vinyl alcohol) gels[166] and can even be negative for

poly(N-isopropylacrylamide) gels near volume transitions.[167] Therefore, if the actual Poisson's ratio of a material is not measured and is lower than that assumed, then a discrepancy between the real elastic modulus of the material and the measured elastic modulus will arise.

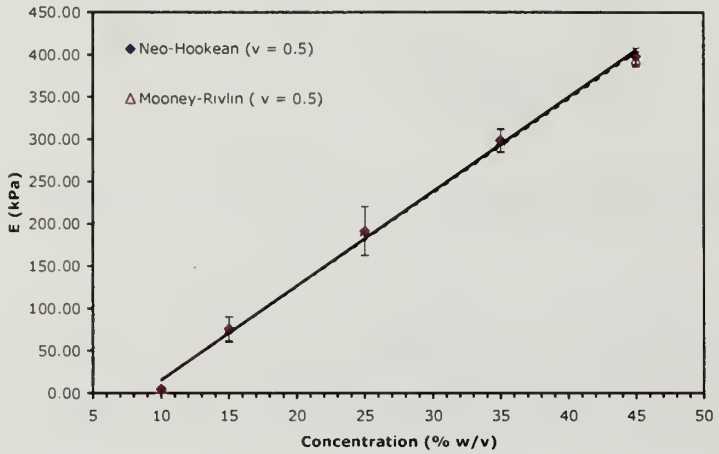

Figure 5.12. Elastic modulus versus concentration using rubber models with an assumed Poisson's ratio of 0.5.

The modulus values for all of the fits are compared in Figure 5.13a. This comparison showed that the Neo-Hookean and Mooney-Rivlin models calculated the highest elastic modulus, while the Hookean model (5% strain) calculated the lowest elastic modulus, and the discrepancies in modulus appeared to be more pronounced at higher concentrations. However, the discrepancies may have only been more pronounced because of the overall higher values. To account for this, Figure 5.13b shows the modulus values normalized to the lowest modulus (Hookean fit at 5% strain). When normalized, the trend was less clear. At low concentrations (10%) all the fits agreed well except for the rubber models. Above a concentration of 10%, the normalized Hookean fits at larger strains started to increase slightly with concentration. Overall, once normalized the discrepancies between fits remained fairly constant; however, the data

still showed that the assumed constitutive equation greatly affected the measured modulus of the material.

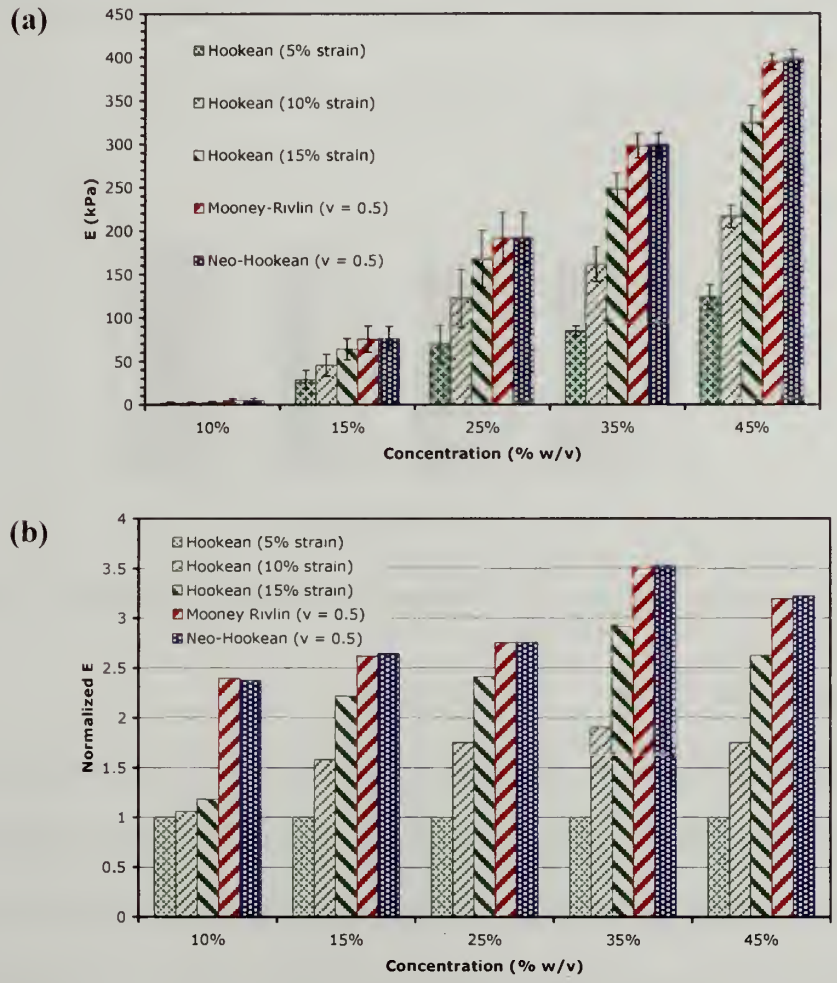

Figure 5.13. Comparing elastic modulus with all fits. (**a**) Elastic modulus versus concentration for all fits. (**b**) Normalized modulus values versus concentration for all fits.

Since the mechanical properties of cartilage are known to be strain rate dependent, we probed the photocrosslinked PLA-PEO-PLA hydrogels for this characteristic. The same hydrogel was compressed at 0.5, 1, 2.5, and 5 mm/min, and the modulus was calculated using a Hookean model at 10% strain, a Neo-Hookean model, and the Mooney Rivlin model. Figure 5.14 shows the measured elastic modulus is

independent of the strain rate (converted to milli-Hertz), at least within the range of rates probed here. So, while the material may approach the proper modulus values to mimic certain soft tissues, it still does not have the same dynamic properties of native tissue.

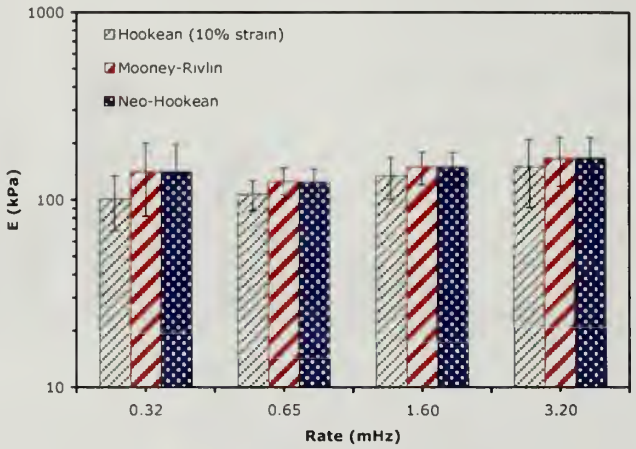

Figure 5.14. Measured modulus of photocrosslinked PLA-PEO-PLA versus strain rate.

5.4.2. Finite Size Effects

One final important consideration when comparing modulus values is that of finite size effects. When probing the compression behavior of a cylinder with measured height (h) and radius (a), work has shown that the determined modulus is only valid if the contact radius is much smaller than the height of the sample. As the ratio of a/h increases, or as the sample becomes flatter and more pancake-shaped, the effective measured modulus increases. The following semi-empirical equation, determined by using finite element methods, captures this effect:[168]

$$E = E_{eff}\left[1 + \frac{4}{3}(a/h) + \frac{4}{3}(a/h)^3\right]^{-1}$$

where E_{eff} is the effective or measured modulus. According to this expression, with even a small a/h ratio equal to 0.1, 10% error is introduced in the modulus measurement.

Therefore, it is essential to know the dimensions of the hydrogel to better compare modulus values from one researcher to another. For example, in this study a 25% photocrosslinked PLA-PEO-PLA hydrogel had a = 4.75 mm and h = 7.9 mm, giving a/h $\approx$ 0.6. Another group may report the same effective modulus as what was measured in this study but have different dimensions leading to a/h $\approx$ 2.5. By using the equation above, the actual modulus of the gel with a/h $\approx$ 0.6 is approximately 12 times greater than that of the gel with a/h $\approx$ 2.5. So, although the reported modulus values may be similar, the actual material properties may be very different once finite size effects are taken into account.

However, the semi-empirical expression above was determined using crosslinked elastomers, not hydrogels. To determine if the expression held for crosslinked PLA-PEO-PLA hydrogels, hydrogels were prepared as previously described and cut to various heights with a razor blade. These samples were tested in compression to approximately 10% strain. An example of the resultant stress-strain curve is shown in Figure 5.15. According to the established expression as a/h increases, the measured modulus should increase, but the strain-strain curve implied the opposite trend. Qualitatively, as a/h increased the material appeared to be softer. This data was fit using a Neo-Hookean constitutive relationship to determine the shear modulus at various a/h ratios, and the results are shown in Figure 5.16. Above a/h = 1, the modulus seemed to reach a plateau value, and as a/h decreased, the measured modulus steeply increased.

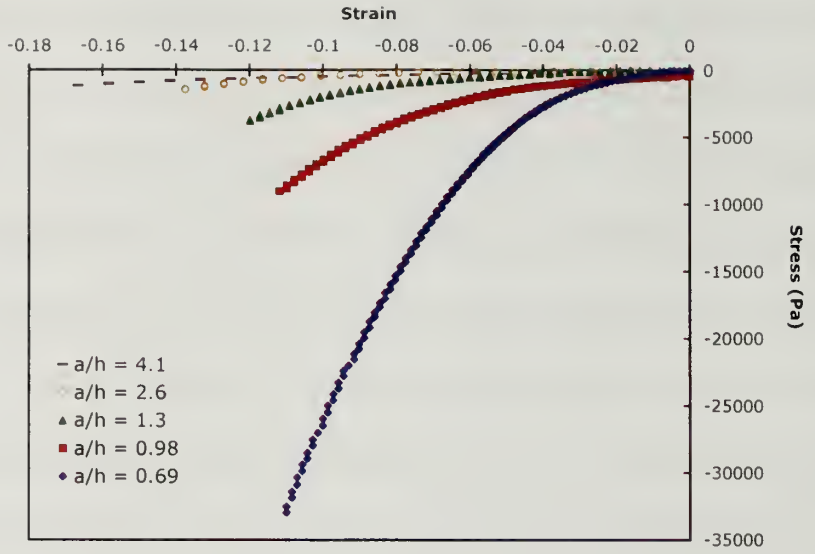

Figure 5.15. Stress versus strain for photocrosslinked PLA-PEO-PLA with varying a/h ratios.

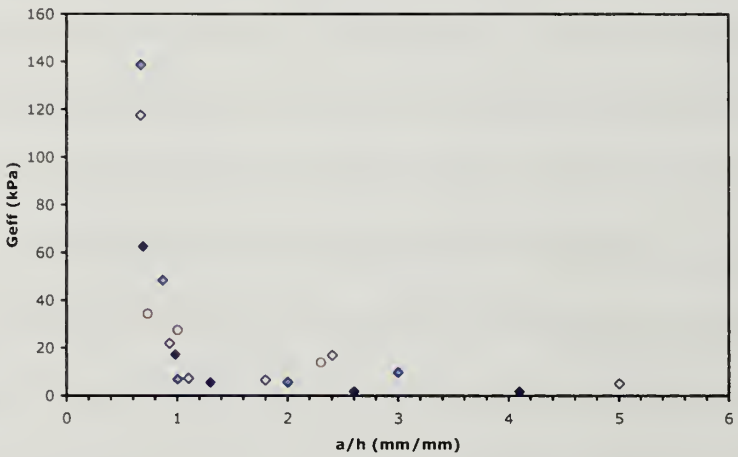

Figure 5.16. Measured modulus versus a/h. The diamond data points had a ≈ 4.9 mm and different shadings correspond to different gel samples that were then cut. The circular data points had a ≈ 8.3 mm.

Since these results showed the opposite trend than that predicted we investigated possible sources of error that might account for the discrepancy. When the samples were prepared, the lowest a/h value was measured first. A section from this same sample that was already compressed was then cut to a smaller height to increase the a/h ratio and compressed again. Although the samples were only compressed to about 10% strain, we

were unsure if repeated compression cycles could change the structure to affect the mechanical properties. To test this, the same sample was repeatedly compressed to see if the measured modulus varied. The results shown in Figure 5.17 indicate that the modulus stayed fairly constant through many cycles regardless of the a/h ratio (the circled data points are likely outliers due to erroneous measurements but were left in the graph for completeness). Therefore, a change in structure does not account for the discrepancy. Another possible factor was that of strain rate. The compression was controlled through the head speed, or extension rate, not by strain rate. So, although the extension rate is held constant, samples with large a/h would undergo a much higher strain rate. However, higher strain rate typically leads to higher modulus values, which is opposite of what we observed. Furthermore, as already discussed in Section 5.4.1, the modulus is independent of the strain rate. Future work will repeat these experiments with a more accurately measured extension and with different geometries including a smaller semi-spherical probe and cavitation rheology[169] to ensure the validity of the data. If the data is accurate then the measured modulus is highly dependent on the dimensions of the sample. A slight difference in a/h can result in a difference of two orders of magnitude in modulus.

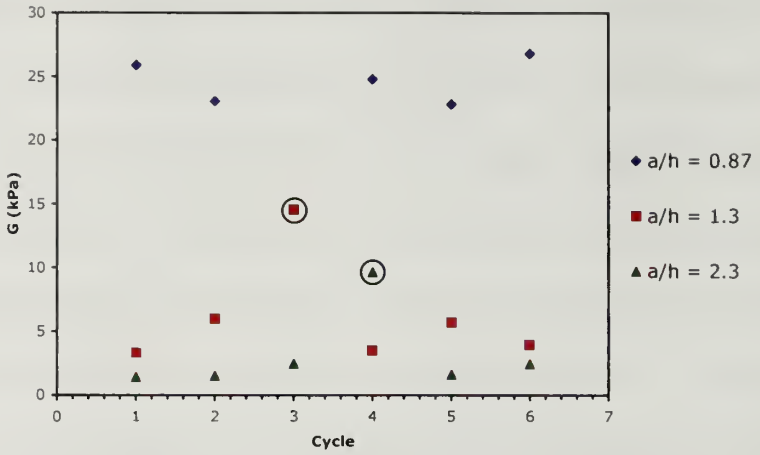

Figure 5.17. Modulus versus compression cycle with varying a/h ratios. Circled data points are likely outliers.

5.5. Conclusions

PLA-PEO-PLA triblock copolymer endgroups were modified with an acrylate functionality for chemical crosslinking. By first forming the physical hydrogel then initiating the photocrosslinking reaction, we templated the structure of the corresponding permanently crosslinked hydrogel. By using this method, the reversible crosslinks were locked in by covalent bonds, which allowed the gel to maintain its mechanical strength in a highly aqueous environment. The degradation properties of these modified hydrogels were characterized by measuring the swelling ratio and mass loss with degradation time. As the hydrogel degraded, the polyester was hydrolyzed, the crosslink density decreased, which led to an exponential increase in swelling ratio with time. The mass lost also increased with degradation time, however the observed kinetics were more complicated than the swelling ratio because the release of molecules only occurred when two hydrolysis events happened on the same chain. After approximately 52 days there was a sharp increase in the mass loss, likely due to the release of polyacrylate chains, and the hydrogel was fully degraded after approximately 63 days. The extended degradation

time as compared to similar photocrosslinked PLA-PEO-PLA hydrogels could be because higher molecular weights were used, or could imply that the self-assembled structure slowed the degradation rate.

The mechanical properties of the hydrogels were evaluated under compression assuming either a Hookean, Neo-Hookean, or Mooney-Rivlin constitutive relationship. As the hydrogel degraded the modulus decreased exponentially with time (analogous to the swelling data), but at a critical time point the modulus dropped sharply (initial G = 64 kPa). This occurred because modulus is dependent on the crosslink density but at a certain time point, we may be measuring a different mechanical parameter such as fracture toughness (measured G = 0.15 kPa after 42 days of degradation). The modulus value had a linear dependence on polymer hydrogel concentration, as would be expected for a physically crosslinked system, and suggests that the original network structure was intact (G = 1.6 – 133 kPa). Both of these observations are consistent, regardless of the assumed constitutive equation, but the overall modulus values are affected. The Hookean model was a poor fit because it did not capture the material's non-linear behavior. While the Mooney-Rivlin model did fit the data well, the Neo-Hookean model was chosen as the best fit because only one fit-parameter was needed, and the model can be statistically derived, giving the fit-parameter physical significance (half of the shear modulus, G).

Finally, we explored the impact of finite size effects. Differences in sample dimensions can lead to similar reported modulus values when the actual material properties are quite different. Previous work showed that as the ratio of a/h increases, so does the measured modulus. However, our work using photocrosslinked PLA-PEO-PLA hydrogels showed the opposite trend. The measured modulus increased as much as two

orders of magnitude as a/h was reduced. Overall, greater care is needed when reporting modulus values so that researchers can know the conditions used for fitting the raw data. By taking greater care, more accurate comparisons and correlations between mechanical properties and cell viability can be made to further progress the field of polymer scaffolds.

BIBLIOGRAPHY

1. Fishman, J.A. and R.H. Rubin, *Infection in Organ-Transplant Recipients.* New England Journal of Medicine, 1998. **338**: p. 1741-1751.

2. *The Organ Procurement and Transplantation Network.* 2008.

3. Gunzburg, W.H. and B. Salmons, *Xenotransplantation: is the risk of viral infection as great as we thought?* Molecular Medicine Today, 2000. **6**: p. 199-208.

4. Langer, R. and J.P. Vacanti, *Tissue Engineering.* Science, 1993. **260**: p. 920-926.

5. Griffith, L.G. and G. Naughton, *Tissue Engineering-Current Challenges and Expanding Opportunities.* Science, 2002. **295**: p. 1009-1014.

6. Stock, U.A. and J.P. Vacanti, *Tissue Engineering: Current State and Prospects.* Annual Review of Medicine, 2001. **52**: p. 443-451.

7. Caplan, A.I. and S.P. Bruder, *Mesenchymal stem cells: building blocks for molecular medicine in the 21st century.* TRENDS in Molecular Medicine, 2001. **7**: p. 259-264.

8. Laurencin, C.T., et al., *Tissue Engineering: Orthopedic Applications.* Annual Review of Biomedical Engineering, 1999. **1**: p. 19-46.

9. Rodkey, W.G., R. Steadman, and S.-T. Li, *A Clinical Study of Collagen Meniscus Implants to Restore the Injured Meniscus.* Clinical Orthopaedics and Related Research, 1999. **3675**: p. 5281-5292.

10. Temenoff, J.S. and A.G. Mikos, *Review: tissue engineering for regeneration of articular cartilage.* Biomaterials, 2000. **21**: p. 431-440.

11. Brittberg, M., et al., *Treatment of Deep Cartilage Defects in the Knee with Autologous Chondrocyte Transplantation.* The New England Journal of Medicine, 1994. **331**(14): p. 889-895.

12. Lutolf, M.P. and J.A. Hubbell, *Synthetic biomaterials as instructive extracellular microenvironments for morphogenesis in tissue engineering.* Nature Biotechnology, 2005. **23**(1): p. 47-55.

13. Boontheekul, T. and D.J. Mooney, *Protein-based signaling systems in tissue engineering.* Current Opinion in Biotechnology, 2003. **14**: p. 559-565.

14. Hubbell, J.A., *Materials as morphogenetic guides in tissue engineering.* Current Opinion in Biotechnology, 2003. **14**: p. 551-558.

15. Hersel, U., C. Dahmen, and H. Kessler, *RGD modified polymers: biomaterials for stimulated cell adhesion and beyond.* Biomaterials, 2003. **24**: p. 4385-4415.

16. Brandl, F., F. Sommer, and A. Goepferich, *Rational design of hydrogels for tissue engineering: Impact of physical factors on cell behavior.* Biomaterials, 2007. **28**: p. 134-146.

17. Yamada, K.M. and B. Geiger, *Molecular interactions in cell adhesion complexes.* Current Opinion in Cell Biology, 1997. **9**: p. 76-85.

18. Pierschbacher, M.D. and E. Ruoslahti, *Cell attachment activity of fibronectin can be duplicated by small synthetic fragments of the molecule.* Nature, 1984. **309**: p. 30-33.

19. Ruoslahti, E., *RGD and other recognition sequences for integrins.* Annual Review of Cell Developmental Biology, 1996. **12**: p. 697-715.

20. Huang, S. and D.E. Ingber, *The structural and mechanical complexity of cell-growth control.* Nat. Cell Bio., 1999. **1**: p. 131-138.

21. Georges, P.C. and P.A. Janmey, *Cell type-specific response to growth on soft materials.* Journal of Applied Physiology, 2005. **98**: p. 1547-1553.

22. Choquet, D., D.P. Felsenfeld, and M.P. Sheetz, *Extracellular Matrix Rigidity Causes Strengthening of Integrin-Cytoskeleton Linkages.* Cell, 1997. **88**: p. 39-48.

23. Wang, H.B., M. Dembo, and Y.L. Wang, *Substrate flexibility regulates growth and apoptosis of normal but not transformed cells.* Am. J. Physiol. Cell Physiol., 2000. **279**: p. C1345-C1350.

24. Engler, A.J., et al., *Myotubes differentiate optimally on substrates with tissue-like stiffness: pathological implications for soft or stiff microenvironments.* Journal of Cell Biology, 2004. **166**(6): p. 877-887.

25. Pelham, R.J. and Y.-L. Wang, *High Resolution Detections of Mechanical Forces Exerted by Locomoting Fibroblasts on the Substrate.* Molecular Biology of the Cell, 1999. **10**: p. 935-945.

26. Pelham, R.J. and Y.-L. Wang, *Cell locomotion and focal adhesions are regulated by substrate flexibility.* Proceedings of the National Academy of Sciences of the United States of America, 1997. **94**: p. 13661-13665.

27. Kim, B.-S., et al., *Cyclic mechanical strain regulates the development of engineering smooth muscle tissue.* Nature Biotechnology, 1999. **17**: p. 979-983.

28. Chicurel, M.E., C.S. Chen, and D.E. Ingber, *Cellular control lies in the balance of forces.* Current Opinion in Cell Biology, 1998. **10**: p. 232-239.

29. Engler, A.J., et al., *Matrix Elasticity Directs Stem Cell Lineage Specification.* Cell, 2006. **126**: p. 677-689.

30. Myers, E.R. and V.C. Mow, *Biomechanics of Cartilage and Its Response to Biomechanical Stimuli*, in *Cartilage: Structure, Function, and Biochemistry*, B.K. Hall, Editor. 1983, Academic Press, Inc.: New York, NY. p. 313-341.

31. Oloyede, A. and N. Broom, *The Biomechanics of Cartilage Load-Carriage.* Connective Tissue Research, 1996. **34**(2): p. 119-143.

32. Oloyede, A., R. Flachsmann, and N.D. Broom, *The Dramatic Influence of Loading Velocity on the Compressive Response of Articular Cartilage.* Connective Tissue research, 1992. **27**: p. 211-224.

33. Silver, F.H., *Biological Materials: Structure, Mechanical Properties, and Modeling of Soft Tissues*. New York University Biomedical Engineering Series, ed. W. Welkowitz. 1987, New York: New York University Press.

34. Lu, Y.-B., et al., *Viscoelastic properties of individual glial cells and neurons in the CNS.* Proceedings of the National Academy of Sciences of the United States of America, 2006. **103**(47): p. 17759-17764.

35. Yu, Q.L., J.B. Zhou, and Y.C. Fung, *Neutral axis location in bending and Young's modulus of different layers of arterial wall.* American Journal of Physiology, 1993. **265**: p. 52-60.

36. Sacks, M.S., et al., *Bioprosthetic heart valve heterograft biomaterials: structure, mechanical behavior, and computational simulation.* Expert Review of Medical Devices, 2006. **3**(6): p. 817-834.

37. Silver, F.H., I. Horvath, and D.J. Foran, *Viscoelasticity of the Vessel Wall: The Role of Collagen and Elastic Fibers.* Critical Reviews in Biomedical Engineering, 2001. **29**(3): p. 279-302.

38. Khatyr, F., et al., *Model of the viscoelastic behavior of skin in vivo and study of anisotropy.* Skin Research and Technology, 2004. **10**: p. 96-103.

39. Wang, J.H.-C., *Mechanobiology of tendon.* Journal of Biomechanics, 2006. **39**: p. 1563-1582.

40. Bates, J.H.T., et al., *Lung Tissue Rheology and 1/f Noise.* Annals of Biomedical Engineering, 1994. **22**: p. 674-681.

41. Nasseri, S., L.E. Bilston, and N. Phan-Thien, *Viscoelastic properties of pig kidney in shear, experimental results and modeling.* Rheologica Acta, 2002. **41**: p. 180-192.

42. Kim, B.-S. and D.J. Mooney, *Development of biocompatible synthetic extracellular matrices for tissue engineering.* TIBTECH, 1998. **16**: p. 224-230.

43. Lee, K.Y. and D.J. Mooney, *Hydrogels for Tissue Engineering.* Chemical Reviews, 2001. **101**(7): p. 1869-1879.

44. Hoffman, A.S., *Hydrogels for biomedical applications.* Advanced Drug Delivery Reviews, 2002. **54**: p. 3-12.

45. Kissel, T., Y. Li, and F. Unger, *ABA-triblock copolymer from biodegradable polyester A-blocks and hydrophilic poly(ethylene oxide) B-blocks as a candidate for in situ forming hydrogel delivery systems for proteins.* Advanced Drug Delivery Reviews, 2002. **54**: p. 99-134.

46. Gutowska, A., B. Jeong, and M. Jasionowski, *Injectable Gels for Tissue Engineering.* The Anatomical Record, 2001. **263**: p. 342-349.

47. Mano, J.F., et al., *Natural origin biodegradable systems in tissue engineering and regenerative medicine: present status and some moving trends.* Journal of the Royal Society Interface, 2007. **4**: p. 999-1030.

48. Riesle, J., et al., *Collagen in Tissue-Engineered Cartilage: Types, Structure, and Crosslinks.* Journal of Cellular Biochemistry, 1998. **71**: p. 313-327.

49. Buma, P., et al., *Cross-linked type I and type II collagenous matrices for the repair of full-thickness articular cartilage defects-A study in rabbits.* Biomaterials, 2003. **24**: p. 3255-3263.

50. Albala, D.M., *Fibrin sealants in clinical practice.* Cardiovascular Surgery, 2003. **11**: p. 5-11.

51. Rowe, S.L., S.Y. Lee, and J.P. Stegemann, *Influence of thrombin concentration on the mechanical and morphological properties of cell-seeded fibrin hydrogels.* Acta Biomaterialia, 2007. **3**: p. 59-67.

52. Sierra, D.H., A.W. Eberhardt, and J.E. Lemons, *Failure characteristics of multiple-component fibrin-based adhesives.* Journal of Biomedical Materials Research, 2002. **59**: p. 1-11.

53. Cummings, C.L., et al., *Properties of engineering vascular constructs made from collagen, fibrin, and collagen-fibrin mixtures.* Biomaterials, 2004. **25**: p. 3699-3706.

54. Remuzzi, A., et al., *Vascular Smooth Muscle Cells on Hyaluronic Acid: Culture and Mechanical Characterization of an Engineered Vascular Construct.* Tissue Engineering, 2004. **10**: p. 699-711.

55. Chung, C., et al., *Effects of Auricular Chondrocyte Expansion on Neocartilage Formation in Photocrosslinked Hyaluronic Acid Networks.* Tissue Engineering, 2006. **12**: p. 2665-2673.

56. Burdick, J.A., et al., *Controlled Degradation and Mechanical Behavior of Photopolymerized Hyaluronic Acid Networks.* Biomacromolecules, 2005. **6**: p. 386-391.

57. Lahiji, A., et al., *Chitosan supports the expression of extracellular matrix proteins in human osteoblasts and chondrocytes.* Journal of Biomedical Materials Research, 2000. **51**: p. 586-595.

58. Kim, I.-Y., et al., *Chitosan and its derivatives for tissue engineering applications.* Biotechnology Advances, 2008. **26**: p. 1-21.

59. Kuo, C.K. and P.X. Ma, *Ionically crosslinked alginate hydrogels as scaffolds for tissue engineering: Part 1. Structure, gelation rate, and mechanical properties.* Biomaterials, 2001. **22**: p. 511-521.

60. Stevens, M.M., et al., *A rapid-curing alginate gel system: utility in periosteum-derived cartilage tissue engineering.* Biomaterials, 2004. **25**: p. 887-894.

61. Gu, W.Y., et al., *New insight into deformation-dependent hydraulic permeability of gels and cartilage, and dynamic behavior of agarose gels in confined compression.* Journal of Biomechanics, 2003. **36**: p. 593-598.

62. Mauck, R.L., et al., *Functional Tissue Engineering of Articular Cartilage Through Dynamic Loading of Chondrocyte-Seeded Agarose Gels.* Journal of Biomechanical Engineering, 2000. **122**: p. 252-260.

63. Duncan, R., *The Dawning Era of Polymer Therapeutics.* Nature Reviews Drug Discovery, 2003. **2**: p. 347-360.

64. Sodergard, A. and M. Stolt, *Properties of lactic acid based polymers and their correlation with composition.* Progress in Polymer Science, 2002. **27**: p. 1123-1163.

65. Sudesh, K., H. Abe, and Y. Doi, *Synthesis, structure and properties of polyhydroxyalkanoates: biological polyesters.* Progress in Polymer Science, 2000. **25**: p. 1503-1555.

66. Okada, M., *Chemical syntheses of biodegradable polymers.* Progress in Polymer Science, 2002. **27**: p. 87-133.

67. Takigawa, T., et al., *Swelling and stress-relaxation of poly(N-isopropylacrylamide) gels in the collapsed state.* Journal of Chemical Physics, 2002. **117**: p. 7306-7312.

68. Hennink, W.E. and C.F. varNostrum, *Novel crosslinking methods to design hydrogels.* Advanced Drug Delivery Reviews, 2002. **54**: p. 13-36.

69. Freemont, T.J. and B.R. Saunders, *pH-Responsive microgel dispersions for repairing damaged load-bearing soft tissue.* Soft Matter, 2008. **4**: p. 919-924.

70. Elisseeff, J., et al., *Transdermal photopolymerization of poly(ethylene oxide)-based injectable hydrogels for tissue-engineered cartilage.* Plastic and Reconstructive Surgery, 1999. **104**(4): p. 1014-1022.

71. Anseth, K.S., et al., *In situ forming degradable networks and their application in tissue engineering and drug delivery.* Journal of Controlled Release, 2002. **78**(1-3): p. 199-209.

72. Sawhney, A.S., C.P. Pathak, and J.A. Hubbell, *Bioerodible Hydrogels Based on Photopolymerized Poly(ethylene glycol)-co-poly(alpha-hydroxy acid) Diacrylate Macromers.* Macromolecules, 1993. **26**: p. 581-587.

73. Bryant, S.J., et al., *Encapsulating Chondrocytes in Degrading PEG Hydrogels with High Modulus: Engineering Gel Structural Changes to Facilitate Cartilaginous Tissue Production.* Biotechnology and Bioengineering, 2004. **86**(7): p. 747-755.

74. Lutolf, M.P., et al., *Cell-Responsive Synthetic Hydrogels.* Advanced Materials, 2003. **15**(11): p. 888-892.

75. Kong, H.J., E. Wong, and D.J. Mooney, *Independent Control of Rigidity and Toughness of Polymeric Hydrogels.* Macromolecules, 2003. **36**(4582-4588).

76. Kong, H.-J., K.Y. Lee, and D.J. Mooney, *Decoupling the dependence of rheological/mechanical properties of hydrogels from solids concentration.* Polymer, 2002. **43**: p. 6239-6246.

77. Mi, L., et al., *Self-Assembling Protein Hydrogels with Modular Integrin Binding Domains.* Biomacromolecules, 2006. **7**: p. 38-47.

78. Reddy, T.T., et al., *Swelling Behavior and Controlled Release of Theophylline and Sulfamethoxazole Drugs in beta-Lactoglobulin Protein Gels Obtained by Phase Separation in Water/Ethanol Mixture.* Biomacromolecules, 2006. **7**: p. 323-330.

79. Ozbas, B., et al., *Salt-Triggered Peptide Folding and Consequent Self-Assembly into Hydrogels with Tunable Modulus.* Macromolecules, 2004. **37**: p. 7331-7337.

80. Haines, L.A., et al., *Light-Activated Hydrogel Formation via the Triggered Folding and Self-Assembly of a Designed Peptide.* Journal of American Chemical Society, 2005. **127**: p. 17025-17029.

81. Deming, T.J., *Polypeptide hydrogels via a unique assembly mechanism.* Soft Matter, 2005. **1**: p. 28-35.

82. Ricciardi, R., et al., *Investigation of the Crystallinity of Freeze/Thaw Poly(vinyl alcohol) Hydrogels by Different Techniques.* Macromolecules, 2004. **37**: p. 9510-9516.

83. Ricciardi, R., et al., *X-ray Diffraction Analysis of Poly(vinyl alcohol) Hydrogels, Obtained by Freezing and Thawing Techniques.* Macromolecules, 2004. **37**: p. 1921-1927.

84. Ricciardi, R., et al., *Investigation of the relationships between the chain organization and rheological properties of atactic poly(vinyl alcohol) hydrogels.* Polymer, 2003. **44**: p. 3375-3380.

85. Ricciardi, R., et al., *Structural Organization of Poly(vinyl alcohol) Hydrogels Obtained by Freezing and Thawing Techniques: A SANS Study.* Chem. Mater., 2005. **17**: p. 1183-1189.

86. Kaneko, T., et al., *Liquid-Crystalline Hydrogels. 1. Enhanced Effects of Incorporation of Acrylic Acid Units on the Liquid-Crystalline Ordering.* Macromolecules, 2000. **33**: p. 412-418.

87. Kaneko, T., et al., *Liquid Crystalline Hydrogels. 2. Effects of Water on the Structural Ordering.* Macromolecules, 2000. **33**: p. 4422-4426.

88. Yamaoka, K., et al., *Liquid Crystalline Gels. 3. Role of Hydrogen Bonding in the Formation and Stabilization of Mesophase Structures.* Macromolecules, 2001. **34**: p. 1470-1476.

89. Yamaoka, K., et al., *Liquid Crystalline Gels. 4. Water- and Stress-Induced Mesophase Transition.* Langmuir, 2003. **19**: p. 8134-8136.

90. Miyazaki, T., et al., *Hydrogels with Crystalline or Liquid Crystalline Structure.* Macromol. Rapid Commun., 2002. **23**: p. 447-455.

91. Tae, G., et al., *Hydrogels with Controlled, Surface Erosion Characteristics from Self-Assembly of Fluoroalkyl-Ended Poly(ethylene glycol).* Macromolecules, 2001. **34**: p. 6409-6419.

92. Berret, J.-F., et al., *Fluorocarbon associative polymers.* Current Opinion in Colloid and Interface Science, 2003. **8**: p. 296-306.

93. Calvet, D., et al., *Perfluoroalkyl End-Capped Poly(ethylene oxide). Synthesis, Characterization, and Rheological Behavior in Aqueous Solution.* Macromolecules, 2003. **36**: p. 449-457.

94. Pham, Q.T., et al., *Micellar Solution of Associative Triblock Copolymer: The Relationship between Structure and Rheology.* Macromolecules, 1999. **32**: p. 5139-5146.

95. Castelletto, V., et al., *Structure and rheology of aqueous micellar solution and gels formed from an associative poly(oxybutylene)-poly(oxyethylene)-poly(oxybutylene) triblock copolymer.* Soft Matter, 2005. **1**: p. 138-145.

96. Hamley, I.W., et al., *Shear-Induced Orientational Transitions in the Body-Centered Cubic Phase of a Diblock Copolymer Gel.* Macromolecules, 1998. **31**: p. 3906-3911.

97. Patrick, J., et al., *Diblock Copoly(oxyethylene/oxybutylene) E41B8 in Water: Liquid Crystal Mesophases Studied by Small Angle X-Ray Scattering.* Macromolecules, 1999. **32**: p. 2058-2060.

98. Alexandridis, P. and T.A. Hatton, *Poly(ethylene oxide)-poly(propylene oxide)-poly(ethylene oxide) block copolymer surfactants in aqueous solutions and at interfaces: thermodynamics, structure, dynamics, and modeling.* Colloids and Surfaces A: Physicochemical and Engineering Aspects, 1995. **96**: p. 1-46.

99. Brown, W., et al., *Micelle and Gel Formation in a Poly(ethylene oxide)/Poly(propylene oxide)/Poly(ethylene oxide) Triblock Copolymer in Water Solution. Dynamic and Static Light Scattering and Oscillatory Shear Measurements.* Journal of Physical Chemistry, 1991. **95**: p. 1850-1858.

100. Lau, B.K., et al., *Micellization to Gelation of a Triblock Copolymer in Water: Thermoreversibility and Scaling.* Journal of Polymer Science: Part B, 2004. **42**: p. 2014-2025.

101. Rashkov, I., et al., *Synthesis, characterization, and hydrolytic degradation of PLA/PEO/PLA with short poly(L-lactic acid) chains.* Macromolecules, 1996. **29**: p. 50-56.

102. Li, S.M., et al., *Synthesis, characterization, and hydrolytic degradation of PLA/PEO/PLA triblock copolymer with long poly(L-lactic acid) blocks.* Macromolecules, 1996. **29**: p. 57-62.

103. Lee, D.S., et al., *Novel Thermoreversible Gelation of Biodegradable PLGA-block-PEO-block-PLGA Triblock Copolymers in Aqueous Solution.* Macromol. Rapid Commun., 2001. **22**: p. 587-592.

104. Zhong, Z., et al., *Synthesis and Aqueous Phase Behavior of Thermoresponsive Biodegradable poly(D,L-3-methylglycolide)-block-poly(ethylene glycol)-block-poly(D,L-3-methylglycolide) triblock copolymers.* Macromol. Chem. Phys., 2002. **203**: p. 1797-1803.

105. Lee, H.T. and D.S. Lee, *Thermoresponsive phase transition of PLA-block-PEO-block-PLA triblock stereo-copolymers in aqueous solution.* Macromol. Res., 2002. **10**: p. 359-364.

106. Kim, M.S., et al., *Preparation of Thermosensitive Diblock Copolymers Consisting of MPEG and Polyesters.* Macromolecules, 2006. **39**(9): p. 3099-3102.

107. Jeong, B., et al., *Thermoreversible Gelation of Poly(Ethylene Oxide) Biodegradable Polyester Block Copolymer.* Journal of Polymer Science: Part A: Polymer Chemistry, 1999. **37**: p. 751-760.

108. Riley, T., et al., *Use of Viscoelastic Measurements for Investigating Interparticle Interactions in Dispersions of Micellar-like Poly(lactic acid)-Poly(ethylene glycol) Nanoparticles.* Langmuir, 2002. **18**: p. 7663-7668.

109. Bae, S.J., et al., *Gelation Behavior of Poly(ethylene glycol) and Polycaprolactone Triblock and Multiblock Copolymer Aqueous Solutions.* Macromolecules, 2006. **39**: p. 4873-4879.

110. Tanodekaew, S., et al., *Gelation of aqueous solution of diblock copolymer of ethylene oxide and D,L-lactide.* Macromolecular Chemistry and Physics, 1997. **198**(11): p. 3385-3395.

111. Choi, S.W., et al., *Thermoreversible Gelation of Poly(ethylene oxide) Biodegradable Polyester Block Copolymers. II.* Journal of Polymer Science: Part A: Polymer Chemistry, 1999. **37**: p. 2207-2218.

112. Lim, D.W. and T.G. Park, *Stereocomplex Formation between Enantiomeric PLA-PEG-PLA Triblock Copolymers: Characterization and Use as Protein-Delivery Microparticulate Carriers.* Journal of Applied Polymer Science, 2000. **75**: p. 1615-1623.

113. Kricheldorf, H.R., et al., *Stereocomplexes of A-B-A Triblock Copolymers Based on Poly(L-lactide) and Poly(D-Lactide) A Blocks.* Macromolecules, 2005. **38**: p. 7018-7025.

114. Fujiwara, T., et al., *Novel Thermo-Responsive Formation of a Hydrogel by Stereo-Complexation between PLLA-PEG-PLLA and PDLA-PEG-PDLA Block Copolymers.* Macromolecular Bioscience, 2001. **1**: p. 204-208.

115. Li, S. and M. Vert, *Synthesis, Characterization, and Stereocomplex-Induced Gelation of Block Copolymers Prepared by Ring-Opening Polymerization of L(D)-Lactide in the Presence of Poly(ethylene glycol).* Macromolecules, 2003. **36**: p. 8008-8014.

116. Kwon, K.-W., et al., *Gelation behavior of PEO-PLGA-PEO triblock copolymers in water.* Polymer, 2002. **43**: p. 3353-3358.

117. Jeong, B., et al., *Biodegradable block copolymer as injectable drug-delivery systems.* Letters to Nature, 1997. **388**: p. 860-862.

118. Molina, I., et al., *Protein release from physically crosslinked hydrogels of the PLA/PEO/PLA triblock copolymer-type.* Biomaterials, 2001. **22**: p. 363-369.

119. Dechy-Cabaret, O., B. Martin-Vaca, and D. Bourissou, *Controlled Ring-Opening Polymerization of Lactide and Glycolide.* Chemical Reviews, 2004. **104**: p. 6147-6176.

120. Kim, Y., G.K. Jnaneshwara, and J.F. Vekade, *Titanium Alkoxides as Initiators for the Controlled Polymerization of Lactide.* Inorganic Chemistry, 2003. **42**: p. 1437-1447.

121. Dove, A.P., et al., *N-Heterocyclic carbenes: Effective organic catalysts for living polymerization.* Polymer, 2006. **47**: p. 4018-4025.

122. Aamer, K.A., et al., *Rheological Studies of PLLA-PEO-PLLA triblock copolymer hydrogels.* Biomaterials, 2004. **25**(6): p. 1087-1093.

123. Sanabria-DeLong, N., et al., *Poly(lactide)-Poly(ethylene oxide)-Poly(lactide) Triblock Copolymers: Synthesis and Thermal Properties*, in *Degradable Polymer and Materials, Principles and Practice*, K.C. Khemani and C. Scholz, Editors. 2006, American Chemical Society: Washington, D.C. p. 156-167.

124. Tanaka, F. and S.F. Edwards, *Viscoelastic Properties of Physically Cross-Linked Networks. Transient Network Theory.* Macromolecules, 1992. **25**: p. 1516-1523.

125. Semenov, A.N., J.-F. Joanny, and A.R. Khokhlov, *Associating Polymers: Equilibrium and Linear Viscoelasticity.* Macromolecules, 1995. **28**: p. 1066-1075.

126. Wang, S.-Q., *Transient Network Theory for Shear-Thickening Fluids and Physically Cross-Linked Systems.* Macromolecules, 1992. **25**: p. 7003-7010.

127. DeSantis, P. and A.J. Kovacs, *Molecular Conformation of Poly(S-lactic acid).* Biopolymers, 1968. **6**: p. 299-306.

128. Sarasua, J.-R., et al., *Crystallization and Melting Behavior of Polylactides.* Macromolecules, 1998. **31**: p. 3895-3905.

129. Pluta, M. and A. Galeski, *Crystalline and Supermolecular Structure of Poly(lactide) in Relation to the Crystallization Method.* Journal of Applied Polymer Science, 2002. **86**: p. 1386-1395.

130. Sanabria-DeLong, N., et al., *Controlling Hydrogel Properties by Crystallization of Hydrophobic Domains.* Macromolecules, 2006. **39**: p. 1308-1310.

131. Agrawal, S.K., et al., *Structural Characterization of PLA-PEO-PLA Solutions and Hydrogels: Crystalline vs. Amorphous PLA Domains.* Macromolecules, 2008. **41**: p. 1774-1784.

132. Lin, E.K. and A.P. Gast, *Semicrystalline Diblock Copolymer Platelets in Dilute Solution.* Macromolecules, 1996. **29**: p. 4432-4441.

133. Fujiwara, T., M. Miyamoto, and Y. Kimura, *Crystallization-Induced Morphological Changes of a Poly(L-lactide)/Poly(oxyethylene) Diblock Copolymer from Sphere to Band via Disk: A Novel Macromolecular Self-Organization Process from Core-Shell Nanoparticles on Surface.* Macromolecules, 2000. **33**: p. 2782-2785.

134. Cao, L., I. Manners, and M.A. Winnik, *Influence of the Interplay of Crystallization and Chain Stretching on Micellar Morphologies: Solution Self-Aseembly of Coil-Crystalline Poly(isoprene-block-ferrocenylsilane).* Macromolecules, 2002. **35**: p. 8258-8260.

135. Xu, J.-T., et al., *The effect of architecture on the morphology and crystallization of oxyethlene/oxybutulene block copolymers from micelles in n-hexane.* Journal of Material Chemistry, 2003. **13**: p. 2740-2748.

136. Fu, J., et al., *Self-Assembly of Crystalline-Coil Diblock Copolymer in Solvents with Varying Selectivity: From Spinodal-like Aggregates to Spheres, Cylinders, and Lamellae.* Macromolecules, 2004. **37**: p. 976-986.

137. Lee, H.B., M.S. Jhon, and J.D. Andrade, *Nature of Water in Synthetic Hydrogels, I. Dilatometry, Specific Conductivity, and Differential Scanning Calorimetry of Polyhydroxyethyl Methacrylate.* Journal of Colloid and Interface Science, 1975. **51**: p. 225-231.

138. Kim, S.J., C.K. Lee, and S.I. Kim, *Characterization of the Water State of Hyaluronic Acid and Poly(vinyl alcohol) Interpenetrating Polymer Networks.* Journal of Applied Polymer Science, 2004. **92**: p. 1467-1472.

139. Qu, X., A. Wirsen, and A.-C. Albertsson, *Novel pH-sensitive chitosan hydrogels: swelling behavior and states of water.* Polymer, 2000. **41**: p. 4589-4598.

140. Kim, S.J., S.J. Park, and S.I. Kim, *Synthesis and characteristics of interpenetrating polymer network hydrogels composed of poly(vinyl alcohol) and poly(N-isopropylacrylamide).* Reactive & Functional Polymers, 2003. **55**: p. 61-67.

141. Agrawal, S.K., et al., *Rheological characterization of biocompatible associative polymer hydrogels with crystalline and amorphous endblocks.* Journal of Materials Research, 2006. **21**(8): p. 2118-2125.

142. Lin, Y.G., et al., *Dynamic Mechanical Measurement of Crystallization-Induced Gelation in Thermoplastic Elastomeric Poly(propylene).* Macromolecules, 1991. **24**: p. 850-854.

143. Chambon, F. and H.H. Winter, *Linear Viscoelasticity at the Gel Point of a Cross-linking PDMS with Imbalanced Stoichiometry.* Journal of Rheology, 1987. **31**: p. 683-697.

144. Chambon, F., et al., *Rheology of Model Polyurethanes at the Gel Point.* Macromolecules, 1986. **19**: p. 2146-2149.

145. Alexander, L.E., *X-Ray Diffraction Methods in Polymer Science.* 1979, c1969, Huntington, NY: Robert E. Kreieger Publishing Co.

146. Mori, T., et al., *Effects of chain end structures on pyrolysis of poly(L-lactic acid) containing tin atoms.* Polymer Degradation and Stability, 2004. **84**: p. 243-251.

147. Wachsen, O., K. Platkowski, and K.-H. Reichert, *Thermal degradation of poly-L-lactide - studies on kinetics, modeling and melt stabilisation.* Polymer Degradation and Stability, 1997. **57**: p. 87-94.

148. Kricheldorf, H.R., C. Boettcher, and K.-U. Tonnes, *Polylactones: 23. Polymerization of racemic and meso D, L-lactide with various organotin catalysts-stereochemical aspects.* Polymer, 1992. **33**(13): p. 2817-2824.

149. Schwach, G., et al., *Stannous octoate- versus zinc-initiated polymerization of racemic lactide.* Polymer Bulletin, 1994. **32**: p. 617-623.

150. Hong, J., et al., *Characterization of Poly(ethylene oxide)-b-Poly(L-lactide) Block Copolymers by Matrix-Assisted Laser Desorption/Ionization Time-of-Flight Mass Spectroscopy.* Macromolecular Research, 2003. **11**(5): p. 341-346.

151. Lee, H., et al., *Characterization of Poly(ethylene oxide)-block-poly(L-lactide) by HPLC and MALDI-TOF Mass Spectrometry.* Macromolecules, 1999. **32**(12): p. 4143-4146.

152. Lee, H., et al., *Characterization of Poly(L-lactide)-block-poly(ethylene oxide)-block-poly(L-lactide) triblock copolymer by Liquid Chromatography at the Crtical Condition and by MALDI-TOF Mass Spectrometry.* Anal. Chem., 2001. **73**: p. 1726-1732.

153. Metters, A.T., K.S. Anseth, and C.N. Bowman, *Fundamental studies of a novel, biodegradable PEG-b-PLA hydrogel.* Polymer, 2000. **41**: p. 3993-4004.

154. Metters, A.T., K.S. Anseth, and C.N. Bowman, *A Statistical Kinetic Model for the Bulk Degradation of PLA-b-PEG-b-PLA Hydrogel Networks: Incorporating Network Non-Idealities.* Journal of Physical Chemistry B, 2001. **105**: p. 8069-8076.

155. Flory, P.J. and J. J. Rehner, *Statistical Mechanics of Cross-Linked Polymer Networks, II. Swelling.* Journal of Chemical Physics, 1943. **11**(11): p. 521-526.

156. Mase, G.T. and G.E. Mase, *Continuum Mechanics for Engineers*. 2 ed. 1999, Boca Raton: CRC Press.

157. Flory, P.J. and J. J. Rehner, *Statistical Mechanics of Cross-Linked Polymer Networks, I. Rubberlike Elasticity.* Journal of Chemical Physics, 1943. **11**(11): p. 512-520.

158. Treloar, L.R.G., *The elasticity of a network of longchain molecules- II.* Transactions of the Faraday Society, 1943. **39**: p. 241-246.

159. Wall, F.T., *Statistical Thermodynamics of Rubber. II.* Journal of Chemical Physics, 1942. **10**: p. 485-488.

160. Gerecht, S., et al., *A porous photocurable elastomer for cell encapsulation and culture.* biomaterials, 2007. **28**: p. 4826-4835.

161. Rice, M.A. and K.S. Anseth, *Encapsulating chondrocytes in copolymer gels: Bimodal degradation kinetics influence cell phenotype and extracellular matrix development.* Journal of Biomedical Materials Research Part A, 2004. **70**: p. 560-568.

162. Mooney, M., *A Theory of Large Elastic Deformation.* Journal of Applied Physics, 1940. **11**: p. 582-592.

163. Rivlin, R.S., *Large Elastic Deformations of Isotropic Materials. IV. Further Developments of General Theory.* Philosophical Transactions of the Royal Society of London. Series A, Mathematical and Physical Sciences, 1948. **241**(835): p. 379-397.

164. De, S.K., et al., *Equilibrium Swelling and Kinetics of pH-Responsive Hydrogels: Models, Experiments, and Simulations.* Journal of Microelectromechanical Systems, 2002. **11**: p. 544-555.

165. Li, Y., Z. Hu, and C. Li, *New Method for Measuring Poisson's Ratio in Polymer Gels.* Journal of Applied Polymer Science, 1993. **50**: p. 1107-1111.

166. Urayama, K., T. Takigawa, and T. Masuda, *Poisson's Ratio of Poly(vinyl alcohol) Gels.* Macromolecules, 1993. **26**: p. 3092-3096.

167. Hirotsu, S., *Softening of bulk modulus and negative Poisson's ratio near the volume phase transition of polymer gels.* Journal of Chemical Physics, 1991. **94**: p. 3949-3957.

168. Shull, K.R., et al., *Axisymmetric adhesion tests of soft materials.* Macromolecular Chemistry and Physics, 1998. **199**: p. 489-511.

169. Zimberlin, J.A., et al., *Cavitation rheology for soft materials.* Soft Matter, 2007. **3**: p. 763-767.